Metal-free Methods Utilizing Single-electron Oxidations

Kelli A. Ogawa

A dissertation submitted in partial fulfillment of the
requirements for the degree of:

Doctor of Philosophy

University of Washington

2015

Reading Committee:

Prof. Andrew J. Boydston, Chair

Prof. Gojko Lalic

Prof. Brandi Cossairt

Program Authorized to Offer Degree:

Department of Chemistry

University of Washington

Abstract

Metal-free Methods Utilizing Single-electron Oxidations

Kelli A. Ogawa

Chairperson of the Supervisory Committee:
Professor Andrew J. Bodyston
Department of Chemistry

Redox transformations are critically important steps in organic syntheses; however, they often require stoichiometric reagents or metal catalysts. Growing interest in "greener" alternatives to traditional processes motivated our group to develop methods that achieve single-electron oxidations under metal-free conditions. This dissertation describes our work toward developing metal-free methods that avoid the use of stoichiometric oxidants, high cell potentials, toxic metal reagents, and produces minimal byproducts. Towards the goal of increasing atom efficiency and reducing waste, we developed a method that integrates organocatalysis with electro-organic synthesis to achieve efficient aldehyde transformations. This method was successfully demonstrated for the one-pot conversion of aldehydes to esters and thioesters. The optimization of the thioesterification reaction emphasized the importance of taking the redox potentials of azolium precatalysts into consideration when developing *N*-heterocyclic carbene (NHC) catalyzed reactions. This led us to systematically characterize the redox properties of a series of azolium and azolinium salts, including benzothiazolium, thiazolinium, thiazolium, triazolium, imidazolium, and imidazolinium salts. The series includes a broad range of *N*-aryl

thiazolium salts that collectively demonstrate the ability to fine tune the reduction potential of the thiazolium ring via electronic modification to the *N*-aryl moiety. Additionally, a novel class of *N*-aryl thiazolinium salts has been synthesized and characterized. In contrast to what has been observed from imidazolium and imidazolinium counterparts, saturation of the thiazolium backbone to give thiazolinium salts results in more facile electrochemical reduction. Finally, we developed a method to achieve ring-opening metathesis polymerization (ROMP) mediated by oxidation of organic initiators in the absence of any transition-metals. Radical cations, generated via one-electron oxidation of vinyl ethers, were found to react with norbornene to give polymeric species with microstructures essentially identical to those traditionally obtained via metal-mediated ROMP. We found that vinyl ether oxidation could be accomplished under mild conditions using an organic photoredox mediator. This led to high yields of polymer and generally good correlation between M_n values and initial monomer to catalyst loadings. Moreover, temporal control over reinitiation of polymer growth was achieved during on/off cycles of light exposure. This method demonstrates the first metal-free method for controlled ROMP.

Table of Contents

List of Figures

List of Schemes

List of Tables

Acknowledgements

I would like to thank my advisor, Prof. Andrew J. Boydston, for his guidance, patience, and encouragement over the past five years. I am grateful for all of the lessons (in chemistry and life) that he has taught me throughout my graduate school career. I would also like to express my gratitude to Dr. Eric Finney and Dr. Adam Goetz for their work on the aldehyde oxidations (chapter 1) and metal-free ROMP (chapter 3), respectively. They were exceptional postdocs in our lab and patiently answered the millions of questions I had every day, for which I am very grateful. I would also like to thank the Boydston group, especially Derek Church, Mike Larsen, and Greg Peterson, who went through the ups and downs of graduate school along with me. I am also indebted to many professors for helpful discussions and encouragement, including all of my committee members, Prof. Gojko Lalic, Prof. Dustin Maly, Prof. Mike Heinekey, Prof. Brandi Cossairt, and Prof. Peter Pauzauskie. Also, a special thanks to Prof. Christine Luscombe, Prof. Werner Kaminsky, Prof. Dean Waldow (Pacific Lutheran University), and Prof. Robert H. Grubbs (California Institute of Technology). I would also like to express my gratitude to the Chemistry department staff and lab technicians (Leesa and Dave) for keeping the department running smoothly every day. I am also indebted to my family and friends, who have provided me with unconditional love and support. Your annual visits helped to keep me sane! Of course all of this would not be possible without my husband, Paul Ogawa. You have taken care of me and supported me without asking for anything in return, for which I am eternally grateful. Finally, I would like to thank the University of Washington, the Washington Technology Center, SpringStar, Inc., and the American Chemical Society Petroleum Research Fund (ACS PRF) for funding my graduate research.

Dedication

To my husband, Paul Ogawa. All of this would not be possible without you.

Chapter 1 – Organocatalyzed Anodic Oxidation of Aldehydes[1,2,3]

Section 1: Introduction

1.1.a Electro-organic Chemistry

Electro-organic chemistry (EOC) has emerged as one of the most powerful methods for executing redox transformations of organic compounds.[1,2] The diverse synthetic capabilities that have been developed in this area stem from the ability to use bulk electrolysis to generate highly reactive, even potentially hazardous, intermediates under mild reaction conditions. For example, highly reactive radical cations and anions can typically be generated under neutral conditions at room temperature. Moreover, EOC is often found to be a more environmentally friendly alternative to traditional redox approaches due largely to the replacement of stoichiometric redox reagents with electrical current. This green approach helps to maximize atom efficiency and minimize toxic reagents, such as heavy metals, in the waste stream. Many of the general principles and synthetic applications of EOC have been reviewed, with particular focus on direct bulk electrolysis, indirect electrolysis using redox mediators, and application of electroauxiliaries.[1,2] Recently, there has been a resurgence of interest in the integration of

[1] Reproduced with permission from Finney, E. E.; Ogawa, K. A.; Boydston, A. J. "Organocatalyzed Anodic Oxidation of Aldehydes" *J. Am. Chem. Soc.* **2012**, *134*, 12374 – 12377. Copyright 2012 American Chemical Society.

[2] Reproduced with permission from Ogawa, K. A.; Boydston, A. J. "Anodic Oxidation of Aldehydes to Thioesters" *Org. Lett.* **2014**, *16*, 1928 – 1931. Copyright 2014 American Chemical Society.

[3] Reproduced with permission from Ogawa, K. A.; Boydston, A. J. "Recent Developments in Organocatalyzed Electro-organic Chemistry" *Chem. Lett.*, **2015**, *44*, 10 – 16. Copyright 2015 The Chemical Society of Japan.

organocatalysis with EOC to achieve oxidative transformations (**Figure 1.1**), which constitutes the focus of this review.

Figure 1.1: Generalized depiction of organocatalyzed anodic oxidation.

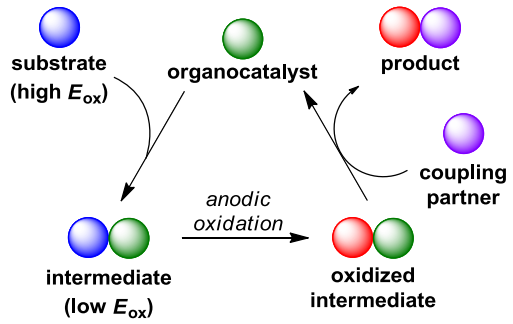

What differentiates organocatalyzed EOC from more traditional approaches are the manner in which the electroactive species is generated and the concentration of that species. For example, most approaches to bulk electrolysis involve oxidation or reduction of a substrate that is in an electroactive form throughout the reaction; it is not altered *in situ* prior to the electrochemical event.

To put the development of organocatalyzed EOC into context, we will first consider some of the basic techniques and principles of electrosynthesis, with a focus toward the use of coulometry to achieve anodic oxidations.[3,4,5] The electrolysis experiments can be performed using either a controlled-current or controlled-potential approach. In both techniques, electrical current is passed between a working and counter electrode. The oxidation and balancing reduction reactions occur at the working and counter electrode, respectively. In controlled-potential experiments, a reference electrode is also used to accurately maintain the voltage of the working electrode. The substrate is then oxidized

and converted to product over time. The decrease in substrate concentration is accompanied by a decrease in the passing current and therefore reaction rate. In controlled-current coulometry, the current demand is held constant throughout the electrolysis and the voltage is gradually increased (for oxidations) to compensate for the depleting concentration of substrate. Since the current remains constant, the rate of substrate consumption can also be maintained provided all electron flow is associated with the desired electrolysis reaction (i.e., a high Faradic efficiency is observed). In either a controlled-potential or –current approach, it is clear that the redox potentials of the substrate in comparison with all other species in solution must be carefully considered in order to achieve high chemoselectivity.

Electroauxiliaries can be a powerful tool for achieving high chemoselectivity. Key examples of such functional groups include organothio groups (thioacetals),[6] organostannanes,[7] silyl groups,[8] enol ethers,[9] and germyl groups.[10] These functional groups manifest lowered oxidation potentials which lead to their more selective electrolysis. Notably, electroauxiliaries are traditionally installed stoichiometrically. Following electrolysis, the remnants of the electroauxiliary can either be further derivatized or removed.

Redox mediators are another attractive tool for achieving efficient anodic oxidations.[1] A redox mediator facilitates *indirect* electrolysis by undergoing electrochemical oxidation at the heterogeneous electrode surface, and then chemically oxidizing the desired substrate in solution (**Figure 1.2**). The ability to regenerate the

active form of the mediator *in situ* permits its use in catalytic quantities; therefore reducing energy consumption and chemical waste. By shifting away from a heterogeneous electron transfer to a homogenous process, higher rates and selectivities can be achieved. The use of redox mediators enables the oxidation to be carried out under milder oxidation conditions than those required for direct electrochemical oxidation.

Figure 1.2: Idealized depiction of a one-electron oxidation facilitated by a redox mediator.

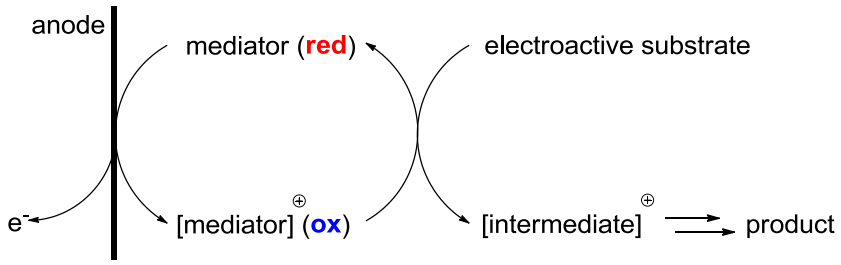

The most commonly used organic redox mediators include triarylamines,[1a,11] triarylimidazoles,[1a,12] and *N*-oxyl radicals.[1a,13] Among these, the most extensively studied are the triarylamines. These compounds provide access to a wide range of oxidation potentials and a variety of applications such as oxidative cleavage of C-S bonds, functionalization of aromatic side chains, and oxidative fluorodesulfurization, have been reported.

As an exciting parallel to the installation of electroauxiliaries and use of mediators to facilitate anodic oxidation, organocatalyzed EOC can be viewed as the *in situ* formation of electroauxiliaries via interaction of an organocatalyst and substrate to generate an electroactive intermediate. To clarify, we view the distinguishing features of organocatalyzed EOC to be the use of an organocatalyst to directly augment the redox

potential of the substrate, and *in situ* electrolysis of the catalytically-generated intermediate.[14] This differs from EOC using redox mediators, which do not change the redox potential of the substrate. This emerging branch of catalyzed anodic oxidations requires overcoming challenges associated with outcompeting homogenous side reactions with heterogeneous oxidations at the anode and reduced current flow due to low concentrations of the electroactive species. With careful tuning of the reaction conditions and electrochemical cell, highly efficient transformations have been achieved. By integrating organocatalysis with electro-organic synthesis, the need for stoichiometric redox reagents and high cell potentials are avoided and minimal byproducts are produced. Although only a few examples have been reported thus far, the advantages associated with this burgeoning field are expected to be of great interest to a broadening community.

1.1.b Cyanide Mediated Aldehyde Oxidations

The first demonstrated example of organocatalyzed anodic oxidations was reported by Chiba et al. in 1982 (**Figure 1.3**).[15] They investigated cyanide mediated anodic oxidation of aldehydes. Specifically, methyl esters were formed via oxidative esterification of aromatic and aliphatic aldehydes in MeOH in the presence of sodium cyanide. Controlled-current experiments were performed using a NaCN/MeOH solution and platinum electrodes. Notably, side products from competing reactions that have been shown to be catalyzed by NaCN, such as benzoin condensation, were observed in only trace amounts. A variety of unactivated, sterically hindered, and electron-deficient

aldehydes gave good yields while aliphatic aldehydes gave a mixture of products due to competing aldol condensation reactions.

Figure 1.3: Representative examples of anodic oxidations of aldehydes in the presence of NaCN in MeOH.

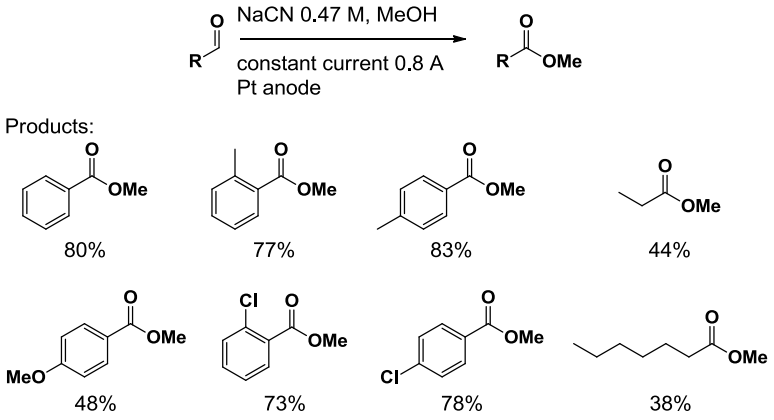

Various mechanisms were considered such as direct oxidation of the aldehyde substrate and oxidation of a cyanohydrin intermediate. Control experiments using $NaClO_4$ or tetraethylammonium *p*-toluenesulfonate instead of NaCN as electrolytes yielded only trace amounts of ester. In addition, electrochemical studies suggested that the electroactive species was likely not the aldehyde. For example, benzaldehyde was found to oxidize at 2.3 V vs SCE in a $LiClO_4/CH_3CN$ solution, whereas changing the electrolyte solution to a NaCN/MeOH mixture decreased the oxidation potential to 1.7 V vs SCE. This decrease in oxidation potential was thought to be the result of cyanohydrin formation prior to oxidation, similar to the MnO_2-mediated oxidation mechanism described by Corey in 1968 (**Scheme 1.1**).[16] The method developed by Corey, which has recently been expanded to include *N*-heterocyclic carbene (NHC) catalysts, typically

utilizes up to 20 molar equivalents of MnO_2. The stoichiometric oxidant is replaced by electrical current in Chiba's approach, thus reducing the amount of by-products.

Scheme 1.1: Cyanohydrin formation.

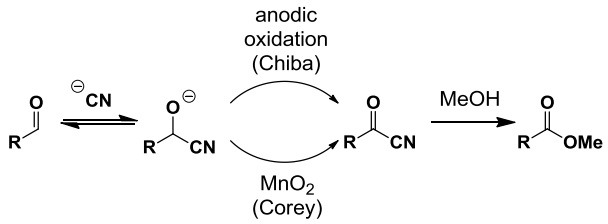

Collectively, these results support a mechanism in which the aldehyde substrate reacts first with cyanide anion to form the cyanohydrin intermediate, which undergoes subsequent oxidation to give the acyl nitrile. Although the use of catalytic (sub-stoichiometric) quantities of cyanide were not explicitly demonstrated, this report was the first to suggest that organocatalyzed anodic oxidations were feasible. Variants using substoichiometric organocatalysts were later reported by Jang, Diederich, and Boydston, as discussed below.

1.1.c Amine Catalyzed α-oxyaminations of Aldehydes via Anodic Oxidation

Enamine catalysis is an attractive avenue for organocatalyzed EOC due to the wealth of knowledge regarding amine-based organocatalysts, the disparate oxidation potentials of aldehyde substrates and enamine intermediates, and the ability to access enantioselective variants via chiral amine catalysts. Capitalizing on these attributes, Jang and coworkers reported an amine catalyzed α-oxyamination of aldehydes in 2009.[17] Specifically, they developed methods involving anodic oxidation of catalytically

generated enamines, and *in situ* trapping of the ensuing radical cations with TEMPO as depicted in **Scheme 1.2**.

Scheme 1.2: Generalized depiction of organocatalytic enamine formation, anodic oxidation, and coupling with TEMPO.

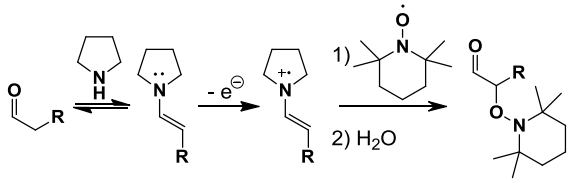

Previous methods of α-oxyamination of aldehydes via enamine catalysis used metal-based oxidants, such as ceric ammonium nitrate (CAN) and Cp_2FeBF_4 in stoichiometric amounts.[18,19] Single-electron oxidation of the enamine intermediate by the stoichiometric oxidant generates a radical cation intermediate, which then couples with a nucleophilic partner to give the desired product. Inspired by the reactivity of these radical cations Jang et al. replaced the stoichiometric metal oxidants with electrochemical oxidation.

Cyclic voltammetry experiments were performed to determine the selectivity of the oxidation and were found to be consistent with one-electron oxidation of the enamine. No redox wave was observed in cyclic voltammograms (CVs) of their initial aldehyde substrate, hydrocinnamaldehyde, up to 2 V vs Ag wire pseudoreference. In the CV of preformed enamine, an irreversible oxidation peak was observed at 0.71 V vs Ag wire, which was less than that observed from the pyrrolidine catalyst (1.41 V) alone. Similarly, a mixture of hydrocinnamaldehyde and pyrrolidine in a 2:1 ratio displayed an irreversible oxidation peak at 0.72 V vs Ag wire.

After confirming the feasibility of a selective oxidation, control experiments were conducted to rule out the possibility of a $TEMPO^+$ pathway involving oxidation of TEMPO followed by electrophilic addition of $TEMPO^+$ to an enolate or enamine intermediate.[20] None of the α-oxyaminoaldehyde product was obtained when preformed enolate or enamine was generated in the presence of $TEMPO^+$. These results were consistent with a mechanism involving formation and anodic oxidation of enamine intermediates.

Figure 1.4: Representative examples of the α-oxyamination of aldehydes using anodic oxidation.

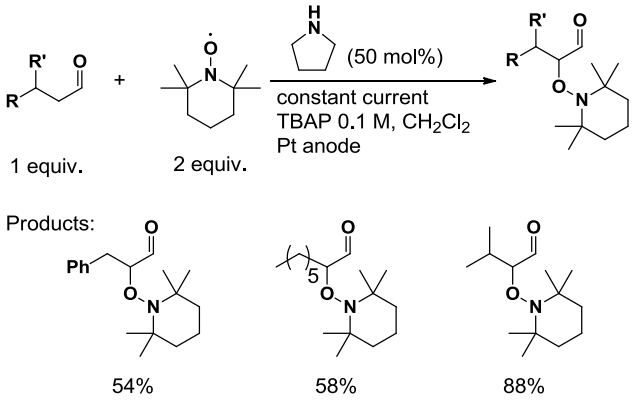

With these results at hand, Jang and coworkers were able to achieve α-oxyamination of aliphatic aldehydes using pyrrolidine as an organocatalyst and controlled-current electrolysis (**Figure 1.4**). Notably, an enantioselective variant was also demonstrated using a chiral *sec*-amine catalyst providing good yields and enantioselectivities (**Figure. 1.5**).

Figure 1.5: Enantioselective α-oxyamination of aldehydes using anodic oxidation.

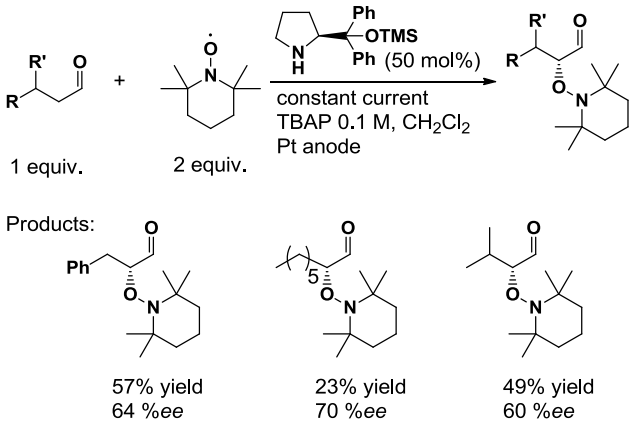

1.1.d Amine Catalyzed α-alkylations of Aldehydes Using Anodic Oxidation

Jang and coworkers extended their work on organocatalyzed EOC to include α-alkylation of aldehydes via anodic oxidation of enamines (**Figure 1.6**).[21] Notably, previous examples of α-alkylations of aldehydes involved photoredox metal catalysts ($[Ru(bpy)_3]^{2+}$; bpy = bipyridine), or stoichiometric organic oxidants (2,3-dichloro-5,6-dicyanobenzoquinone) to promote the desired redox transformation.[22,23] These methods involve the one-electron oxidation of the coupling partner or preactivation prior to attack of the enamine and do not involve the direct oxidation of the enamine intermediate. In contrast to these previous methods, Jang et al. envisioned tandem one-electron oxidations of the enamine intermediate and nucleophilic coupling partner to generate radical intermediates. The resulting radicals species would then couple to form the desired C–C bond.

Jang's enantioselective α-alkylation of aldehydes (**Figure 1.6**) was conducted using 20 – 50 mol % of a chiral *sec*-amine catalyst and controlled-current conditions. A series

of aliphatic aldehydes were successfully coupled with xanthene; however, poor yields and enantioselectivities were obtained with cycloheptatriene as the coupling partner in place of xanthene. Increasing the catalyst loading to 50 mol% with hydrocinnamaldehyde as the substrate resulted in a minor increase in yield (68% yield using 20 mol% catalyst and 74% yield using 50 mol% catalyst). Additionally, the yield listed for octanal was obtained with 50 mol% catalyst.

Figure 1.6: Representative examples of the electro-organocatalyzed α-alkylation of aliphatic aldehydes.

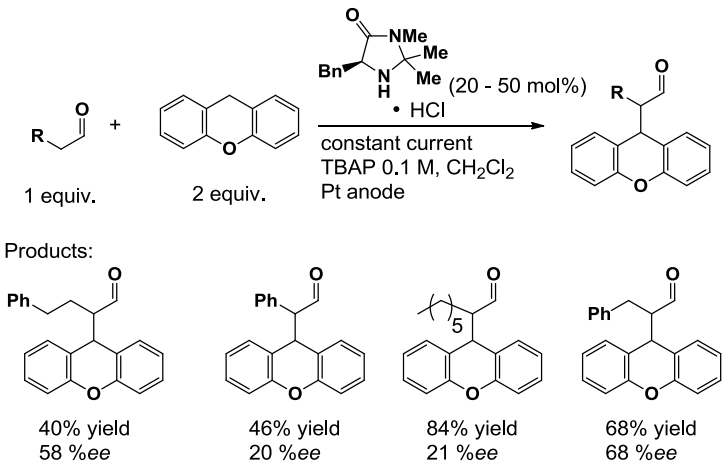

To determine the selectivity of the electrochemical oxidation, the electrochemical properties of all substrates and the reaction mixture were evaluated using cyclic voltammetry. The individual substrates exhibited irreversible oxidation peaks at 2.7, 1.4, and 2.0 V vs Ag wire for the aldehyde, pyrrolidine, and xanthene, respectively. The CV of a mixture of aldehyde and pyrrolidine (2:1 ratio) showed an oxidation peak at 0.8 V vs Ag wire, which was consistent with the oxidation of the enamine intermediate. Finally, the CV of a mixture of all three substrates exhibited three oxidation peaks at 0.8, 2.3, and

2.9 V vs Ag wire. These oxidation potentials supported the selective electrochemical oxidation of the enamine intermediate.

The presence of radical intermediates was further supported using two control experiments. The addition of a radical inhibitor (2,6-di-*tert*-butyl-4-methylphenol) suppressed product formation and the use of an aldehyde substrate containing a cyclopropyl ring resulted in the consumption of the cyclopropyl group. These two results supported the formation of radical intermediates, although the cationic xanthene pathway could not be definitively ruled out.

Section 2: Results and Discussion

1.2.a N-heterocyclic Carbene Catalyzed Anodic Oxidation of Aldehydes to Esters

The use of NHCs to mediate aldehyde oxidations has garnered considerable attention from the synthetic community.[24] NHCs react with aldehydes to give direct addition adducts (**A**) in equilibrium with the Breslow intermediate (**B**), as depicted in **Scheme 1.3**.[25] Each of these species can undergo subsequent oxidation to give an activated ester in the form of an acyl azolium cation (**C**), and a number of chemical oxidants for this transformation have been demonstrated. In the presence of nucleophilic species, the acyl azolium is converted to the desired carboxylic acid derivative (**D**) with concomitant regeneration of the NHC catalyst.

Scheme 1.3: Generalized pathways of NHC-catalyzed aldehyde oxidations.

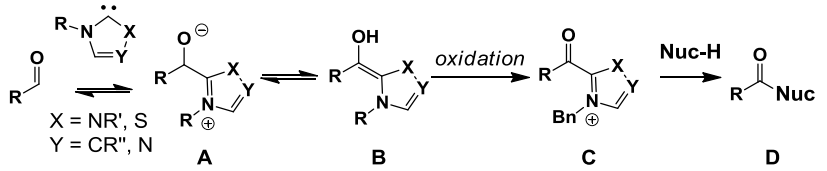

Diederich and coworkers demonstrated that MeFl can be used as an oxidant in catalytic amounts by regenerating the oxidized form electrochemically during the reaction (**Scheme 1.4**).[26] They achieved high yields and good Faradaic efficiencies in MeOH solutions to produce methyl esters from aromatic and aliphatic aldehydes. This study established that the overall biomimetic transformation can be facilitated electrochemically, provided the right combination of substrate, catalyst, and co-catalyst is employed. For example, the best yields were obtained using a supramolecular approach to the NHC catalyst structure, which overcame limitations in the reactivity of more common thiazolylidene-based NHC catalysts.

Scheme 1.4: NHC-catalyzed and Flavin-mediated oxidative esterification of aldehydes.

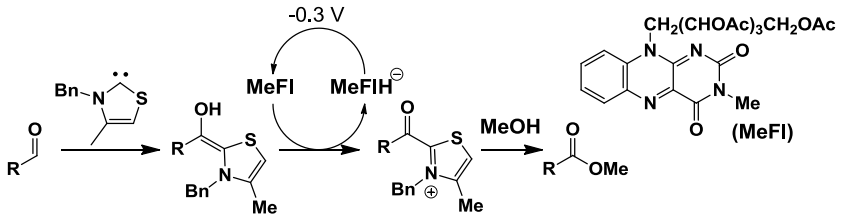

In 2012, our group investigated the use of NHC catalysts to accomplish direct anodic oxidation of the Breslow intermediate, absent redox mediators, and an expanded scope of alcohol coupling partners.[27] Although direct bulk electrolysis of Breslow intermediates

were previously unknown, cyclic voltammetry studies of Breslow intermediates derived from thiazolium precatalysts showed that these intermediates have much lower oxidation potentials than their parent aldehydes (-0.9 V and > 2 V vs SCE, respectively).[28]

As depicted in **Figure 1.7**, we envisioned in situ formation of the Breslow intermediate followed by two-electron anodic oxidation to produce an electrophilic 2-acylazolium species. Nucleophilic attack from the alcohol produces an ester with concomitant regeneration of the NHC catalyst. Oxidations at the anode are balanced by the formation of H_2 gas at the cathode.

Figure 1.7: Proposed catalytic cycle for NHC-catalyzed anodic oxidation of aldehydes.

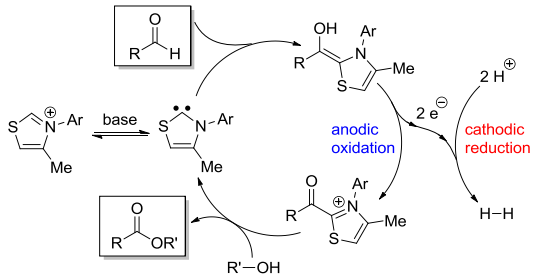

Our initial setup for bulk electrolysis of *p*-tolualdehyde involved using a 3-neck round-bottom flask as an undivided cell, RVC anode, Pt wire cathode, and Bu_4NClO_4 (0.045 M) as supporting electrolyte. The cell potential was maintained at +0.1 V vs $Ag/AgNO_3$. We found potentiostatic experiments to be more successful than using a constant current, which may be expected at low concentrations of anolyte.[1] Considering the propensity for competitive (hemi)acetal formation at high alcohol concentrations,[29] we introduced the alcohol (BnOH) in stoichiometric amounts relative to aldehyde. Initial

screenings revealed DBU and CH_3CN to be an optimal base and solvent combination (THF, DME, DMSO, and DMF as solvents gave similar results).

An initial catalyst screen indicated that thiazolylidenes were more effective than their imidazolylidene, triazolylidene, and acyclic diaminocarbene counterparts. We speculate that the better performance of the thiazolylidene-derived catalysts may be attributed to more favorable access to the Breslow intermediate in comparison with NHCs bearing an additional ring substituent at the 1-position (i.e., NR in place of S). Although observation of aldehyde-derived Breslow intermediates remains challenging,[28] it is expected that those comprising thiazoles would encounter less $A^{1,3}$ strain than those derived from classes of NHCs bearing additional exocyclic substituents.

Using our initial conditions, oxidation of *p*-tolualdehyde proceeded in 46% yield after 48 h using 10 mol% of 4-methyl-3-(2,4,6-trimethylphenyl)thiazolium perchlorate as precatalyst. Analysis of the product mixture revealed a significant amount of benzil-type product. Notably, aerobic oxidation of benzoins is catalyzed by NHC/DBU combinations, presumably proceeding through the corresponding enol(ate) of the benzoin species.[30] Interestingly, under N_2 atmosphere and without an applied cell potential, we still observed benzil products. Further experiments indicated perchlorate as the culprit oxidant. Changing the electrolyte to Bu_4NBr (TBAB) and thiazolium counterion to tetrafluoroborate improved the yield of ester to 94% after 48 h. Benzoin-type product was still observed by ^1H NMR spectroscopy, but was confirmed to be equilibrating under the reaction conditions (see experimental).

Electrode materials and dimensions are an important consideration in bulk electrolyses.[1] Increasing the surface area of the counter electrode from Pt wire (ca. 7.2 cm^2) to a Pt basket (ca. 20 cm^2) gave nearly quantitative formation of the desired ester after 17 h. Excellent yields were maintained when the RVC anode (surface area = 40 cm^2) was replaced with an inexpensive graphite drawing stick (0.6 × 0.6 × 7.5 cm, submerged surface area = 4.5 cm^2). We observed gas formation at the cathode consistent with the production of H_2, as expected considering the low hydrogen overvoltage of the Pt cathode.[1j,k] This mechanistic detail was further confirmed by trapping of the gas formed in the headspace of the electrochemical cell with Vaska's complex to form the corresponding dihydride (see experimental).[31] Using a carbon cathode in place of Pt resulted in decreased reaction efficiency. Notably, no ester production was observed in the absence of thiazolium precatalyst or DBU.

We next focused on the scope of aldehyde and alcohol substrates; key data are summarized in **Table 1.1**. In general, good to excellent yields were obtained for most aldehydes. Substitution at the *ortho* position was tolerated (entries 2 and 3), and excellent chemoselectivity was observed in the presence of electrophilic groups such as carboxylic acid (entry 4), cyano (entries 5 and 6) and ester (entry 26) functionalities. Other electron-deficient benzaldehydes were also viable, such as 4-fluoro-, 4-chloro-, and 4-bromobenzaldehyde (entries 7, 8, and 9, respectively). In general, in the presence of an *N*-(2,4,6-trimethylphenyl)-substituted catalyst, electron-deficient aldehydes displayed an increased extent of benzoin formation that severely inhibited efficient ester production.

Taking advantage of the increased electrophilicity of the aldehydes, however, permitted the use of a bulkier NHC catalyst. Specifically, the *N*-(2,6-diisopropylphenyl) analogue shepherded reactivity away from benzoin condensation and furnished high yields of ester products in short reaction times. Not surprisingly, 4-nitrobenzaldehyde yielded a mixture of products containing only ca. 10% of the desired ester, likely due to reductive coupling of the nitroarene.[32]

Although anodic oxidation of electron-rich heteroaromatic 2-furfural proceeded in good yield (97%, entry 12), electron-rich benzaldehydes such as 4-methoxy- and 4-dimethylaminobenzaldehyde were sluggish to react even at elevated temperatures. These latter results are consistent with other approaches toward NHC-catalyzed oxidation of electron-rich benzaldehydes that are considered deactivated toward formation of the Breslow intermediate.[26,33] Moving the electron-donating group out of conjugation with the aldehyde (i.e., 3-anisaldehyde, entry 13) restored reactivity and the desired ester was obtained in 87% isolated yield.

Oxidation of nonaromatic cyclohexane carboxaldehyde also proceeded smoothly (entry 14), as did oxidation of α,β-unsaturated cinnamaldehyde and 4-methoxycinnamaldehyde (entries 15 and 16, respectively). This latter substrate class indicated to us that the electrochemical oxidation of the Breslow intermediate was sufficiently rapid to avoid competitive reaction pathways such as Stetter reactions, lactone formation, and conjugate reduction.[34,35]

Table 1.1: Substrate scope of NHC-catalyzed anodic oxidation of aldehydes.[a]

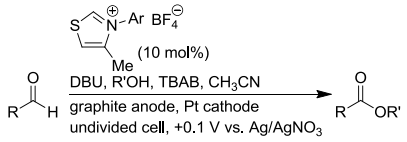

entry	R	R'	Ar	time (h)[b]	FE (%)[c]	yield (%)[d]
1	4-MeC_6H_4	Bn	Mes	17	74	98 (97)
2	2,4-$Me_2C_6H_3$	Bn	Mes	22	91	94 (93)
3	2,4-$Cl_2C_6H_3$	Bn	DiPP	7	93	91
4	4-$CO_2HC_6H_4$	Bn	Mes	15	49	97
5	4-CNC_6H_4	Bn	DiPP	2	99	65
6	3-CNC_6H_4	Bn	DiPP	6	91	94
7	4-FlC_6H_4	Bn	Mes	14	82	97 (92)
8	4-ClC_6H_4	Bn	DiPP	8	98	98
9	4-BrC_6H_4	Bn	DiPP	8	94	98
10	4-IC_6H_4	Bn	DiPP	7	83	88
11	2-pyr	Me	DiPP	4	83	71 (60)
12	2-fur	Bn	Mes	5	92	97 (91)
13	3-$MeOC_6H_4$	Bn	Mes	11	97	92 (87)
14	Cyclohexyl	Bn	Mes	56	99	87 (85)
15	Cinnamyl	Bn	Mes	7	99	90 (83)
16	4-MeO-cinnamyl	Bn	Mes	27	72	98
17	4-MeC_6H_4	Et	Mes	12	70	98 (95)
18	4-MeC_6H_4	2-PhEt	Mes	36	50	72 (70)
19[e]	4-MeC_6H_4	*s*-Bu	Mes	24	97	45
20	4-MeC_6H_4	*t*-Bu	Mes	4	0	0
21	4-MeC_6H_4	allyl	Mes	36	49	72 (66)
22	2,4-$Me_2C_6H_3$	allyl	Mes	13	91	91 (83)
23	4-MeC_6H_4	propargyl	Mes	13	97	96 (89)
24	4-MeC_6H_4	4-pentynyl	Mes	25	85	88 (74)
25	4-MeC_6H_4	Me_3SiEt	Mes	30	98	96 (94)
26	4-MeC_6H_4	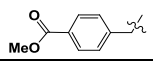	Mes	24	72	91 (90)

[a]Reactions conducted in dry CH_3CN (15 mL) at RT in a 3-neck flask under N_2 with a graphite anode, Pt basket cathode, 0.150 M RCHO, 0.165 M ROH, 0.150 M DBU, 0.015 M thiazolium salt, 0.045 M TBAB, and constant cell potential of +0.1 V (vs $Ag/AgNO_3$). Mes = 2,4,6-trimethylphenyl, DiPP = 2,6-diisopropylphenyl. [b]Reactions were monitored by ^1H NMR spectroscopy until ester production had ceased. [c]Faradaic efficiencies assuming two-electron oxidations. [d]Determined by ^1H NMR spectroscopy using 1,3,5-trimethoxybenzene as internal standard (average of two runs); isolated yields in parentheses. [e]Reaction conducted at 45 °C.

A range of alcohols were found to be compatible (**Table 1.1**, entries 17 – 26). As expected, *s*-BuOH (entry 19) displayed lower reactivity than did primary alcohols, and no ester product was obtained when *t*-BuOH was employed (entry 20). Functionalized and activated alcohols such as benzyl alcohol, allyl alcohol, propargyl alcohol, 4-pentyn-1-ol, and 2-(trimethylsilyl)ethanol each furnished the corresponding esters in good to excellent yields.

To improve the overall practicality of the organocatalyzed anodic oxidations, we considered replacement of the potentiostat with a simple battery, similar to what has been demonstrated for constant-current oxidations.[36] Our initial conditions involved oxidation of *p*-tolualdehyde to benzyl toluate using a two-electrode setup driven by commercial batteries (**Table 1.2**). Use of a 6 V lantern battery (entry 1) failed to produce ester product, possibly due to destructive oxidation of the NHC catalyst. Reducing the voltage (1.5 V AA-cell, entry 2) gave the desired ester in 22% yield. Increasing the current while maintaining the voltage by assembling multiple batteries in parallel and using D-cell batteries led to improved reaction efficiencies (entries 3 – 6), although ester production remained modest. Switching to a to 1.2 V NiCd battery (entry 7) resulted in a more promising 67% yield after 26 h.

Table 1.2: NHC-catalyzed anodic oxidation of aldehydes using batteries as a voltage source.[a]

entry	battery arrangement	time (h)[b]	yield (%)[c]
1	1 × 6 V, lantern battery	24	0
2	1 × 1.5 V, AA-cell	48	22
3	2 × 1.5 V, AA-cell (parallel)	24	31
4	4 × 1.5 V, AA-cell (parallel)	36	32
5	1 × 1.5 V, D-cell	24	50
6	2 × 1.5 V, D-cell (parallel)	48	56
7	1 × 1.2 V, rechargeable NiCd	26	67

[a]Reactions conducted at RT in a cylindrical vial under N_2 with 0.045 M TBAB, 0.150 M aldehyde, 0.165 M ROH, 0.150 M DBU, 0.015 M 4-methyl-3-(2,4,6-trimethylphenyl)thiazolium tetrafluoroborate in CH_3CN. [b]Reactions were monitored by ^1H NMR spectroscopy until ester production had ceased. [c]Determined by ^1H NMR spectroscopy using 1,3,5-trimethoxybenzene as internal standard.

To achieve the necessary controlled potential, we assembled a simple voltage divider (**Figure 1.8**) consisting of a 10 Ω resistor in parallel with the reaction cell, which together were in series with a 100 Ω resistor. Two 1.5 V D-cell batteries were arranged in parallel as the voltage source. This setup gave a measured voltage of +0.14 V across the cell during the experiment and furnished benzyl toluate in 78% isolated yield after 27 h at RT, and 85% isolated yield after 27 h at 45 °C. Similar success at 45 °C was achieved for 4-chlorobenzaldehyde (40 h, 90% yield), cinnamaldehyde (20 h, 94% yield), 4-methoxycinnamaldehyde (40 h, 93% yield), and nicotinaldehyde (6 h, 58% yield).

Figure 1.8: Circuit diagram for the organocatalyzed anodic aldehyde oxidation using a voltage divider and batteries.

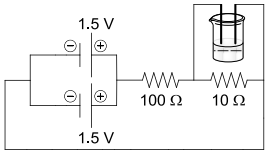

In summary, we have demonstrated the organocatalyzed anodic oxidation of aldehydes at low controlled potentials. This process involves formation of electroactive

intermediates which can be viewed as catalytically-generated electroauxiliaries. Application of this approach provides a direct conversion of aldehydes to esters that circumvents the need for stoichiometric exogenous oxidants, high potentials, or redox mediators, and produces minimal byproducts. This ester formation reaction is successful for a broad range of aldehyde and alcohol coupling partners. Additionally, we have shown that the process is successful using simplified electrochemical equipment such as alkaline batteries, resistors, and graphite sticks in place of potentiostats and more expensive electrodes.

1.2.b N-heterocyclic Carbene Catalyzed Anodic Oxidation of Aldehydes to Thioesters

Although direct aldehyde-to-ester conversions have received the greatest focus, access to a range of other functional groups have also been reported.[37] Among them, direct thioesterifcation of aldehydes has received relatively little attention, which is unfortunate considering the importance of thioesters as synthetic intermediates and biologically active compounds.[38,39]

Despite the superficial similarities with more familiar NHC-catalyzed oxidative esterification of aldehydes, thioester formation poses unique challenges due to potentially deleterious formation of disulfides. This not only consumes the thiol coupling partner, but may also lead to rapid irreversible sulfenylation of NHC catalysts, as reported by Rastetter.[40] While Yadav recently reported the successful use of diaryl disulfides in aldehyde thioesterifications (**Scheme, 1.5**); it is unclear if moderate to good yields are attainable with lower than 30 mol % catalyst loadings.[38d]

Scheme 1.5: Representative methods for conversion of aldehydes to thioesters using NHC catalysts and stoichiometric oxidants, in comparison with the present work.

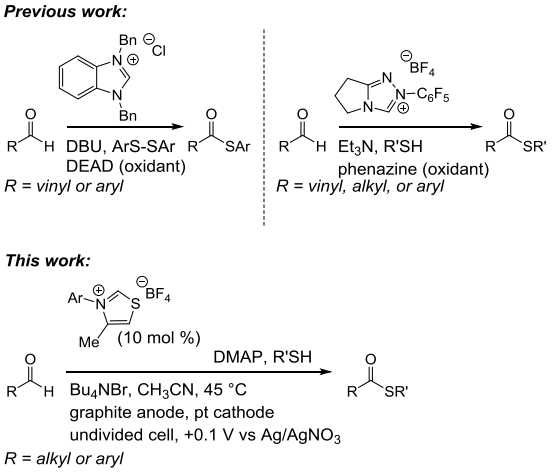

The delicate reactivity of thiols and thiolates signifies the importance of selecting a compatible oxidant. This task was highlighted in the report by Takemoto, in which phenazine emerged as an optimal stoichiometric oxidant after screening several candidates (**Scheme 1.5**).[38c] Notably, each reported general method of NHC-catalyzed aldehyde thioesterification requires a *stoichiometric* exogenous oxidant. This reduces overall efficiency, can limit chemoselectivity, and may give deleterious byproducts (e.g., hydrazides are produced from hydrazobenzenes when azobenzene is used as an oxidant).[38f]

Figure 1.9: Proposed catalytic cycle for NHC-catalyzed anodic oxidation of aldehydes to thioesters.

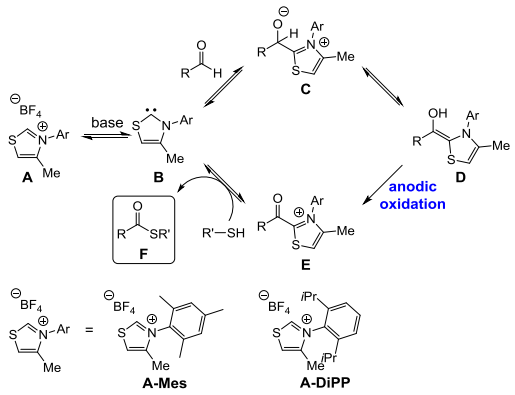

We recently demonstrated a highly atom-efficient method of NHC-catalyzed oxidative esterification via integration of organocatalysis and electrosynthesis.[27] This approach enables one-pot oxidative couplings without the need for stoichiometric oxidants, which we speculated would provide an improved method of thioester synthesis. The catalytic cycle (**Figure 1.9**) involves in situ deprotonation of a thiazolium pre-catalyst (**A**) to give the active NHC catalyst **B**. Reaction of the NHC with aldehyde substrates leads to an equilibrium mixture strongly favoring the addition adduct **C** over the electroactive Breslow intermediate **D**. While oxidation of (pseudo)benzylic alcohols such as **C** have been demonstrated, the oxidation potentials measured via cyclic voltammetry and used herein for potentiostatic oxidation are consistent with oxidation of the Breslow intermediate **D**. The irreversible anodic oxidation of **D** provides acyl thiazolium species **E**, which is intercepted by the thiol substrate to give the thioester product (**F**) and regenerate the active catalyst **B**. Notably, oxidations at the anode are balanced by the formation of H_2 gas at the cathode.

We began our attempts at direct thioesterification by applying the conditions we previously developed for esterifications. Specifically, reactions were conducted in an undivided cell using a graphite anode and Pt basket cathode, with DBU and CH_3CN as base and solvent, respectively. After screening a series of azolium precatalysts, we found 4-methyl-3-(2,4,6-trimethylphenyl)thiazolium tetrafluoroborate (**A**-**Mes**) and 4-methyl-3-(2,6-diisopropylphenyl)thiazolium tetrafluoroborate (**A**-**DiPP**) to be most effective (see experimental). Unfortunately, these conditions gave only 26% yield of thioester when *p*-tolualdehyde and butanethiol were used in the initial screenings. Analysis of the reaction mixture revealed that the remainder of the butanethiol had been oxidized to the corresponding disulfide. We speculated that electrochemical oxidation of either the thiol or thiolate anion was a likely cause. Notably, the Breslow intermediates display two one-electron oxidations clustered around -1.0 V and -0.8 V vs SCE; butanethiol and butanethiolate anion display oxidation potentials at +1.12 and -0.85 V vs SCE, respectively. This suggested to us that cell potentials capable of oxidizing the Breslow intermediate would also be capable of oxidizing thiolates, but that thiols would not be readily oxidized.

Interestingly, our investigations also revealed results consistent with an azolium-mediated oxidation of thiolates. Specifically, in the absence of an applied voltage, the combination of a thiazolium cation and thiolate anion resulted in efficient formation of disulfides (**Table 1.3**).

Table 1.3: Investigation into disulfide formation.[a]

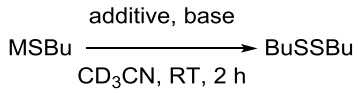

entry	additive	MSBu	base	% BuSSBu[b]
1	**A-Mes**	HSBu	None	0
2	None	HSBu	DBU	0
3	**A-Mes**	HSBu	DBU	25
4	None	NaSBu	None	0
5	**A-Mes**	NaSBu	None	15
6	None	HSBu	DMAP	0
7	**A-Mes**	HSBu	DMAP	4

[a]Reactions conducted at rt in a screw cap NMR tube under N_2 with 0.150 M **A-Mes** (as indicated), 0.150 M MSBu, and 0.150 M base in CD_3CN. [b]Determined by ^1H NMR spectroscopy using 1,3,5-trimethoxybenzene as internal standard.

In the absence of either reactant, no disulfide was observed (entries 1 and 2). DBU was found to be a sufficiently strong base to facilitate thiolate and thus disulfide formation (entry 3). Similarly, sodium butanethiolate was easily oxidized in the presence of the thiazolium salt (entries 4 and 5). In an attempt to minimize thiolate formation, we investigated DMAP and found that disulfide was formed to a much lesser extent (entry 7).

We further investigated the influence of base strength and concentration during the anodic oxidation to form thioesters (**Table 1.4**). After 2 h, DBU (100 mol % relative to aldehyde) gave 57% yield of disulfide (entry 1) and only trace amounts of thioester. Use of K_2CO_3 or DMAP each resulted in improved yields of thioester (entries 2 and 3, respectively), with DMAP giving 21% yield of thioester while producing 10% yield of disulfide. To further minimize thiolate formation, we reduced the amount of DMAP to 50

mol % (entry 4). Although the yield of thioester dropped to only 11% in the 2 h run, the ratio of thioester to disulfide (2.75:1) was improved in comparison with those having higher base loadings. With the exception of pyridine (entry 6), which was found to be completely ineffective, we continued to observe greater yield of thioester than disulfide when maintaining a 50 mol % base loading (entries 7 – 10).

Table 1.4: Base screen for NHC-catalyzed anodic oxidation of aldehydes to thioesters.[a]

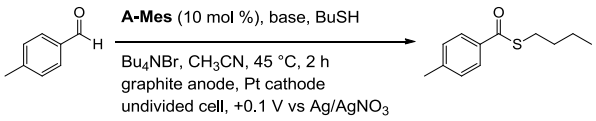

entry	base (M)	% thioester[b]	% BuSSBu[b]
1	DBU (0.15)	<1	57
2	K_2CO_3 (0.15)	15	15
3	DMAP (0.15)	21	10
4	DMAP (0.075)	11	4
5	DBU (0.075)	3	58
6	Pyridine (0.075)	0	0
7	K_2CO_3 (0.075)	5	3
8	DIPEA (0.075)	20	13
9	DABCO (0.075)	15	10
10	NEt_3 (0.075)	30	12

[a]Reactions conducted at 45 °C in a three-neck flask under N_2 with a graphite anode, Pt basket cathode, 0.045 M Bu_4NBr, 0.150 M aldehyde, 0.300 M R'SH, and constant cell potential of +0.1 V (vs $Ag/AgNO_3$). [b]Determined by GC-MS and ^1H NMR spectroscopy using 1,3,5-trimethoxybenzene as internal standard.

We next explored the aldehyde and thiol substrate scope; key results are depicted in **Scheme 1.6**. Unactivated and *ortho*-substituted aldehydes gave good yields of thioester, as did cyclohexane carboxaldehyde. In general, electron-deficient aldehydes proceeded in good to excellent yields, including heteroaromatic 2-pyridinecarboxylaldehyde. Attempts with α,β-unsaturated aldehydes were met with

limited success. In addition to butanethiol, we found that other primary thiols such as benzyl, 2-chlorobenzyl, and 2-furfuryl each gave good yields of the desired thioester. Additionally, cyclohexanethiol gave the secondary thioester in 63% yield.

Scheme 1.6: Substrate scope of NHC-catalyzed anodic oxidation of aldehydes to thioesters.[a]

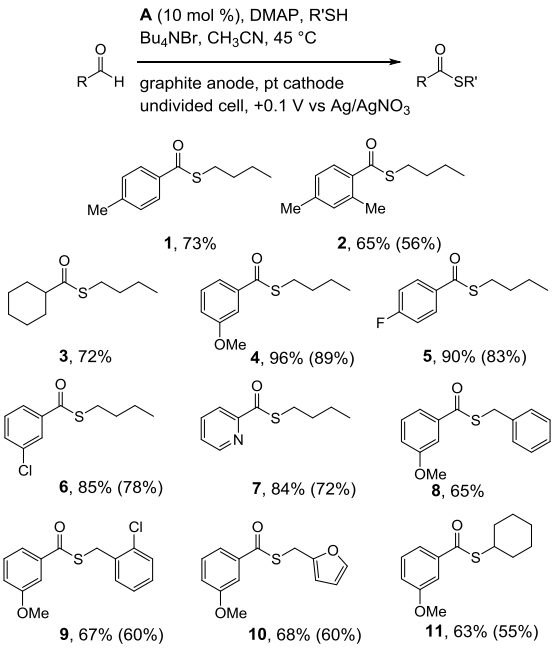

[a]Reactions conducted at 45 °C in a three-neck flask under N_2 with a graphite anode, Pt basket cathode, 0.045 M Bu_4NBr, 0.150 M aldehyde, 0.300 M R'SH, 0.075 M DMAP, and constant cell potential of +0.1 V (vs $Ag/AgNO_3$). For **1 – 5** and **6 – 11** precatalysts **A-Mes** and **A-DiPP** were used, respectively. Reaction times ranged from 8 – 44 h and were monitored by ^1H NMR spectroscopy and GC-MS until production of thioester had ceased. Yields were determined by GC-MS using 1,3,5-trimethoxybenzene as internal standard (average of two runs); isolated yields in parentheses. See supporting information for experimental details.

In summary, we have demonstrated a direct conversion of aldehydes to thioesters. This integrated organocatalyzed electrosynthetic approach achieves efficient anodic oxidation of catalytically generated species and circumvents the need for stoichiometric exogenous oxidants, high cell potentials, or redox mediators while producing minimal

byproducts. Optimization of the strength and concentration of base was essential for minimizing unwanted disulfide formation and achieving efficient thioesterification. This thioesterification reaction provides good to excellent yields for a broad range of aldehyde and thiol substrates.

Section 3: Conclusions

The growing use of electrochemical techniques in organic synthesis has led to the development of novel integrative methods. By integrating organocatalysis with electrosynthesis, highly efficient alternatives to traditional oxidation methods have been developed that involve the efficient anodic oxidation of catalytically generated species. A notable challenge in this area is the need to efficiently oxidize catalytically-generated intermediates present in very low concentrations. This has been partially addressed through the use of redox mediators, high catalyst loadings, and optimization of catalyst reactivity. Organocatalyzed anodic oxidations circumvent the use of stoichiometric exogenous oxidants and high cell potentials, and produce minimal byproducts. In recent examples, relatively low catalyst loadings have been successful for oxidative esterification and thioesterification of aldehydes, with H_2 gas as the only stoichiometric byproduct. We anticipate that the incentives of environmentally friendly and synthetically versatile oxidative transformations will lead to expanded scope and application of organocatalyzed EOC.

Section 4: Experimental

General Considerations

DME and THF were obtained from a solvent purification system. ^{1}H and ^{13}C NMR spectra were recorded on a Bruker AVance 300 MHz spectrometer. Chemical shifts are reported in delta (δ) units, expressed in parts per million (ppm) downfield from tetramethylsilane using the residual protio-solvent as an internal standard ($CDCl_3$, ^{1}H: 7.26 ppm and ^{13}C: 77.0 ppm; DMSO-d_6, ^{1}H: 2.49 ppm and ^{13}C: 39.5 ppm). All GC-MS experiments were taken on a Hewlett Packard 5971A mass spectrometer/5890 gas chromatograph with electron impact ionization. Electrochemical experiments were performed on either a CH Instruments 1100B potentiostat or an EZ Stat-Basic potentiostat using a 25 mL 3-neck round bottom flask as an undivided cell equipped with a graphite working electrode (General's brand), Pt counter electrode (Premier Lab Supply), and Ag/0.01 M $AgNO_3$ (0.1 M tetrabutylammonium bromide in CH_3CN) double junction reference electrode. The working electrode potential was +0.1 V vs. Ag/$AgNO_3$. For electrolyses performed using batteries in place of a potentiostat, commercial batteries and resistors were used and voltages were measured using a multi-meter. No reference electrode was used for bulk electrolyses using batteries. The 4-methyl-3-(2,4,6-trimethylphenyl)thiazolium and 3-(2,6-diisopropylphenyl)-4-methylthiazolium precatalysts were prepared according to literature procedures.[41] Additionally, (4-(1,3-dioxolan-2-yl)phenyl)methanol[42] and 4-iodobenzaldehyde[43] were prepared according to

literature procedures. All other reagents and solvents were obtained from commercial sources and stored in the drybox.

General procedure for bulk electrolysis (esterification). In the drybox, a 3-neck round bottom flask was charged with a magnetic stir bar, thiazolium precatalyst (0.225 mmol) and anhydrous CH_3CN (15 mL). To the solution was added tetrabutylammonium bromide (0.675 mmol) and aldehyde (2.25 mmol). The electrode leads were fitted through rubber septa and the electrodes inserted into the flask. The distance between the lower (closest) ends of the electrodes were: C anode → Pt cathode: 0.3 cm, C anode → reference electrode: 0.2 cm, Pt cathode → reference electrode: 0.9 cm. The flask was sealed with the rubber septa, and the electrochemical cell was then removed from the dry box and placed under a positive pressure of N_2. To the stirred solution was added alcohol (2.36 mmol) and DBU (2.25 mmol). The solution typically changed from colorless to red-orange upon addition of DBU. The electrodes were connected to the potentiostat and bulk electrolysis was started with constant stirring.

Aliquots (0.1 mL) were removed with a disposable syringe, a known quantity of 1,3,5-trimethoxybenzene was added as an internal standard, and the mixture was analyzed by ^{1}H NMR spectroscopy in DMSO-d_6. When ester formation ceased as judged by ^{1}H NMR spectroscopy, the electrolysis was stopped. The cell and the electrodes were rinsed with solvent, and the combined solutions were concentrated under reduced

pressure. The residue was then extracted with ethyl acetate (4 × 15 mL). The combined extracts were then washed with H_2O (2 × 50 mL), and then dried over Na_2SO_4. When all of the aldehyde was consumed and a volatile alcohol used, the extraction was sufficient to isolate the ester; however, when aldehyde was still present or a higher boiling alcohol was used, the extraction was followed by flash chromatography on silica gel using a mixture of ethyl acetate and hexanes. ^{1}H and ^{13}C NMR spectra for new compounds are reported below; other spectra were consistent with literature data: benzyl 4-methylbenzoate,[44] terephthalic acid monobenzyl ester,[45] benzyl 4-cyanobenzoate,[46] benzyl 3-cyanobenzoate,[47] benzyl 4-fluorobenzoate,[48] benzyl 4-chlorobenzoate,[49] benzyl 4-bromobenzoate,[50] benzyl 4-iodobenzoate,[51] benzyl cyclohexanecarboxylate,[52] benzyl *trans*-cinnamate,[53] benzyl *trans*-4-methoxycinnamate,[54] benzyl 3-methoxybenzoate,[55] ethyl 4-methylbenzoate,[56] allyl 4-methylbenzoate,[57] propargyl 4-methylbenzoate.[57]

Reactions were found to be equally successful without the use of a drybox when proper air-free handling was performed. In open air, reaction progress typically ceased within 2 h for *p*-tolualdehyde oxidation (< 20% yield of benzyl toluate as determined by ^{1}H NMR spectroscopy using 1,3,5-trimethoxybenzene as internal standard). In the absence of a drybox, a typical procedure was as follows: an oven-dried 3-neck round bottom flask containing a magnetic stir bar was fitted with electrodes and rubber septa as described above and cooled under N_2 atmosphere. Solid reagents were added under a positive pressure of N_2, followed by CH_3CN and liquid reagents each by syringe. The

electrodes were connected to the potentiostat and bulk electrolysis was started with constant stirring.

Benzyl 2,4-dimethylbenzoate

^{1}H NMR (300 MHz, $CDCl_3$) δ = 2.35 (s, 3 H) 2.59 (s, 3 H) 5.33 (s, 2 H) 7.01 - 7.09 (m, 2 H) 7.31 - 7.48 (m, 5 H) 7.88 (d, *J* =7.7 Hz, 1 H). ^{13}C NMR (500 MHz, $CDCl_3$) δ = 21.2, 21.8, 66.1, 126.3, 127.95, 127.99, 128.38, 128.41, 130.81, 132.39, 136.2, 140.4, 142.4, 167.0.

Benzyl 2,4-dichlorobenzoate

^{1}H NMR (300 MHz, $CDCl_3$) δ = 5.37 (s, 2 H) 7.29 (dt, *J* = 8.5, 1.9 Hz, 8 H) 7.36 - 7.49 (m, 43 H) 7.83 (dd, *J* = 8.5, 1.45 Hz, 1 H). ^{13}C NMR (500 MHz, $CDCl_3$) δ = 67.6, 127.1, 128.2, 128.5, 128.6, 128.8, 131.2, 132.8, 135.2, 135.5, 138.5, 164.6.

Benzyl 2-furoate

^{1}H NMR (300 MHz, $CDCl_3$) δ = 5.35 (s, 2 H) 6.50 - 6.56 (m, 1 H) 7.21 (dd, *J* = 3.4, 1.0 Hz, 1 H) 7.33 - 7.44 (m, 5 H) 7.58 (dd, *J* = 1.7, 0.8 Hz, 1 H). ^{13}C NMR (500 MHz, $CDCl_3$) δ = 66.3, 111.7, 118.0, 128.17, 128.20, 128.4, 135.4, 144.4, 146.3, 158.3.

2-Phenylethyl 4-methylbenzoate

^{1}H NMR (300 MHz, $CDCl_3$) δ = 2.41 (s, 3 H) 3.07 (t, *J* = 7.0 Hz, 2 H) 4.52 (t, *J* = 7.0 Hz, 2 H) 7.24 - 7.34 (m, 7 H) 7.88 - 7.94 (m, 2 H). ^{13}C NMR (300 MHz, $CDCl_3$) δ = 21.5, 35.1, 65.2, 126.4, 127.4, 128.4, 128.8, 128.9, 129.4, 137.8, 143.3, 166.4.

Allyl 2,4-dimethylbenzoate

^{1}H NMR (300 MHz, $CDCl_3$) δ = 2.35 (s, 3 H) 2.59 (s, 3 H) 4.79 (dt, *J* = 5.5, 1.4 Hz, 2 H) 5.25 - 5.33 (m, 1 H) 5.40 (dq, *J* = 17.2, 1.6 Hz, 1 H) 5.97 - 6.12 (m, z1 H) 7.01 - 7.09 (m, 2 H) 7.84 - 7.91 (m, 1 H). ^{13}C NMR (400 MHz, $CDCl_3$) δ = 21.4, 21.8, 65.1, 118.0, 126.4, 126.5, 130.8, 132.47, 132.49, 140.4, 142.5, 167.1.

(4-pentyn-1-yl) 4-methylbenzoate

^{1}H NMR (300 MHz, $CDCl_3$) δ = 1.97 - 2.00 (m, 2 H) 2.35 - 2.39 (m, 2 H) 2.41 (s, 3 H) 4.39 - 4.43 (m, 2 H) 7.21 - 7.26 (m, 2 H) 7.90 - 7.96 (m, 2 H). ^{13}C NMR (500 MHz, $CDCl_3$) δ = 15.3, 21.5, 27.6, 63.1, 69.0, 83.0, 127.3, 129.0, 129.5, 143.5, 166.4.

2-(Trimethylsilyl)ethyl 4-methylbenzoate

^{1}H NMR (500 MHz, $CDCl_3$) δ = 0.00 (s, 9 H) 1.02 - 1.08 (m, 2 H) 2.29 (s, 3 H) 4.29 - 4.36 (m, 2 H) 7.12 (d, *J* = 7.8 Hz, 2 H) 7.85 (d, *J* = 8.3 Hz, 2 H). ^{13}C NMR (500 MHz, $CDCl_3$) δ = -1.6, 17.2, 21.4, 62.7, 127.8, 128.8, 129.4, 143.1, 166.6.

4-(Carbomethoxy)benzyl 4-methylbenzoate

^{1}H NMR (300 MHz, $CDCl_3$) δ = 2.41 - 2.46 (m, 3 H) 3.93 (s, 3 H) 5.41 (s, 2 H) 7.24 - 7.28 (m, 2 H) 7.51 (d, *J* = 8.2 Hz, 2 H) 7.98 (d, *J* = 8.2 Hz, 2 H) 8.03 - 8.09 (m, 2 H). ^{13}C NMR (500 MHz, $CDCl_3$) δ = 21.9, 52.2, 62.7, 127.0, 127.5, 129.1, 129.7, 129.79, 129.83, 141.2, 144.0, 166.3, 166.7.

Control experiment forming benzil in the absence of an applied potential. In the drybox, a vial was charged with DME (15 mL) and a stir bar. To the vial were added sequentially *p*-tolualdehyde (0.27 mL, 2.25 mmol), 4-methyl-3-(2,4,6-

trimethylphenyl)thiazolium perchlorate (71.5 mg, 0.225 mmol), benzyl alcohol (0.25 mL, 2.36 mmol), DBU (0.34 mL, 2.25 mmol), and lithium perchlorate (71.8 mg, 0.675 mmol, 30 mol% with respect to *p*-tolualdehyde). Upon addition of perchlorate, a white solid precipitated from the solution. The solution was stirred for 2 h, and the vial was brought out of the drybox. The white solid was collected via vacuum filtration and characterized as 4,4'-dimethylbenzil by ^{1}H NMR spectroscopy (yield: 95% based on perchlorate).[58] An analogous experiment using 0.225 mmol of lithium perchlorate (10 mol% with respect to *p*-tolualdehyde) gave 9% yield of 4,4'-dimethylbenzil based on perchlorate.

Control experiment showing the equilibration between benzoin and aldehyde. In the drybox, CD_3CN (0.5 mL) was added to a screw cap NMR tube. To the tube were added sequentially 4,4'-dimethylbenzoin (18.02 mg, 0.075 mmol), 4-methyl-3-(2,4,6-trimethylphenyl)thiazolium tetrafluoroborate (2.29 mg, 0.008 mmol), tetrabutylammonium bromide (7.25 mg, 0.023 mmol), 1,3,5-trimethoxybenzene (internal standard, 8.20 mg, 0.049 mmol), and DBU (0.01 mL, 0.075 mmol). The solution was monitored by ^{1}H NMR spectroscopy. As shown in **Figure 1.10**, the mole fraction of 4,4'-dimethylbenzoin was initially 1.0 and decreased over time with concomitant increase in the concentration of *p*-tolualdehyde. No other products were observed, and mass balance as judged by NMR spectroscopy was in accordance with a 2:1 benzoin/aldehyde stoichiometry.

Figure 1.10: Equilibration of 4,4'-dimethylbenzoin to *p*-tolualdehyde under reaction conditions consistent with anodic aldehyde oxidations, but without electrodes or applied voltage.

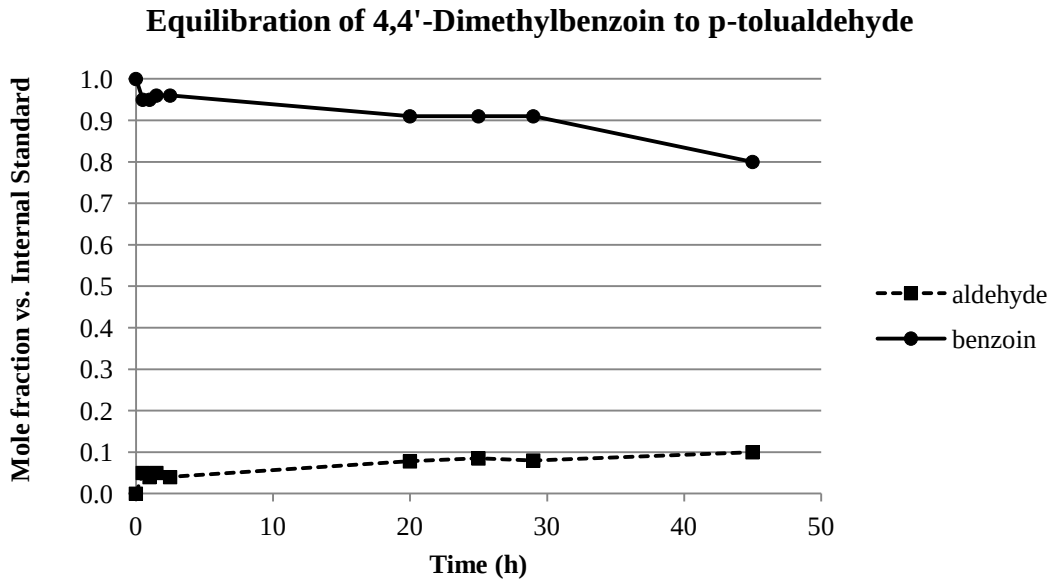

Cyclic Voltammetry. Representative cyclic voltammograms are depicted in **Figure 1.11**, with E_{ox} values for Breslow intermediates listed in **Table 1.5**. The general procedure was as follows: In the drybox, a 3-neck round bottom flask was charged with a magnetic stir bar and CH_3CN (15 mL), and tetrabutylammonium tetrafluoroborate (1.50 mmol). For CVs of each aldehyde, the indicated aldehyde (0.075 mmol) was added to the mixture. Alternatively, for CVs of the Breslow intermediates in the absence of alcohol, aldehyde (3.75 mmol), thiazolium precatalyst (0.075 mmol), and DBU (0.15 mmol) were added to the mixture. The flask was equipped with a Pt wire anode, Pt wire cathode, and $Ag/AgNO_3$ reference electrode (0.01 M $AgNO_3$/0.1 M tetrabutylammonium tetrafluoroborate in CH_3CN) and then the apparatus was sealed using rubber septa. The electrochemical cell was then removed from the drybox and the solution was placed

under a positive pressure of N_2 and stirred at room temperature or in an ice bath for the aldehydes and Breslow intermediates, respectively. Stirring was stopped prior to connecting to the potentiostat. The cyclic voltammograms for the aldehydes were typically taken from -1.0 V to +3.0 V vs. Ag/NO_3 and the cyclic voltammograms for the Breslow intermediates were typically taken from -1.4 V to +0.6 V vs. $Ag/AgNO_3$ with a sweep rate of 0.10 V/s. Ferrocene (0.15 mmol) was added as an internal standard after each voltammogram.[59] All potentials are reported in V vs. SCE.

Figure 1.11: Cyclic voltammograms using conditions as described above.

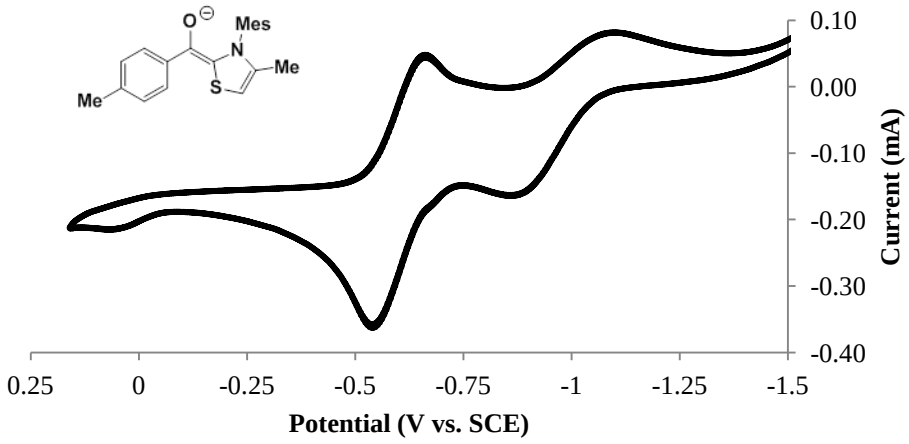

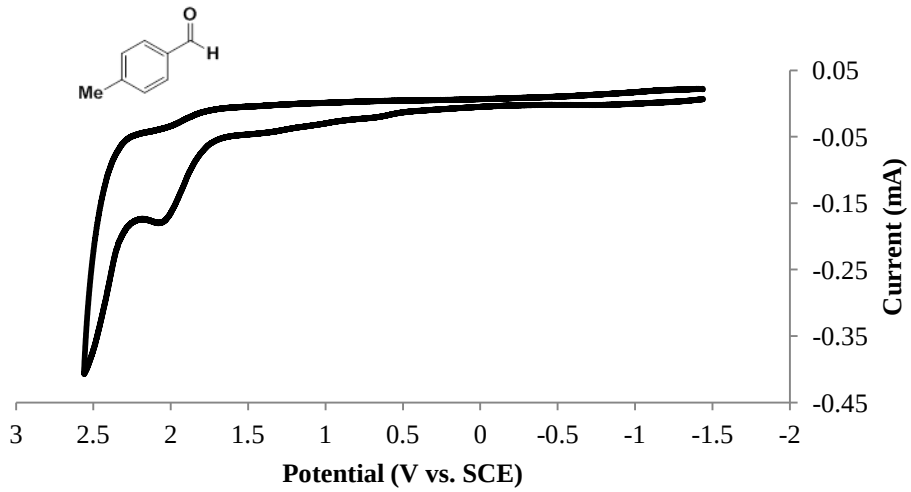
O
H
Me
0.05
-0.05
-0.15
-0.25
-0.35
-0.45
Current (mA)
3
2.5
2
1.5
1
0.5
0
-0.5
-1
-1.5
-2
Potential (V vs. SCE)

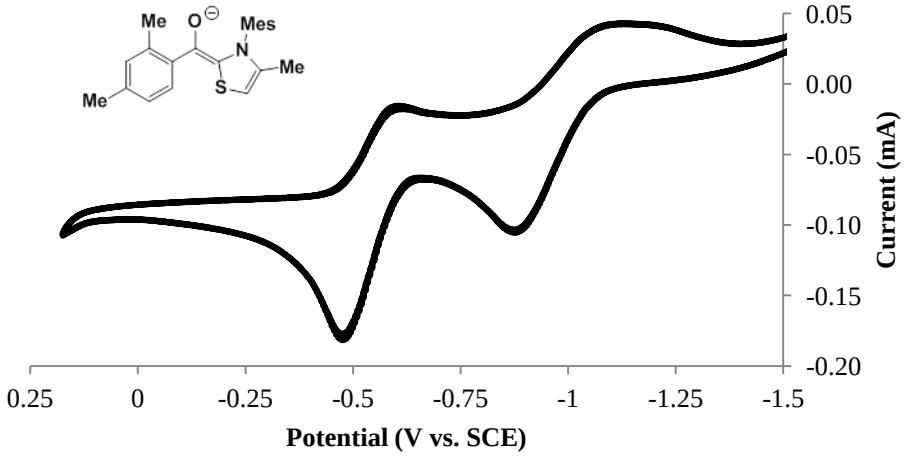
Me
O
Mes
N
Me
Me
S
0.05
0.00
-0.05
-0.10
-0.15
-0.20
Current (mA)
0.25
0
-0.25
-0.5
-0.75
-1
-1.25
-1.5
Potential (V vs. SCE)

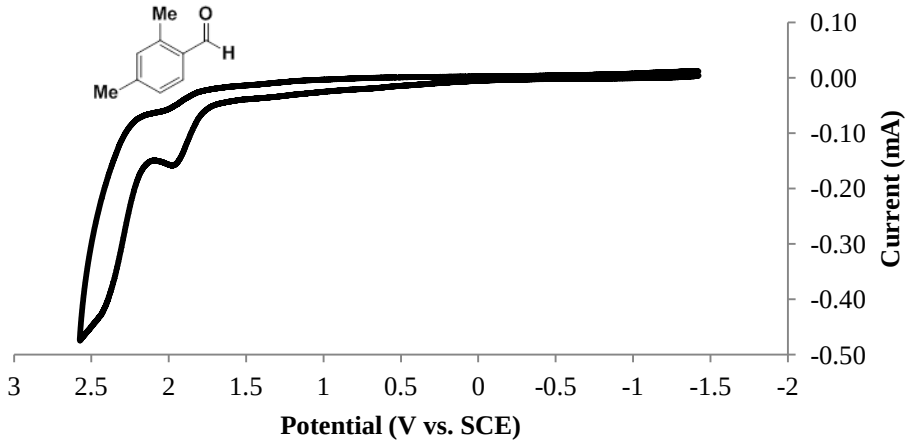
Me
O
H
Me
0.10
0.00
-0.10
-0.20
-0.30
-0.40
-0.50
Current (mA)
3
2.5
2
1.5
1
0.5
0
-0.5
-1
-1.5
-2
Potential (V vs. SCE)

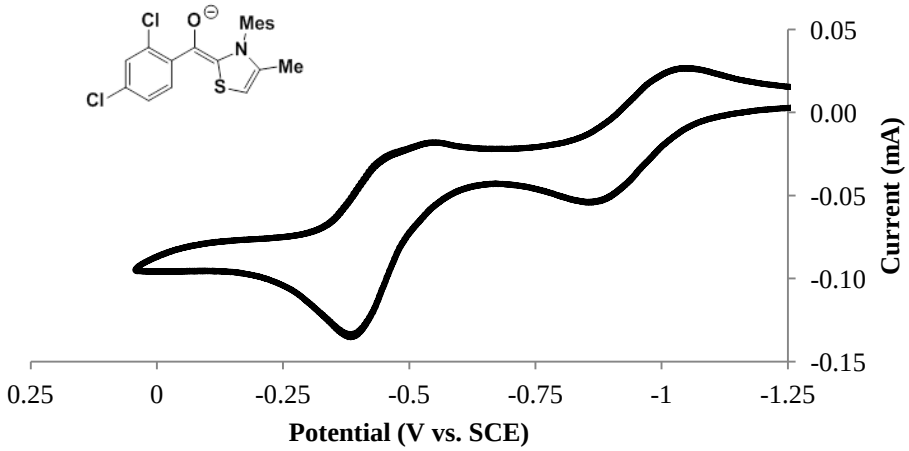
Cl
O
Mes
N
Me
S
Cl
0.05
0.00
-0.05
-0.10
-0.15
Current (mA)
0.25
0
-0.25
-0.5
-0.75
-1
-1.25
Potential (V vs. SCE)

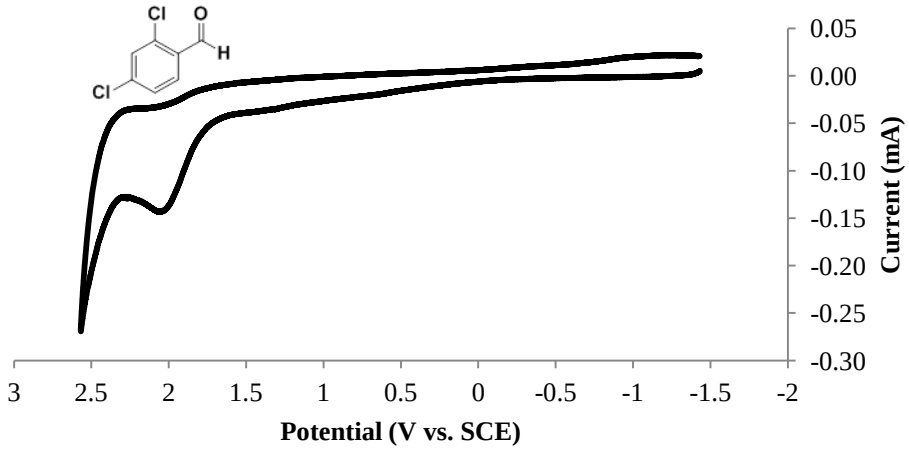
Cl
O
H
Cl
0.05
0.00
-0.05
-0.10
-0.15
-0.20
-0.25
-0.30
Current (mA)
3
2.5
2
1.5
1
0.5
0
-0.5
-1
-1.5
-2
Potential (V vs. SCE)

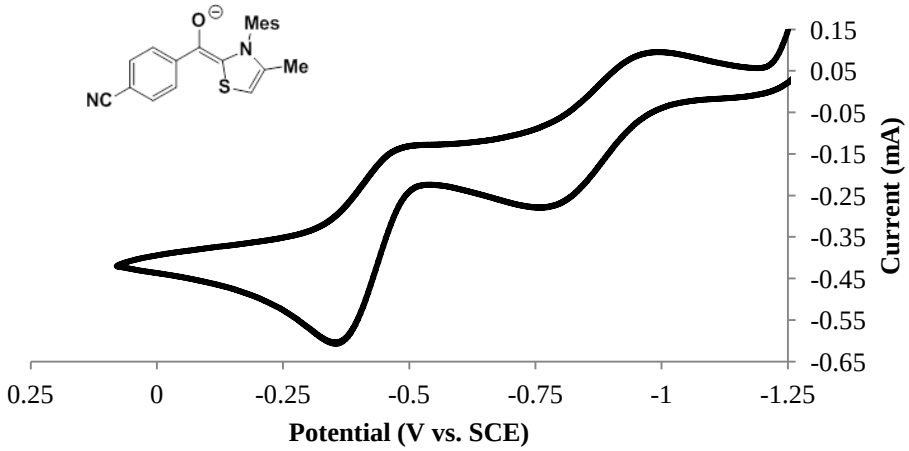
O
Mes
N
Me
S
NC
0.15
0.05
-0.05
-0.15
-0.25
-0.35
-0.45
-0.55
-0.65
Current (mA)
0.25
0
-0.25
-0.5
-0.75
-1
-1.25
Potential (V vs. SCE)

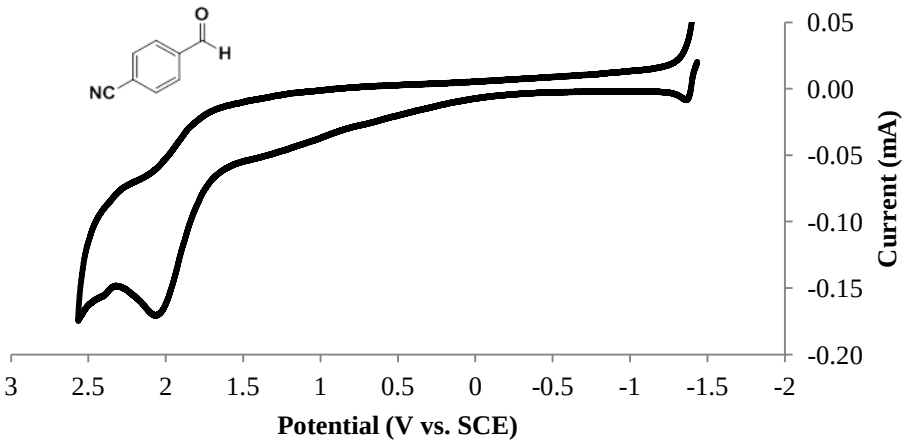
O
H
NC
0.05
0.00
-0.05
-0.10
-0.15
-0.20
Current (mA)
3
2.5
2
1.5
1
0.5
0
-0.5
-1
-1.5
-2
Potential (V vs. SCE)

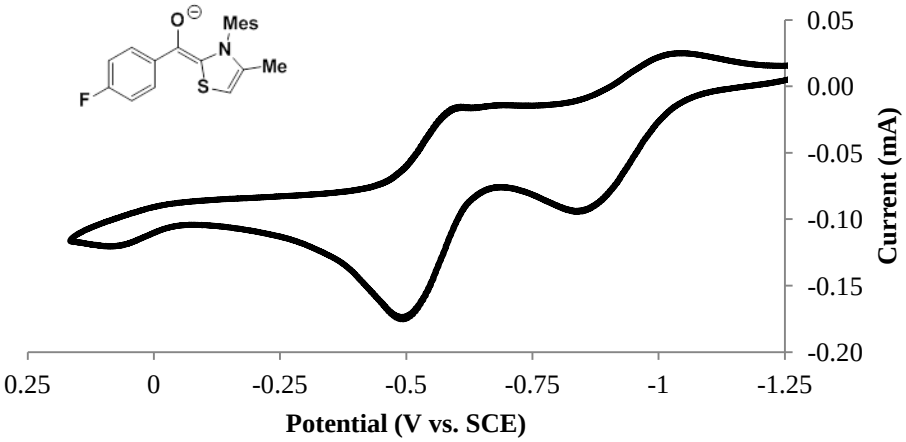
O
Mes
N
Me
S
F
0.05
0.00
-0.05
-0.10
-0.15
-0.20
Current (mA)
0.25
0
-0.25
-0.5
-0.75
-1
-1.25
Potential (V vs. SCE)

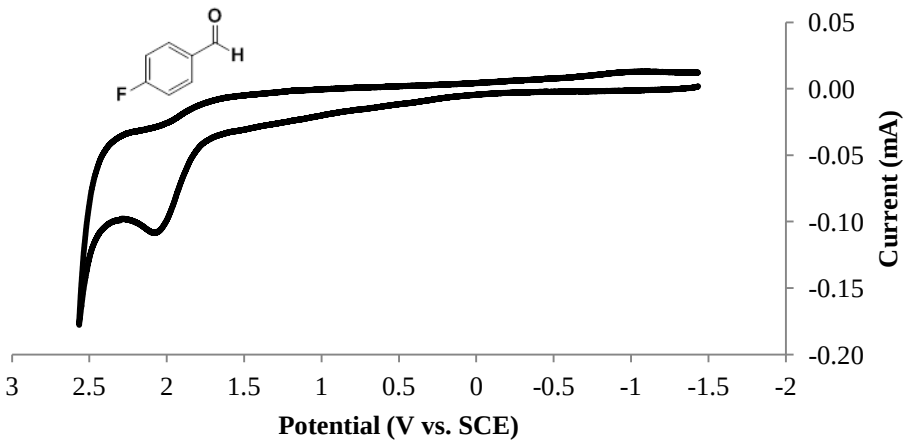
O
H
F
0.05
0.00
-0.05
-0.10
-0.15
-0.20
Current (mA)
3
2.5
2
1.5
1
0.5
0
-0.5
-1
-1.5
-2
Potential (V vs. SCE)

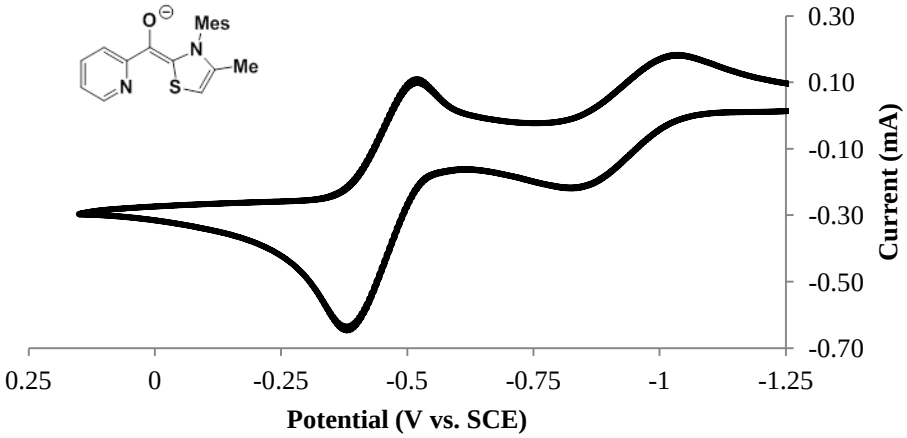
O
Mes
N
Me
N
S
0.30
0.10
-0.10
-0.30
-0.50
-0.70
Current (mA)
0.25
0
-0.25
-0.5
-0.75
-1
-1.25
Potential (V vs. SCE)

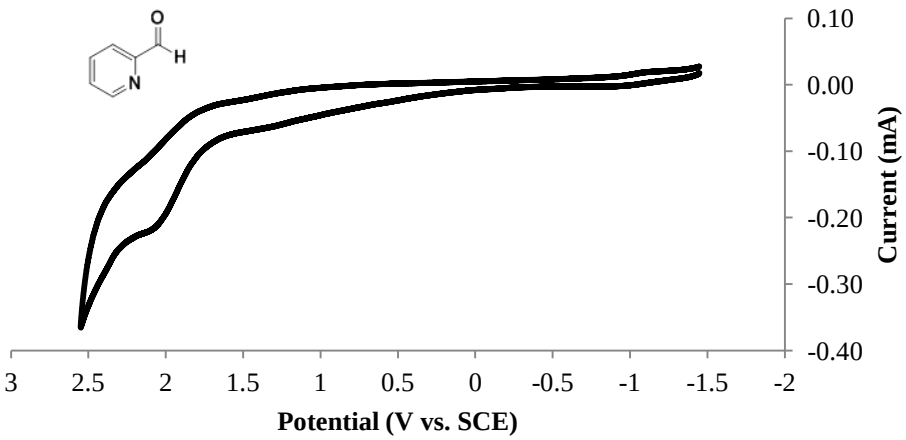
O
H
N
0.10
0.00
-0.10
-0.20
-0.30
-0.40
Current (mA)
3
2.5
2
1.5
1
0.5
0
-0.5
-1
-1.5
-2
Potential (V vs. SCE)

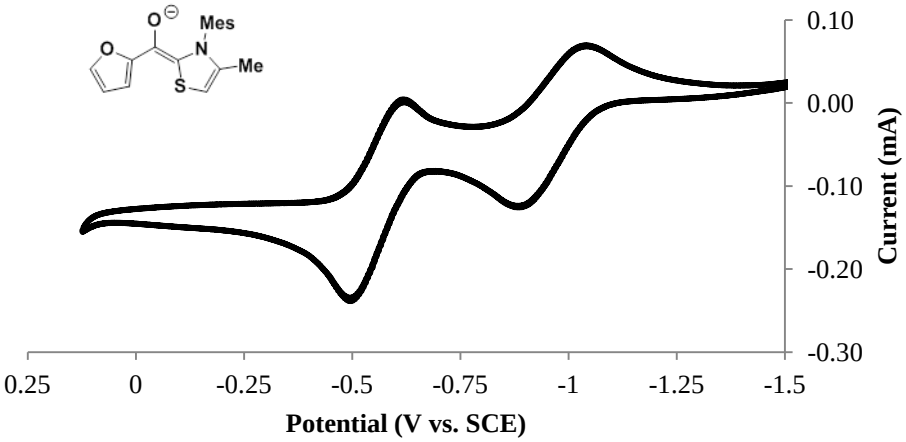
O
Mes
N
O
Me
S
0.10
0.00
-0.10
-0.20
-0.30
Current (mA)
0.25
0
-0.25
-0.5
-0.75
-1
-1.25
-1.5
Potential (V vs. SCE)

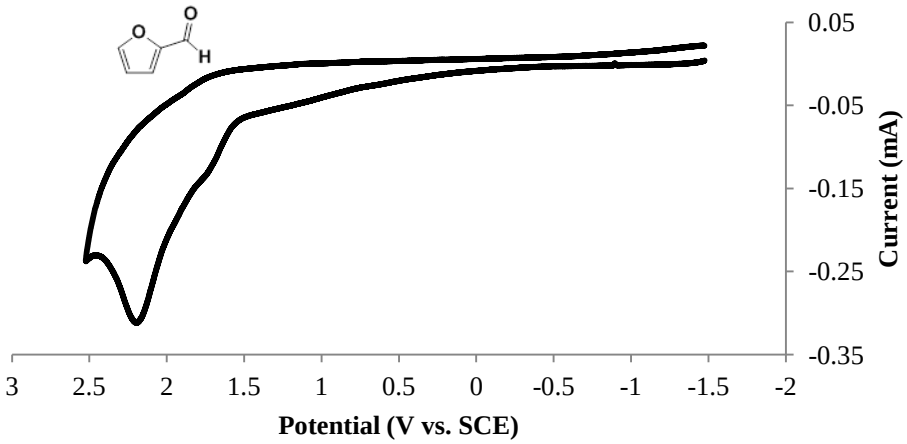
O
O
H
0.05
-0.05
-0.15
-0.25
-0.35
Current (mA)
3
2.5
2
1.5
1
0.5
0
-0.5
-1
-1.5
-2
Potential (V vs. SCE)

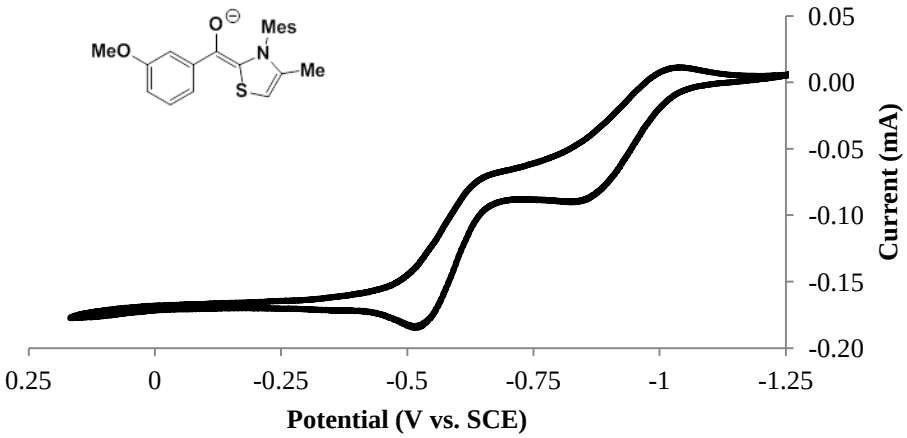
O
Mes
MeO
N
Me
S
0.05
0.00
-0.05
-0.10
-0.15
-0.20
Current (mA)
0.25
0
-0.25
-0.5
-0.75
-1
-1.25
Potential (V vs. SCE)

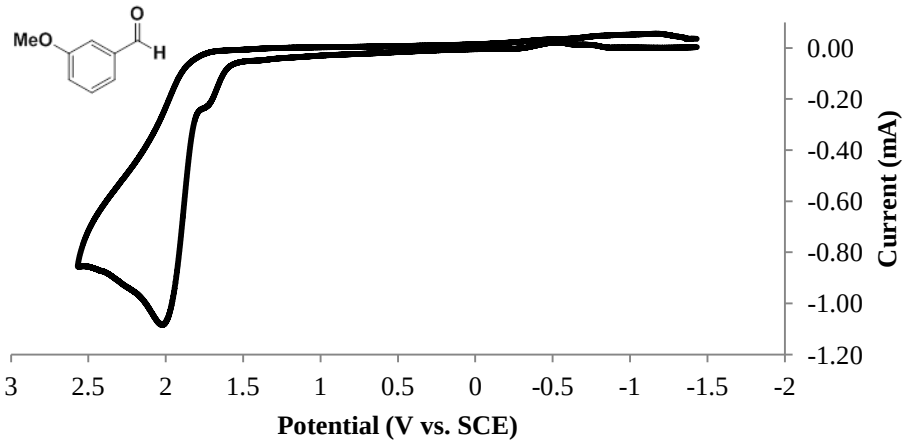
MeO
O
H
0.00
-0.20
-0.40
-0.60
-0.80
-1.00
-1.20
Current (mA)
3
2.5
2
1.5
1
0.5
0
-0.5
-1
-1.5
-2
Potential (V vs. SCE)

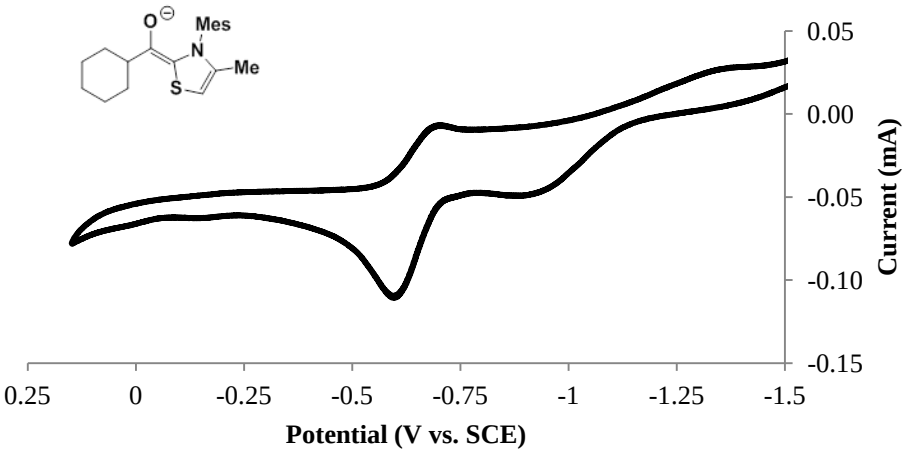
O
Mes
N
Me
S
0.05
0.00
-0.05
-0.10
-0.15
Current (mA)
0.25
0
-0.25
-0.5
-0.75
-1
-1.25
-1.5
Potential (V vs. SCE)

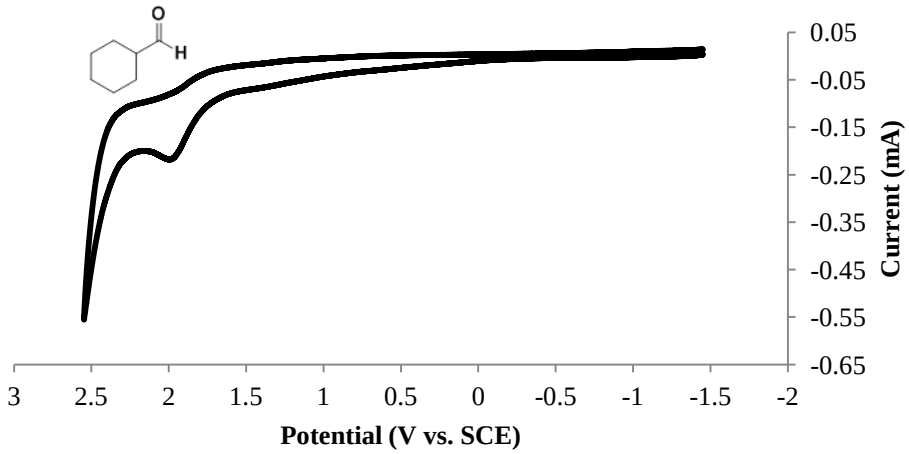
O
H
0.05
-0.05
-0.15
-0.25
-0.35
-0.45
-0.55
-0.65
Current (mA)
3
2.5
2
1.5
1
0.5
0
-0.5
-1
-1.5
-2
Potential (V vs. SCE)

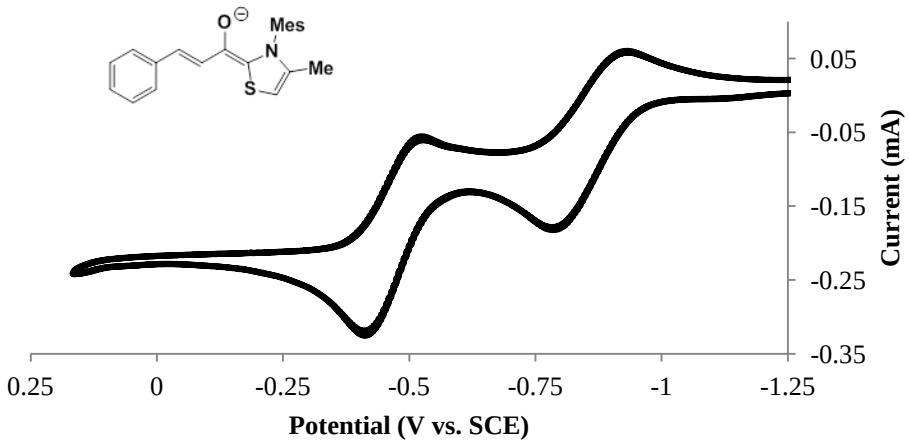
O
Mes
N
Me
S
0.05
-0.05
-0.15
-0.25
-0.35
Current (mA)
0.25
0
-0.25
-0.5
-0.75
-1
-1.25
Potential (V vs. SCE)

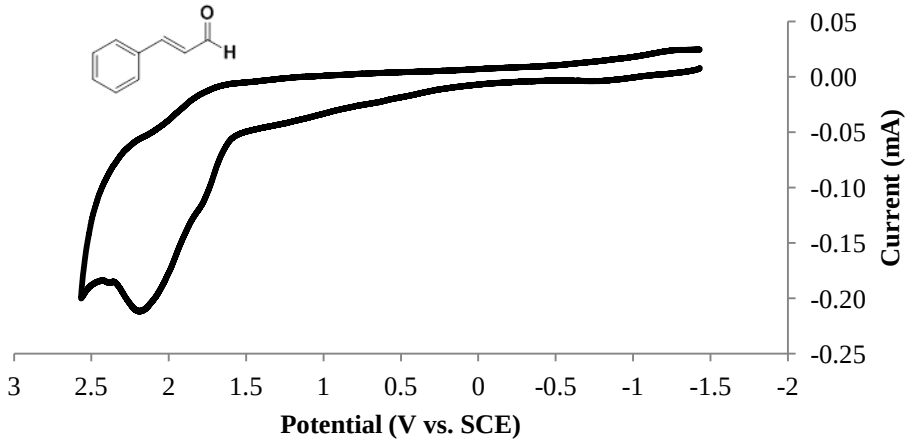
O
H
0.05
0.00
-0.05
-0.10
-0.15
-0.20
-0.25
Current (mA)
3
2.5
2
1.5
1
0.5
0
-0.5
-1
-1.5
-2
Potential (V vs. SCE)

Table 1.5: Potentials (vs. SCE) of Breslow intermediates determined by cyclic voltammetry as described above.

aldehyde used	E_{ox1}	E_{ox2}
p-tolualdehyde	-0.86	-0.54
2,4-dimethylbenzaldehyde	-0.88	-0.48
2,4-dichlorobenzaldehyde	-0.86	-0.38
4-cyanobenzaldehyde	-0.78	-0.35
4-fluorobenzaldehyde	-0.84	-0.49
2-pyridinecarboxaldehyde	-0.83	-0.38
2-furaldehyde	-0.89	-0.50
3-methoxybenzaldehyde	-0.87	-0.51
cyclohexanecarboxaldehyde	-0.94	-0.60
trans-cinnamaldehyde	-0.79	-0.42

Current-time plots during bulk electrolysis. Representative current versus time plots are given below. The corresponding overall aldehyde-to-ester conversion is depicted on each graph. Large spikes in current during the electrolyses corresponded to aliquots being withdrawn from the reaction mixtures.

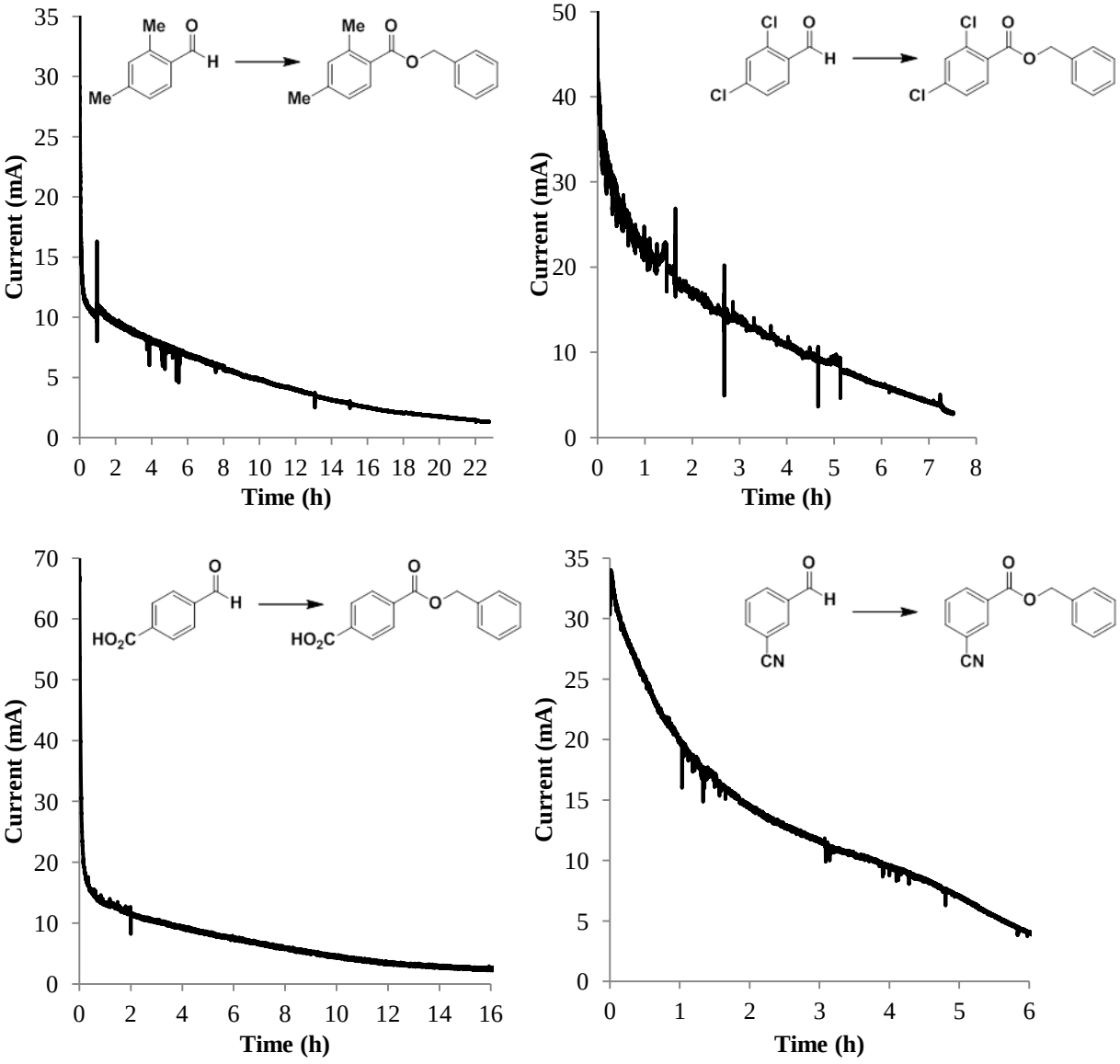
Me
O
H
Me
Me
O
O
Me
Current (mA)
Time (h)
0 2 4 6 8 10 12 14 16 18 20 22
0 5 10 15 20 25 30 35
Cl
O
H
Cl
Cl
O
O
Cl
Current (mA)
Time (h)
0 1 2 3 4 5 6 7 8
0 10 20 30 40 50
O
H
HO2C
O
O
HO2C
Current (mA)
Time (h)
0 2 4 6 8 10 12 14 16
0 10 20 30 40 50 60 70
O
H
CN
O
O
CN
Current (mA)
Time (h)
0 1 2 3 4 5 6
0 5 10 15 20 25 30 35

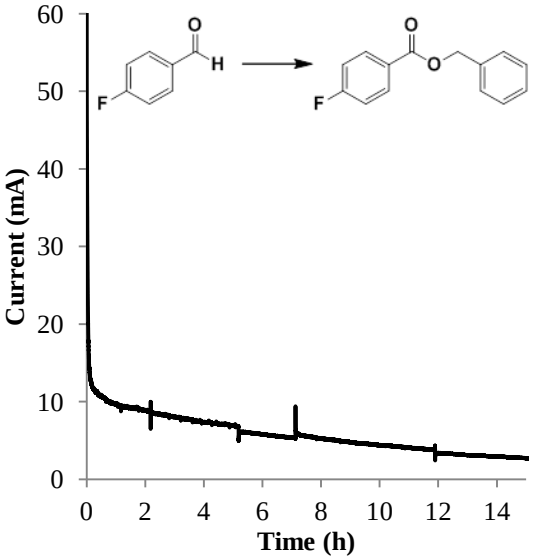
Current (mA)
Time (h)
F
F

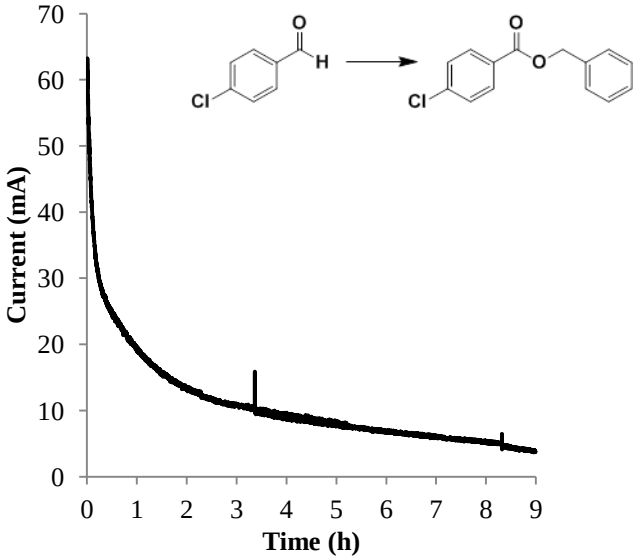
Current (mA)
Time (h)
Cl
Cl

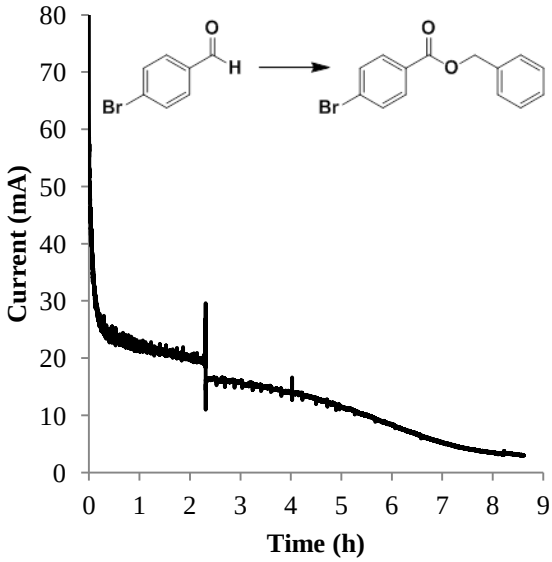
Current (mA)
Time (h)
Br
Br

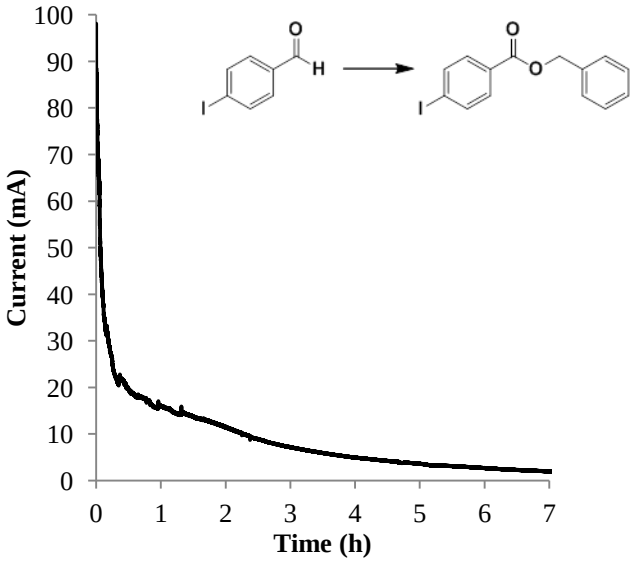
Current (mA)
Time (h)
I
I

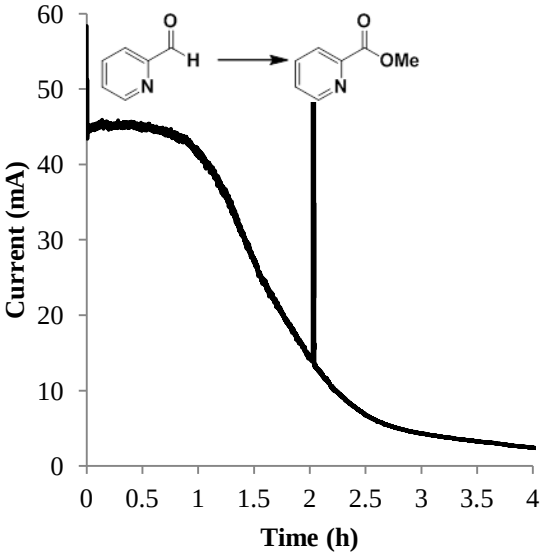
Current (mA)
Time (h)
OMe

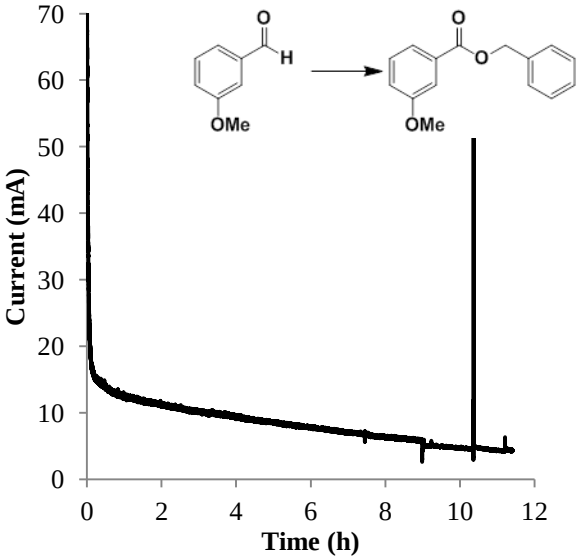
Current (mA)
Time (h)
OMe
OMe

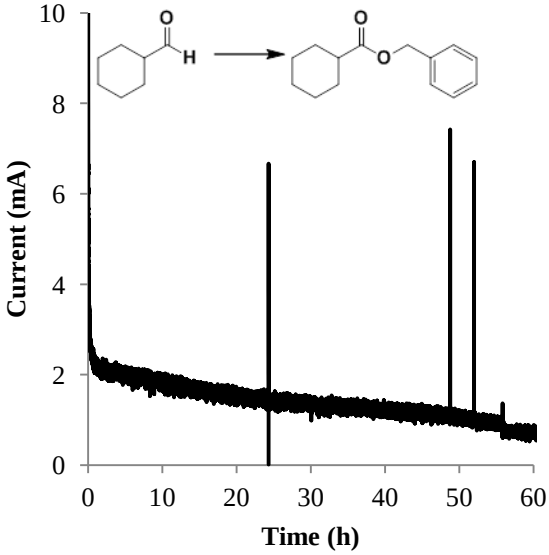
Current (mA)
Time (h)

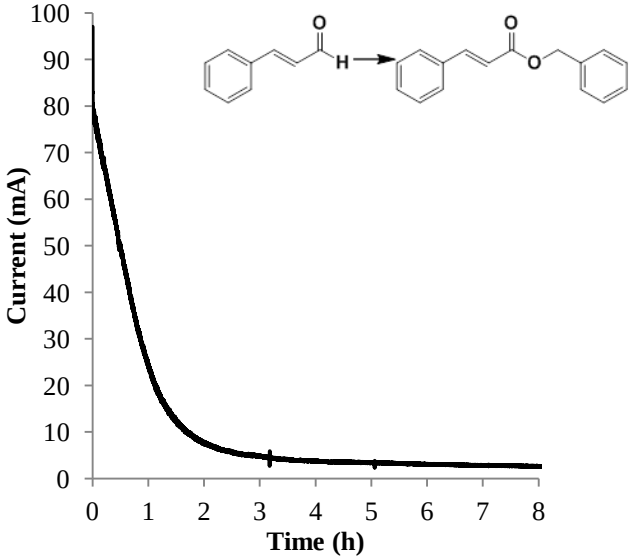
Current (mA)
Time (h)

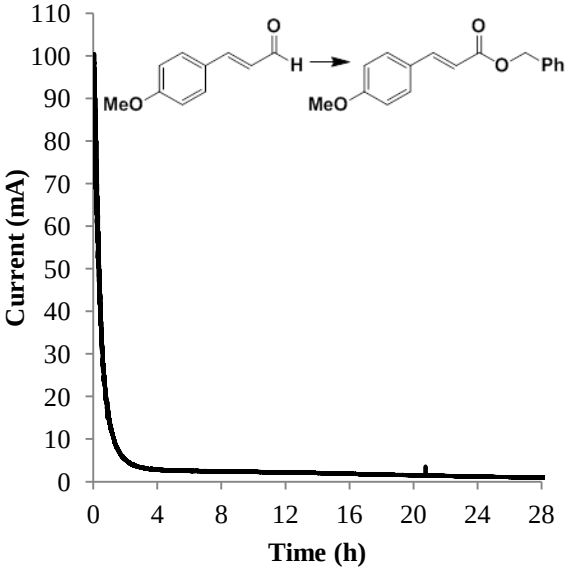
MeO
MeO
O
H
O
O
Ph
Current (mA)
Time (h)
0 4 8 12 16 20 24 28
0 10 20 30 40 50 60 70 80 90 100 110

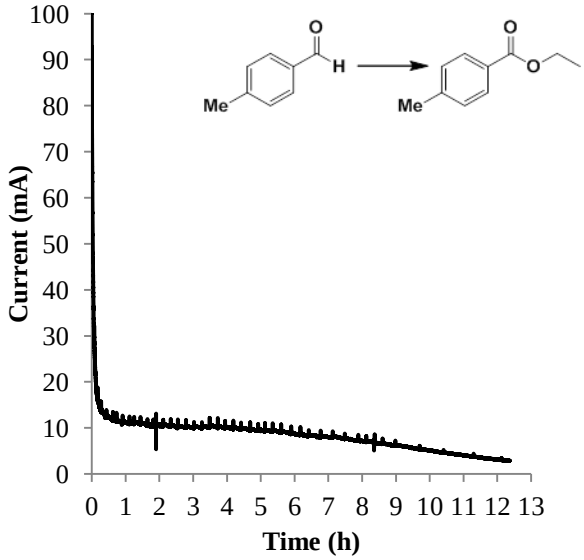
Me
Me
O
H
O
Current (mA)
Time (h)
0 1 2 3 4 5 6 7 8 9 10 11 12 13
0 10 20 30 40 50 60 70 80 90 100

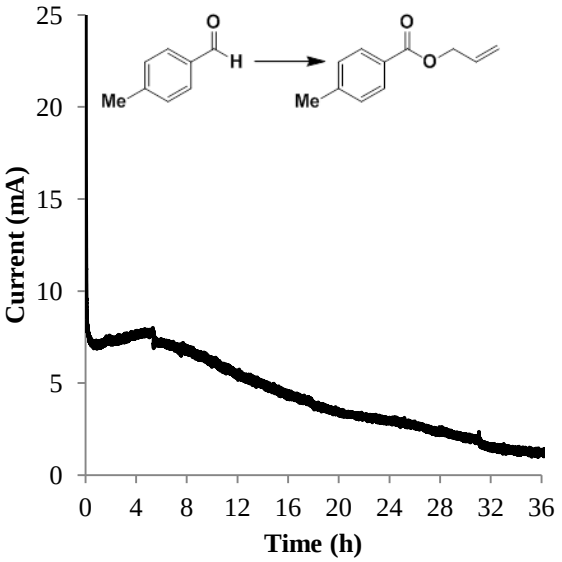
Me
Me
O
H
O
Current (mA)
Time (h)
0 4 8 12 16 20 24 28 32 36
0 5 10 15 20 25

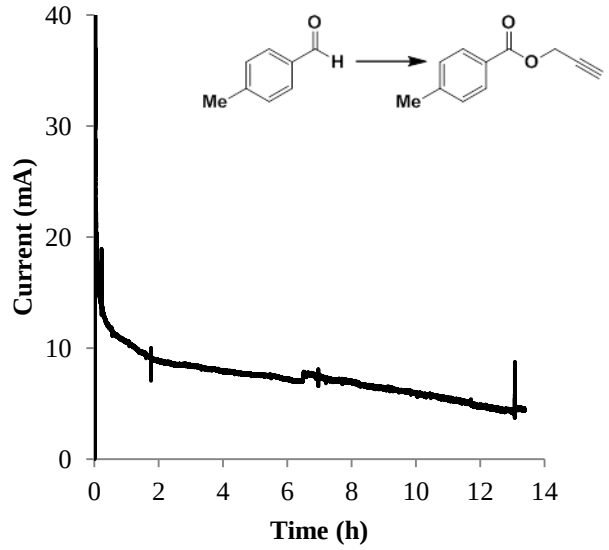
Me
Me
O
H
O
Current (mA)
Time (h)
0 2 4 6 8 10 12 14
0 10 20 30 40

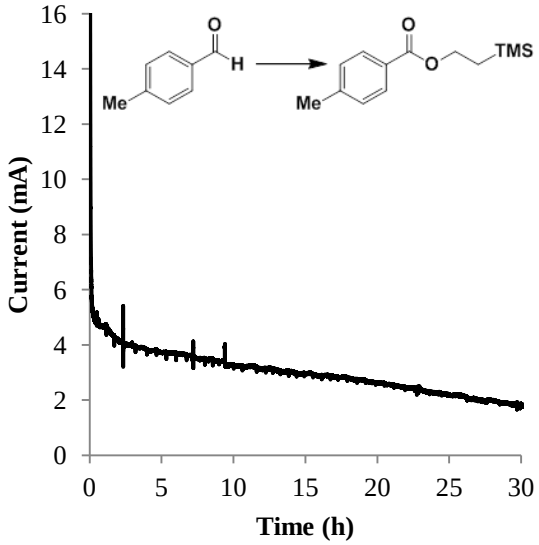

Anodic oxidations using alkaline batteries. In the drybox, thiazolium precatalyst (0.225 mmol) TBAB (0.675 mmol) added to a 25 mL 3-neck round bottom flask. To the flask was added dry CH_3CN (15 mL), aldehyde (2.25 mmol), and benzyl alcohol (2.36 mmol□. The vial was fitted with a graphite stick anode and Pt wire coil cathode, capped with a rubber septum, and brought out of the drybox. The solution was stirred under N_2, and DBU (2.25 mmol) was added to the mixture via syringe. The electrodes were connected to the battery source through a voltage regulator to maintain a potential of ca. +0.14 V as determined using a multi-meter connected across the graphite and Pt electrodes. Aliquots were taken as described above.

Detection of H_2 gas produced during the reaction. Anodic oxidation of *p*-tolualdehyde in the presence of benzyl alcohol was conducted using a potentiostat as described above. Separately, $IrCl(CO)(PPh_3)_2$ (Vaska's complex, 39 mg, 0.05 mmol) was dissolved in

C_6D_6 (0.6 mL) in a screw-cap NMR tube. The tube was sealed with a septum-lined screw-cap under N_2 atmosphere. The atmosphere in the electrochemical cell was bubbled through the NMR tube containing Vaska's complex via cannula, with an exit needle inserted into the NMR tube. The solution in the NMR tube was monitored by ^{1}H and ^{31}P NMR spectroscopy. All spectra were consistent with literature data.[60,61,62]

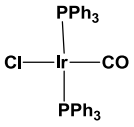

(^{1}H NMR spectrum of Vaska's complex as received from commercial source)

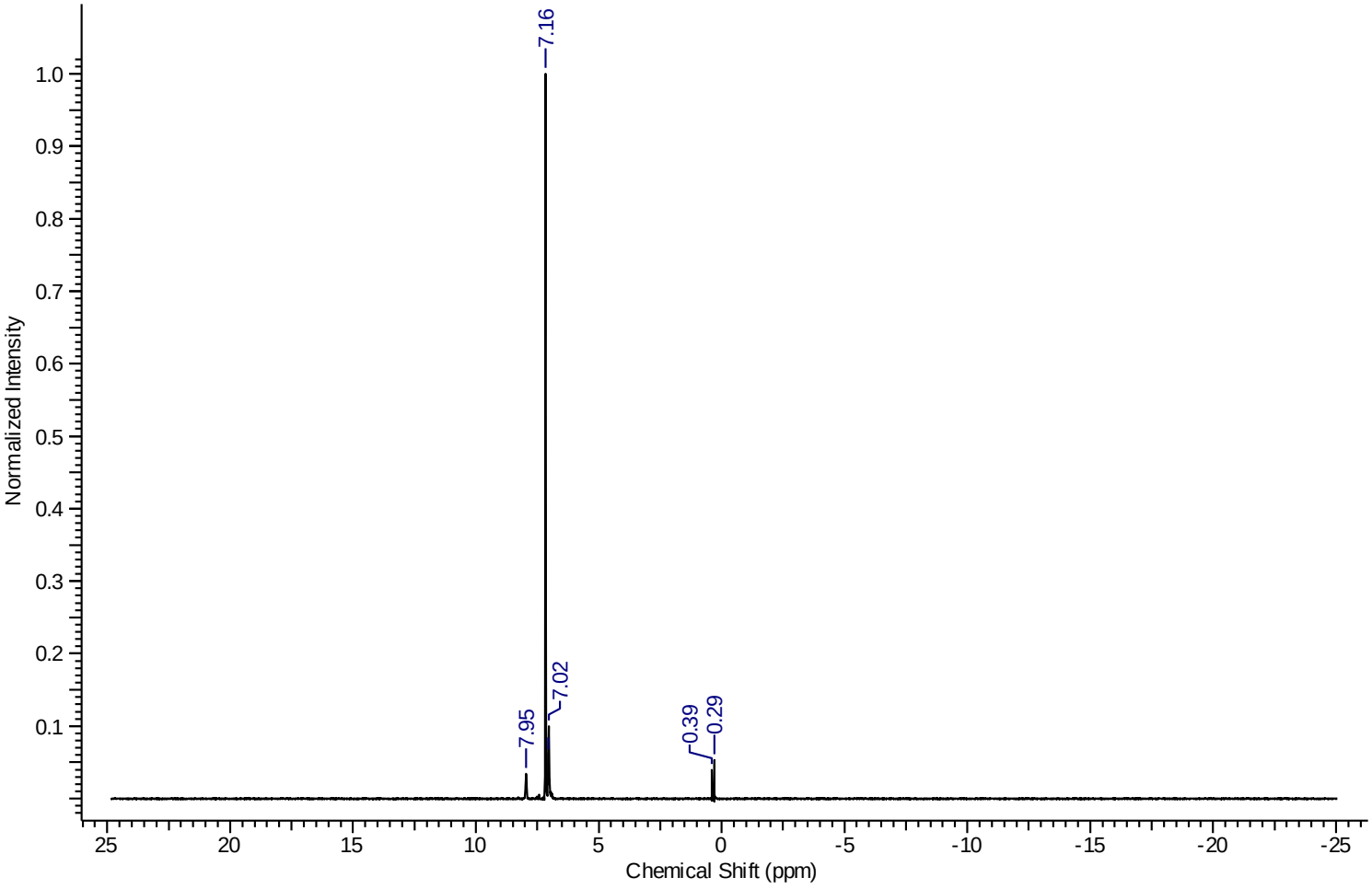

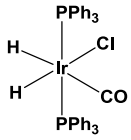

(^{1}H NMR spectrum of dihydride produced after 7 h of anodic aldehyde oxidation)

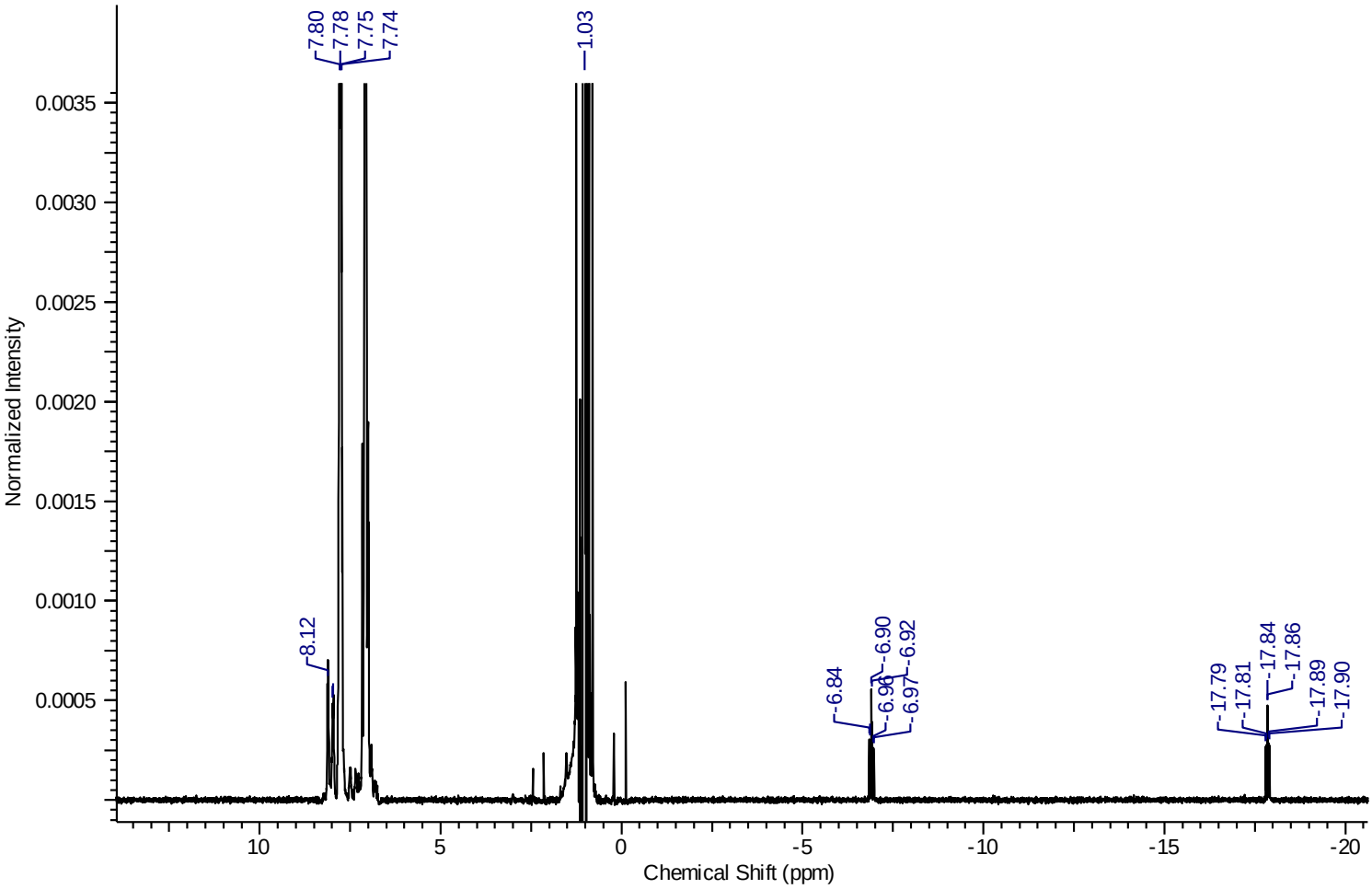

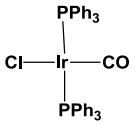

(^{31}P NMR spectrum of Vaska's complex as received from commercial source)

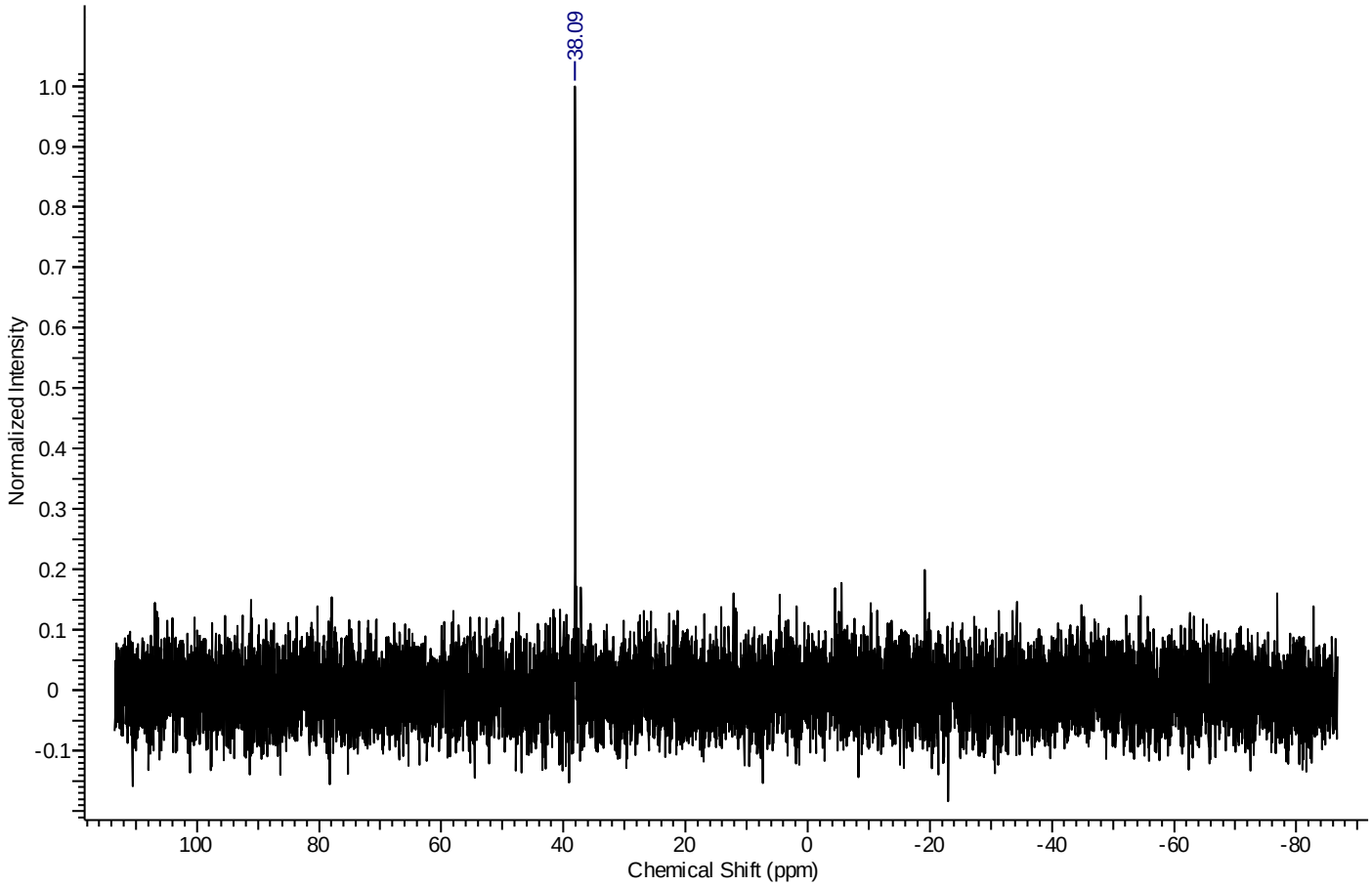

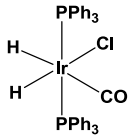

(^{31}P NMR spectrum of dihydride produced after 7 h of anodic aldehyde oxidation)

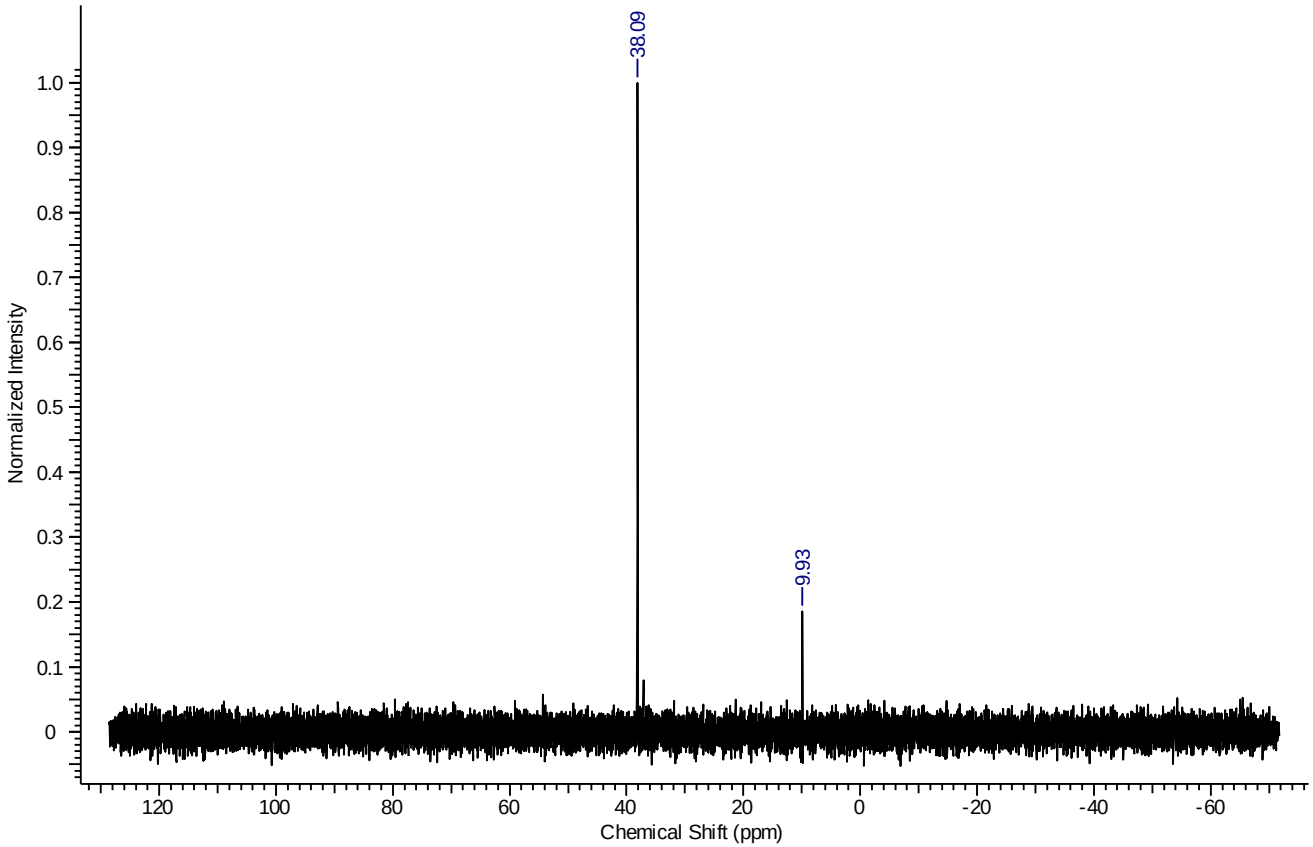

General procedures for bulk electrolysis (thioesterification): In a nitrogen-filled drybox, a 3-neck round bottom flask was charged with a magnetic stir bar, tetrabutylammonium bromide (0.675 mmol, 0.045 M), 4-methyl-3-(2,4,6-trimethylphenyl)thiazolium tetrafluoroborate (**A-Mes**) (0.229 mmol, 0.10 equiv), aldehyde (2.29 mmol, 1.0 equiv), and anhydrous CH_3CN (15 mL). The electrode leads were fitted through rubber septa and the electrodes inserted into the flask. The flask was sealed with the rubber septa, and the electrochemical cell was then removed from the dry box and placed under a positive pressure of N_2. To the stirred solution was added thiol (4.58 mmol, 2.0 equiv) and 4-dimethylaminopyridine (DMAP) (1.15 mmol, 0.50 equiv). The solution typically changed from colorless to orange upon addition of DMAP. The electrodes were connected to the potentiostat and bulk electrolysis was started with constant stirring.

Aliquots (0.1 mL) were removed with a disposable syringe, a known quantity of 1,3,5-trimethoxybenzene was added as an internal standard, and the mixture was analyzed by ^1H NMR spectroscopy in $CDCl_3$ and tandem gas chromatography-mass spectrometry (GC-MS). When thioester formation ceased as judged by ^1H NMR spectroscopy, the electrolysis was stopped. The cell and the electrodes were rinsed with solvent, and the combined solutions were concentrated under reduced pressure. The residue was then extracted with ethyl acetate (4 × 15 mL). The combined extracts were then washed with H_2O (2 × 50 mL), and then dried over Na_2SO_4. The extraction was followed by flash chromatography on silica gel using a (10:90) mixture of ethyl acetate

and hexanes to provide the product. ^{1}H and ^{13}C NMR spectra for new compounds are reported below; other spectra were consistent with literature data: *S*-butyl-cyclohexanecarbothioate[63] and *S*-benzyl-3-methoxythiobenzoate.[64]

***S*-butyl-4-methylthiobenzoate ^{1}H NMR** (300 MHz, $CDCl_3$) δ = 7.88 (d, *J* = 9.0 Hz, 2 H) 7.24 (d, *J* = 9.0 Hz, 2 H) 3.07 (t, *J* = 6.0, 6.0 Hz, 2 H) 2.40 (s, 3 H) 1.66 (m, 2 H) 1.48 (m, 2 H) 0.96 (t, *J* = 6.0, 9.0 Hz, 3 H). ^{1}H and ^{13}C NMR spectra were consistent with literature data.[65] **LRMS:** calculated for $C_{12}H_{16}OS$: 208.09; **found:** 208.05.

***S*-butyl-2,4-dimethylthiobenzoate ^{1}H NMR** (300 MHz, $CDCl_3$) δ = 7.73 (m, 1 H) 7.06 (m, 2 H) 3.03 (t, *J* = 9.0, 6.0 Hz, 2 H) 2.48 (s, 3 H) 2.35 (s, 3 H) 1.66 (m, 2 H) 1.48 (m, 2 H) 0.96 (t, *J* = 9.0, 6.0 Hz, 3 H). **^{13}C NMR** (125 MHz, $CDCl_3$) δ = 194.0, 142.0, 136.9, 134.9, 132.3, 128.7, 126.3, 31.7, 29.2, 22.1, 21.3, 20.6, 13.6. **LRMS:** calculated for $C_{13}H_{18}OS$: 222.11; **found:** 222.10.

***S*-butyl-3-methoxythiobenzoate ^{1}H NMR** (300 MHz, $CDCl_3$) δ = 7.59 (d, *J* = 9.0 Hz, 1 H) 7.47 (m, 1 H) 7.34 (t, *J* = 9.0, 6.0 Hz, 1 H) 7.11 (m, 1 H) 3.85 (s, 3 H) 3.07 (t, *J* = 9.0, 6.0 Hz, 2 H) 1.66 (m, 2 H) 1.46 (m, 2 H) 0.95 (t, *J* = 9.0, 6.0 Hz, 3 H). **^{13}C NMR** (125 MHz, $CDCl_3$) δ = 192.0, 159.7, 138.5, 129.5, 119.7, 119.6, 111.4, 55.4, 31.5, 28.8, 22.0, 13.6. **LRMS:** calculated for $C_{12}H_{16}O_2S$: 224.09; **found:** 224.10.

***S*-butyl-4-fluorothiobenzoate ^{1}H NMR** (300 MHz, $CDCl_3$) δ = 8.00 (dd, *J* = 6.0, 3.0 Hz, 2 H) 7.12 (t, *J* = 9.0, 9.0 Hz, 2 H) 3.08 (t, *J* = 6.0, 9.0 Hz, 2 H) 1.66 (m, 2 H) 1.46 (m, 2 H) 0.95 (t, *J* = 9.0, 6.0 Hz, 3 H). **^{13}C NMR** (125 MHz, $CDCl_3$) δ = 190.5, 166.8, 164.8,

133.6, 129.7, 139.6, 115.7, 115.5, 31.5, 28.8, 22.0, 13.5. **LRMS:** calculated for $C_{11}H_{13}FOS$: 212.07; **found:** 212.00.

***S*-butyl-3-chlorothiobenzoate ^{1}H NMR** (300 MHz, $CDCl_3$) δ = 7.94 (m, 1 H) 7.85 (m, 1 H) 7.54 (m, 1 H) 7.39 (t, *J* = 9.0, 6.0 Hz, 1 H) 3.09 (t, *J* = 9.0, 6.0 Hz, 2 H) 1.67 (m, 2 H) 1.45 (m, 2 H) 0.96 (t, *J* = 9.0, 6.0 Hz, 3 H). **^{13}C NMR** (125 MHz, $CDCl_3$) δ = 190.9, 138.7, 134.8, 133.0, 129.8, 127.2, 125.3, 31.5, 28.9, 22.0, 13.6. **LRMS:** calculated for $C_{11}H_{13}ClOS$: 228.04; **found:** 228.00.

***S*-butyl-2-pyridinecarbothioate ^{1}H NMR** (300 MHz, $CDCl_3$) δ = 8.66 (m, 1 H) 7.93 (m, 1 H) 7.82 (m, 1 H) 7.47 (m, 1 H) 3.02 (t, *J* = 6.0, 9.0 Hz, 2 H) 1.64 (m, 2 H) 1.43 (m, 2 H) 0.91 (t, *J* = 6.0, 6.0 Hz, 3 H). **^{13}C NMR** (125 MHz, $CDCl_3$) δ = 193.6, 151.9, 149.0, 137.1, 127.6, 120.2, 31.2, 28.2, 22.0, 13.5. **LRMS:** calculated for $C_{10}H_{13}NOS$: 195.07; **found:** 195.00.

***S*-(2-chloro)benzyl-3-methoxythiobenzoate ^{1}H NMR** (300 MHz, $CDCl_3$) δ = 7.52 (m, 2 H) 7.42 (m, 1 H) 7.32 (m, 2 H) 7.19 (m, 2 H) 7.08 (m, 1 H) 4.39 (s, 2 H) 3.80 (s, 3 H). **^{13}C NMR** (125 MHz, $CDCl_3$) δ = 191.3, 160.0, 138.3, 135.8, 134.5, 131.5, 129.9, 129.8, 129.1, 127.3, 120.3, 120.2, 111.7, 55.7, 31.6. **LRMS:** calculated for $C_{15}H_{13}ClO_2S$: 292.03; **found:** 292.00.

***S*-furfuryl-3-methoxythiobenzoate ^{1}H NMR** (500 MHz, $CDCl_3$) δ = 7.58 (d, *J* = 10 Hz, 1 H) 7.48 (br, 1 H) 7.36 (t, *J* = 5.0, 10 Hz, 2 H) 7.12 (m, 1 H) 6.32 (br, 2 H) 4.36 (s, 2 H) 3.85 (s, 3 H). **^{13}C NMR** (125 MHz, $CDCl_3$) δ = 190.6, 159.7, 150.3, 142.2, 137.9, 129.6,

120.0, 119.9, 111.4, 110.6, 108.1, 55.4, 25.8. **LRMS:** calculated for $C_{13}H_{12}O_3S$: 248.05; **found:** 248.00.

***S*-cyclohexyl-3-methoxythiobenzoate ^{1}H NMR** (300 MHz, $CDCl_3$) δ = 7.57 (d, *J* = 9.0 Hz, 1 H) 7.48 (m, 1 H) 7.34 (t, *J* = 6.0, 9.0 Hz, 1 H) 7.10 (m, 1 H) 3.85 (s, 3 H). 3.72 (br, 1 H) 2.03 (br, 2 H) 1.74 (br, 2 H) 1.51 (br, 4 H) 1.32 (br, 2 H). **^{13}C NMR** (125 MHz, $CDCl_3$) δ = 191.7, 159.6, 138.8, 129.5, 119.7, 119.5, 111.3, 55.4, 42.6, 33.1, 26.0, 25.6. **LRMS:** calculated for $C_{14}H_{18}O_2S$: 250.10; **found:** 250.10.

Control experiments for disulfide formation. Sodium thiolate was formed via deprotonation of the 1-butane thiol (8.0 µL, 0.075 mmol, 1.0 equiv) with NaH (95%, 1.9 mg, 0.075 mmol, 1.0 equiv) in 0.25 mL CD_3CN. A screw cap NMR tube was sealed under a N_2 atmosphere with a Teflon lined cap. **A** (0.023 g, 0.075 mmol, 1.0 equiv) was dissolved in 0.25 mL of CD_3CN and transferred into the NMR tube. Either a combination of 1-butane thiol (8.0 µL, 0.075 mmol, 1.0 equiv) and corresponding base (0.075 mmol, 1.0 equiv) or sodium thiolate (0.075 mmol, 1.0 equiv) were dissolved in 0.25 mL CD_3CN and then added via syringe. Disulfide formation was monitored by ^{1}H NMR spectroscopy and quantified using 1,3,5-trimethoxy benzene as an internal standard.

General procedures for catalyst screen. In a drybox, a 3-neck round bottom flask was charged with a magnetic stir bar, precatalyst (0.225 mmol, 0.10 equiv) and anhydrous CH_3CN (15 mL). To the solution was added tetrabutylammonium bromide (0.218 g, 0.675 mmol, 0.045 M), *p*-tolualdehyde (0.27 mL, 2.25 mmol, 1.0 equiv), and 1,3-

bis(2,4,6-trimethylphenylimidazolinium chloride (0.077 g, 0.225 mmol, 0.10 equiv). The electrode leads were fitted through rubber septa and the electrodes inserted into the flask. The flask was sealed with the rubber septa, and the electrochemical cell was then removed from the dry box and placed under a positive pressure of N_2. To the stirred solution was added 1-butane thiol (0.48 mL, 4.50 mmol, 2.0 equiv) and DMAP (0.138 g, 1.13 mmol, 0.50 equiv). The electrodes were connected to the potentiostat and bulk electrolysis was started with constant stirring.

Aliquots (0.1 mL) were removed with a disposable syringe, a known quantity of 1,3,5-trimethoxybenzene was added as an internal standard, and the mixture was analyzed by ^{1}H NMR spectroscopy in $CDCl_3$ and GC-MS. See **Table 1.6** for results.

Table 1.6: Catalyst screen

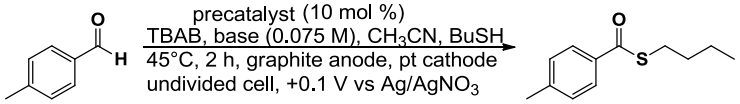

precatalyst	base (0.075 M)	% thioester	% disulfide
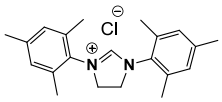	DMAP	<1	0
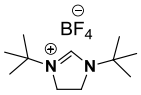	NEt_3	0	0
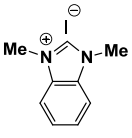	NEt_3	0	0
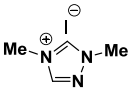	NEt_3	0	0

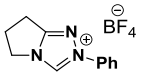	DMAP	3	4
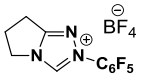	DMAP	5	7
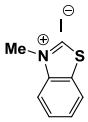	NEt_3	0	5
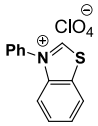	DMAP	1	0
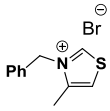	DMAP	4	3
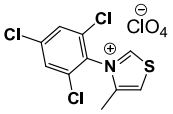	DMAP	9	4
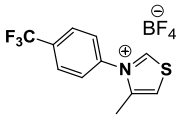	DMAP	0	12
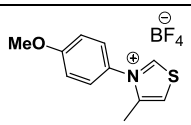	DMAP	2	6
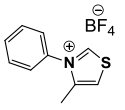	DMAP	1	3
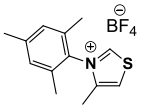	DMAP	11	4

General procedures for base screen. In the drybox, a 3-neck round bottom flask was charged with a magnetic stir bar, **A** (0.069 g, 0.225 mmol, 0.10 equiv) and anhydrous CH_3CN (15 mL). To the solution was added tetrabutylammonium bromide (0.218 g 0.675

mmol, 0.045 M) and *p*-tolualdehyde (0.27 mL, 2.25 mmol, 1.0 equiv). The electrode leads were fitted through rubber septa and the electrodes inserted into the flask. The flask was sealed with the rubber septa, and the electrochemical cell was then removed from the dry box and placed under a positive pressure of N_2. To the stirred solution was added 1-butane thiol (0.48 mL, 4.50 mmol, 2.0 equiv) and base (2.25 mmol, 1.0 equiv 1.13 mmol, 0.5 equiv). The electrodes were connected to the potentiostat and bulk electrolysis was started with constant stirring.

Aliquots (0.1 mL) were removed with a disposable syringe, a known quantity of 1,3,5-trimethoxybenzene was added as an internal standard, and the mixture was analyzed by ^{1}H NMR spectroscopy in $CDCl_3$ and GC-MS.

General procedures for cyclic voltammetry. In the drybox, a 3-neck round bottom flask was charged with a magnetic stir bar and anhydrous CH_3CN (15 mL), tetrabutylammonium tetrafluoroborate (0.494 g, 1.50 mmol, 0.10 M), and substrate (0.023 g, 0.075 mmol, 5.0 mM) were added (sodium butane thiolate was made in situ with 8 µL 1-butane thiol and 19 mg 95% NaH, 0.075 mmol, 5.0 mM). The flask was equipped with a glassy carbon anode (3 mm diameter), Pt basket cathode, and $Ag/AgNO_3$ reference electrode (0.01 M $AgNO_3$/0.1 M tetrabutylammonium tetrafluoroborate in CH_3CN) and then the apparatus was sealed using rubber septa. The electrochemical cell was then removed from the drybox and the solution was placed under a positive pressure of N_2 and stirred at room temperature. Stirring was stopped prior to connecting to the potentiostat. The cyclic voltammogram was typically taken

with a sweep rate of 0.10 V/s. Ferrocene (0.15 mmol) was added as an internal standard after each voltammogram.[66] All potentials are reported in V vs. SCE. See **Figure 1.12 – 1.14**.

Figure 1.12: Cyclic voltammogram of 4-methyl-3-(2,4,6-trimethylphenyl) thiazolium tetrafluoroborate (**A**).

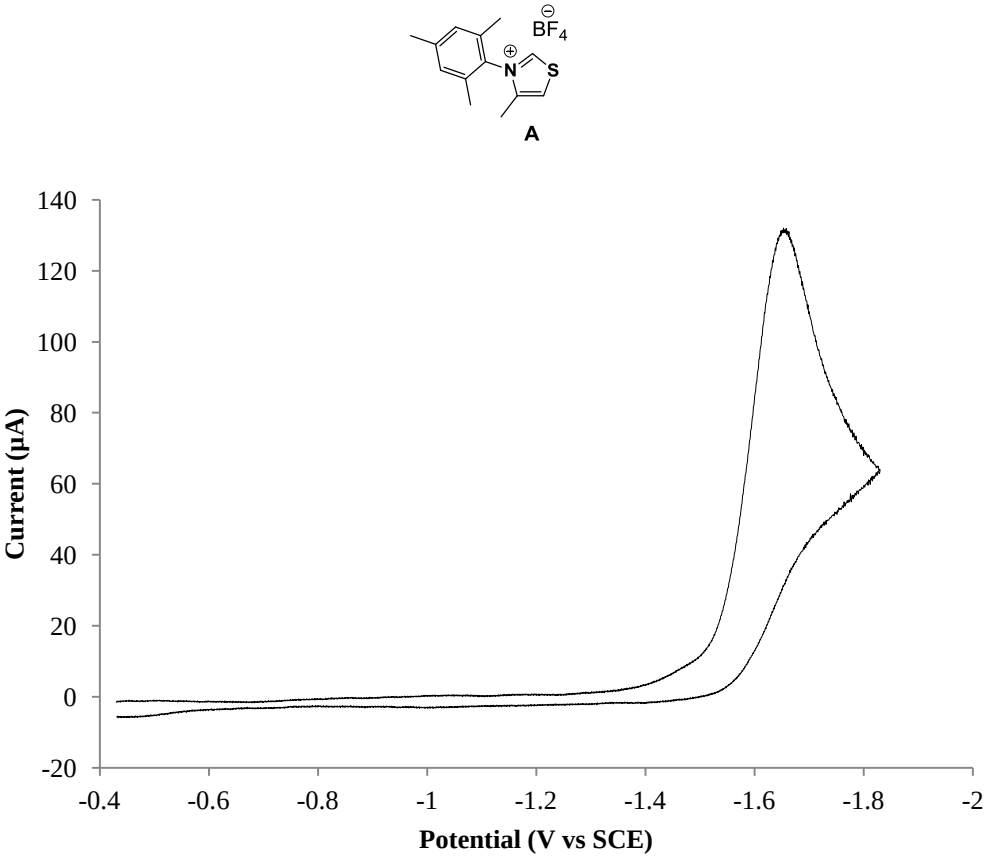

Figure 1.13: Cyclic voltammogram of 1-butane thiol.

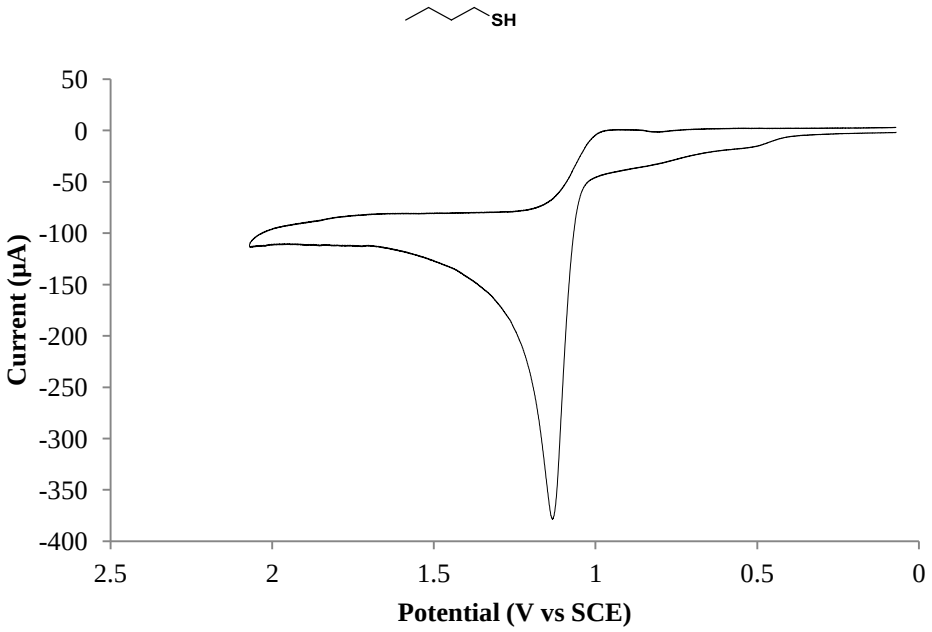

Figure 1.14: Cyclic voltammogram of sodium 1-butane thiolate.

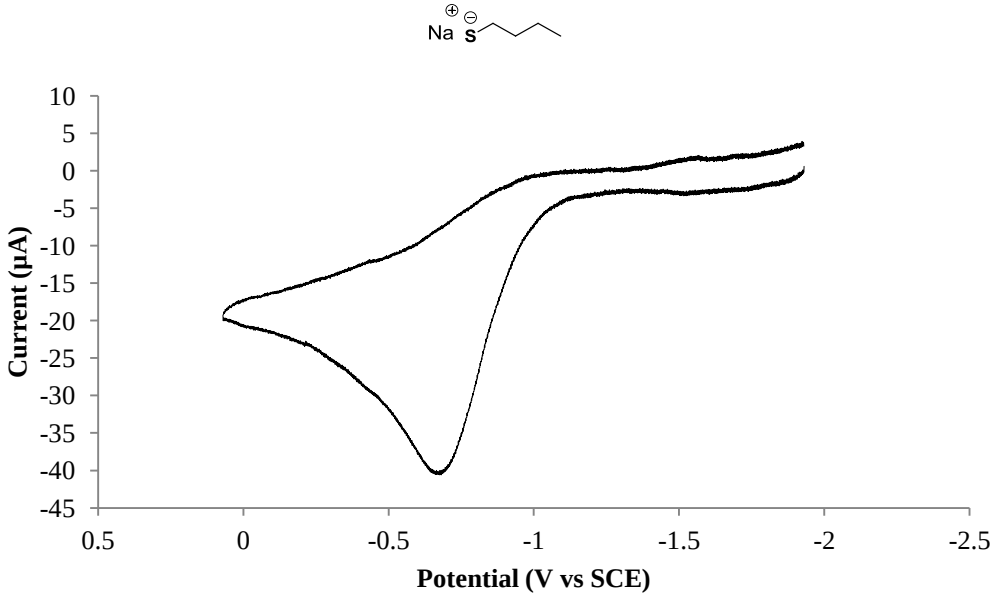

Notes and References to Chapter 1

[1] For recent reviews, see: (a) Francke, R.; Little, R. D. *Chem. Soc. Rev.* **2014**, *43*, 2492. (b) Yoshida, J.-i.; Ashikari, Y.; Matsumoto, K.; Nokami, T. *J. Synth. Org. Chem., Jpn.* **2013**, *71*, 1136. (c) Savéant, J. M. *Chem. Rev.* **2008**, *108*, 2348. (d) Yoshida, J.-i.; Kataoka, K.; Horcajada, R.; Nagaki, A. *Chem. Rev.* **2008**, *108*, 2265. (e) Tang, F.; Chen, C.; Moeller, K. D. *Synthesis* **2007**, *21*, 3411. (f) Sperry, J. B.; Wright, D. L. *Chem. Soc. Rev.* **2006**, *35*, 605. (g) Moinet, C.; Hurvois, J.-P.; Jutand, A. *Adv. Org. Synth.* **2005**, *1*, 403. (h) Little, R. D.; Moeller, K. D. *Electrochem. Soc. Interface* **2002**, *11*, 36. (i) Ogibin, Y. N.; Nikishin, G. I. *Russ. Chem. Rev.* **2001**, *70*, 543. (j) Bard, A. J.; Faulkner, L. R. *Electrochemical Methods Fundamentals and Applications*, 2nd ed.; John Wiley & Sons, Inc.: New York, NY, 2001. (k) *Organic Electrochemistry*, 4th ed., Lund, H.; Hammerich, O. Eds., M. Dekker, New York, NY, 2001. (l) Moeller, K. D. *Tetrahedron* **2000**, *56*, 9527.

[2] Yoshida, J.-i.; Takada, K.; Ishichi, Y.; Isoe, S. *J. Chem. Soc., Chem. Commun.* **1994**, 2361.

[3] Note that while significant developments in EOC have been made in the area of cathodic reductions, we are not aware of any demonstrations of *organocatalyzed* variants. For examples of bulk cathodic reduction, see: reference 1 and Kulisch, J.; Nieger, M.; Stecker, F.; Fischer, A.; Waldvogel, S. R. *Angew. Chem., Int. Ed*. **2011**, *50*, 5564.

[4] For an example involving hydrogen bonding organocatalysis in parallel with cathodic reduction, see: Costero, A. M.; Rodríguez-Muñiz, G. M.; Gaviña, P.; Gil, S.; Domenech, A. *Tetrahedron Lett.* **2007**, *48*, 6992.

[5] For other examples of integrated electrosynthesis, see: (a) Ashikari, Y.; Kiuchi, Y.; Takeuchi, T.; Ueoka, K.; Suga, S.; Yoshida, J.-i. *Chem. Lett.* **2014**, *43*, 210. (b) Morofuji, T.; Shimizu, A.; Yoshida, J.-i. *J. Am. Chem. Soc.* **2014**, *136*, 4496. (c) Morofuji, T.; Shimizu, A.; Yoshida, J.-i. *J. Am. Chem. Soc.* **2013**, *135*, 5000. (d) Ashikari, Y.; Nokami, T.; Yoshida, J.-i. *J. Am. Chem. Soc.* **2011**, *133*, 11840.

[6] (a) Xu, H. C.; Moeller, K. D. *J. Am. Chem. Soc.* **2010**, *132*, 2839. (b) Tanaka, H.; Tokumaru, Y.; Fukui, K.-i.; Kuroboshi, M.; Torii, S.; Jutand, A.; Amatore, C. *Synthesis* **2009**, 3449. (c) Matsumoto, K.; Fujie, S.; Ueoka, K.; Suga, S.; Yoshida, J.-i. *Angew. Chem., Int. Ed.* **2008**, *47*, 2506. (d) Cao, Y.; Hidaka, A.; Tajima, T.; Fuchigami, T. *J. Org. Chem.* **2005**, *70*, 9614. (e) Suzuki, S.; Matsumoto, K.; Kawamura, K.; Suga, S.; Yoshida, J.-i. *Org. Lett.* **2004**, *6*, 3755. (f) Sun, Y.; Moeller, K. D. *Tetrahedron Lett.* **2002**, *43*, 7159. (g) Chiba, K.; Uchiyama, R.; Kim, S.; Kitano, Y.; Tada, M. *Org. Lett.* **2001**, *3*, 1245. (h) Yoshida, J.-i.; Sugawara, M.; Tatsumi, M.; Kise, N. *J. Org. Chem.* **1998**, *63*, 5950. (i) Sugawara, M.; Mori, K.; Yoshida, J.-i. *Electrochim. Acta* **1997**, *42*, 1995. (j) Yoshida, J.-i.; Sugawara, M.; Kise, N. *Tetrahedron Lett.* **1996**, *37*, 3157.

[7] (a) Yoshida, J.-i.; Watanabe, M.; Toshioka, H.; Imagawa, M.; Suga, S. *J. Electroanal. Chem.* **2001**, *507*, 55. (b) Jinno, M.; Kitano, Y.; Tada, M.; Chiba, K. *Org. Lett.* **1999**, *1*, 435. (c) Yoshida, J.-i.; Nishiwaki, K. *J. Chem. Soc. Dalton. Trans.* **1998**, 2589. (d)

Yoshida, J.-i.; Izawa, M. *J. Am. Chem. Soc.* **1997**, *119*, 9361. (e) Glass, R.; Guo, Q.; Liu, Y. *Tetrahedron* **1997**, *53*, 12273. (f) Yoshida, J.-i.; Ishichi, Y.; Nishiwaki, K.; Shiozawa, S.; Isoe, S. *Tetrahedron Lett.* **1992**, *33*, 2599. (g) Glass, R.; Radspinner, A.M.; Singh, W. P. *J. Am. Chem. Soc.* **1992**, *114*, 4921.

[8] (a) Kesselring, D.; Maurer, K.; Moeller, K. D. *Org. Lett.* **2008**, *10*, 2501. (b) Sun, H.; Martin, C.; Kesselring, D.; Keller, R.; Moeller, K. D. *J. Am. Chem. Soc.* **2006**, *128*, 13761. (c) Suga, S.; Suzuki, S.; Yoshida, J.-i. *Org. Lett.* **2005**, *7*, 4717. (d) Suga, S.; Watanabe, M.; Yoshida, J.-i. *J. Am. Chem. Soc.* **2002**, *124*, 14824. (e) Suga, S.; Suzuki, S.; Yamamoto, A.; Yoshida, J.-i. *J. Am. Chem. Soc.* **2000**, *122*, 10244. (f) Yoshida, J.-i.; Suga, S.; Fuke, K.-i.; Watanabe, M. *Chem. Lett.* **1999**, 251. (g) Yoshida, J.-i.; Maekawa, T.; Murata, T.; Matsunaga, S.-i.; Isoe, S. *J. Am. Chem. Soc.* **1990**, *112*, 1962.

[9] (a) Yamaguchi, Y.; Okada, Y.; Chiba, K. *J. Org. Chem.* **2013**, *78*, 2626. (b) Redden, A.; Perkins, R. J.; Moeller, K. D. *Angew. Chem., Int. Ed.* **2013**, *52*, 12865. (c) Okada, Y.; Akaba, R.; Chiba, K. *Org. Lett.* **2009**, *11*, 1033. (d) Tang, F.; Moeller, K. D. *Tetrahedron* **2009**, 65, 10863.

[10] Yoshida, J.-i.; Morita, Y.; Itoh, M.; Ishichi, Y.; Isoe, S. *Synlett* **1992**, 843.

[11] (a) Takahashi, K.; Furusawa, T.; Swamura, T.; Kuribayashi, S.; Inagi, S.; Fuchigami, T. *Electrochim. Acta* **2012**, *77*, 47. (b) Park, Y. S.; Little, R. D. *Electrochim. Acta* **2009**, *54*, 5077. (c) Park, Y. S.; Little, R. D. *J. Org. Chem.* **2008**, *73*, 6807. (d) Park, Y. S.; Wang, S. C.; Tantillo, D. J.; Little, R. D. *J. Org. Chem.* **2007**, *72*, 4351. (e) Wu, X.; Davis, A. P.; Fry, A. J. *Org. Lett.* **2007**, *9*, 5633. (f) Shen, Y.; Hattori, H.; Ding, K.; Atobe, M.; Fuchigami, T.; *Electrochim. Acta* **2006**, *51*, 2819. (g) Shen, Y.; Suzuki, K.; Atobe, M.; Fuchigami, T. *J. Electroanal. Chem.* **2003**, *540*, 189. (h) Fuchigami, T.; Tetsu, M.; Tajima, T.; Ishii, H. *Synlett* **2001**, 1269. (i) Gunic, J.; Tabakovic, I. *Electrochim. Acta* **1990**, *35*, 225. (j) Grosse K. H.; Brinkhaus, Steckhan, E. *Tetrahedron* **1986**, *42*, 553.

[12] (a) Francke, R.; Little, R. D. *J. Am. Chem. Soc.* **2014**, *136*, 427. (b) Zhang, N.-T.; Zeng, C.-C.; Lam, C. M.; Gbur, R. K.; Little, R. D. *J. Org. Chem.* **2013**, *78*, 2104. (c) Zeng, C.-C.; Zhang, N.-T.; Lam, C. M.; Little, R. D. *Org. Lett.* **2012**, *14*, 1314.

[13] (a) Li, C.; Zeng, C.-C.; Hu, L.-M.; Yang, F.-L.; Yoo, S. J.; Little, R. D. *Electrochim. Acta* **2013**, *114*, 560. (b) Inokuchi, T.; Matsumoto, S.; Tsuji, M.; Torii, S. *J. Org. Chem.* **1992**, *57*, 5023. (c) Semmelhack, M. F.; Schmid, C. R. *J. Am. Chem. Soc.* **1983**, *105*, 6732. (d) Semmelhack, M. F.; Chou, C. S.; Cortes, D. A. *J. Am. Chem. Soc.* **1983**, *105*, 4492.

[14] A related, but distinct concept involves parallel anodic oxidation and organocatalysis. For example, see: Jensen, K.; Franke, P. T.; Nielsen, L. T.; Daasbjerg, K.; Jørgensen, A. K. *Angew. Chem., Int. Ed.* **2009**, *49*, 129.

[15] Chiba, T.; Okimoto, M.; Nagai, H.; Takata, Y. *Bull. Chem. Soc. Jpn.* **1982**, *55*, 335.

[16] Corey, E. J.; Gilman, N. W.; Ganem, B. E. *J. Am. Chem. Soc.* **1968**, *90*, 5616.

[17] Bui, N.-N; Ho, X.-H.; Mho, S.-i.; Jang, H.-Y. *Eur. J. Org. Chem.* **2009**, 5309.

[18] (a) Kim, H.; MacMillan, D. W. C. *J. Am. Chem. Soc.* **2008**, *130*, 398. (b) Jang, H.-Y.; Hong, J.-B.; MacMillan, D. W. C. *J. Am. Chem. Soc.* **2007**, *129*, 7004. (c) Beeson, T. D.; Mastracchio, A.; Hong, J.-B.; Ashton, K.; MacMillan, D. W. C. *Science* **2007**, *316*, 582.
[19] Sibi, M.- P.; Hasegawa, M. *J. Am. Chem. Soc.* **2007**, *129*, 4124.
[20] Schämann, M.; Schäfer, H. J. *Electrochim. Acta* **2005**, *50*, 4956.
[21] Ho, X.-H.; Mho, S.-i.; Kang, H.; Jang, H.-Y. *Eur. J. Org. Chem.* **2010**, 4436.
[22] (a) Nagib, D. A.; Scott, M. E.; MacMillan, D. W. C. *J. Am. Chem. Soc.* **2009**, *131*, 10875. (b) Nicewicz, D. A.; MacMillan, D. W. C. *Science*, **2008**, *322*, 77.
[23] Benfatti, F.; Capdevila, M. G.; Zoli, L.; Benedetto, E.; Cozzi, P. G. *Chem. Commun.* **2009**, 5919.
[24] For reviews focusing on NHC-catalyzed oxidative transformations, see: (a) De Sarkar, S.; Biswas, A.; Samanta, R. C.; Studer, A. *Chem. Eur. J.* **2013**, *19*, 4664. (b) Maki, B. E.; Chan, A.; Phillips, E. M.; Scheidt, K. A. *Tetrahedron* **2009**, *65*, 3102. (c) Ekoue-Kovi, K.; Wolf, C. *Chem. Eur. J.* **2008**, *14*, 6302.
[25] Breslow, R. *J. Am. Chem. Soc.* **1958**, *80*, 3719.
[26] Tam-Chang, S.-W.; Jimenez, L.; Diederich, F. *Helv. Chim. Acta* **1993**, *76*, 2616. (b) Tam, S.-W.; Jimenez, L.; Diederich, F. *J. Am. Chem. Soc.* **1992**, *114*, 1503.
[27] Finney, E. E.; Ogawa, K. A.; Boydston, A. J. *J. Am. Chem. Soc.* **2012**, *134*, 12374.
[28] (a) DiRocco, D. A.; Oberg, K. M.; Rovis, T. *J. Am. Chem Soc.* **2012**, *134*, 6143. (b) Nakanishi, I.; Itoh, S.; Fukuzumi, S. *Chem. Eur. J.* **1999**, *5*, 2810. (c) Barletta, G.; Chung, A. C.; Rios, C. B.; Jordan, F.; Schlegel, J. M. *J. Am. Chem. Soc.* **1990**, *112*, 8144.
[29] For electrochemical oxidation of aldehydes to esters via hemiacetal intermediates using halide mediators, see: (a) Shono, T.; Matsumura, Y.; Hayashi, J.; Inoue, K.; Iwasaki, F.; Itoh, T. *J. Org. Chem.* **1985**, *50*, 4967. (b) Okimoto, M.; Chiba, T. *J. Org. Chem.* **1988**, *53*, 218.
[30] Shimakawa, Y.; Morikawa, T.; Sakaguchi, S. *Tetrahedron Lett.* **2010**, *51*, 1786.
[31] Vaska, L.; DiLuzio, J. W. *J. Am. Chem. Soc.* **1969**, *84*, 679.
[32] Yang, J. Y.; McEwen, W. E.; Kleinberg, J. *J. Am. Chem. Soc.* **1958**, *80*, 4300.
[33] (a) Biswas, A.; De Sarkar, S.; Tebben, L.; Studer, A. *Chem. Commun.* **2012**, *48*, 5190. (b) Lee, K.; Kim, H.; Hong, J. *Angew. Chem. Int. Ed.* **2012**, *51*, 5735. (c) Kuwano, S.; Harada, S.; Oriez, R.; Yamada, K.-i. *Chem. Commun.* **2012**, *48*, 145. (d) De Sarkar, S.; Grimme, S.; Studer, A. *J. Am. Chem. Soc.* **2010**, *132*, 1190. (e) Goswami, S.; Hazra, A. *Chem. Lett.* **2009**, *38*, 484. (f) Yoshida, M.; Katagiri, Y.; Zhu, W.-B.; Shishido, K. *Org. Biomol. Chem.* **2009**, *7*, 4062. (g) Wong, F. T.; Patra, P. K.; Seayad, J.; Zhang, Y.; Ying, J. Y. *Org. Lett.* **2008**, *10*, 2333. (h) Maki, B. E.; Scheidt, K. A. *Org. Lett.* **2008**, *10*, 4331. (i) Noonan, C.; Baragwanath, L.; Connon, S. J. *Tetrahedron Lett.* **2008**, *49*, 4003. (j) Guin, J.; De Sarkar, S.; Grimme, S.; Studer, A. *Angew. Chem. Int. Ed.* **2008**, *47*, 8727. (k) Liu, Y.-K.; Li, R.; Yue, L.; Li, B.-J.; Chen, Y.-C.; Wu, Y.; Ding, L.-S. *Org. Lett.* **2006**, *8*, 1521. (l) Miyashita, A.; Suzuki, Y.; Nagasaki, I.; Ishiguro, C.; Iwamoto, K.-i.; Higashino, T. *Chem. Pharm. Bull.* **1997**, *45*, 1254.

[34] For a recent review, see: Vora, H. U.; Wheeler, P.; Rovis, T. *Adv. Synth. Catal.* **2012**, *354*, 1617. For excellent recent examples, see: (a) Zhang, B.; Feng, P.; Cui, Y.; Jiao, N. *Chem. Commun.* **2012**, *48*, 7280. (b) Feroci, M.; Chiarotto, I.; Orsini, M.; Pelagalli, R.; Inesi, A. *Chem. Commun.* **2012**, *48*, 5361. (c) Zhao, Y.-M.; Tam, Y.; Wang, Y.-J.; Li, Z.; Sun, J. *Org. Lett.* **2012**, *14*, 1398. (d) Sohn, S. S.; Bode, J. W. *Angew. Chem. Int. Ed.* **2006**, *45*, 6021. (e) Chan, A.; Scheidt, K. A. *Org. Lett.* **2005**, *7*, 905. (f) Reynolds, N.; Alaniz, J.; Rovis, T. *J. Am. Chem. Soc.* **2004**, *126*, 9518. (g) Sohn, S. S.; Rosen, E. L.; Bode, J. W. *J. Am. Chem. Soc.* **2004**, *126*, 14370. (h) Chow, K. Y.-K.; Bode, J. W. *J. Am. Chem. Soc.* **2004**, *126*, 8126.

[35] (a) Chiang, P.-C.; Bode, J. W. in *N-Heterocyclic Carbenes: From Laboratory Curiosities to Efficient Synthetic Tools*; Díez-Gonzáles, S.; Ed.; RSC Catalysis Series No. 6; Royal Society of Chemistry: Cambridge, 2010; pp 399-435. (b) Moore, J. L.; Rovis, T. *Top. Curr. Chem.* **2009**, *291*, 77. (c) Enders, D.; Niemeier, O., Henseler, A. *Chem. Rev.* **2007**, *107*, 5606.

[36] Frey, D. A.; Wu, N.; Moeller, K. D. *Tetrahedron Lett.* **1996**, *37*, 8317.

[37] For selected recent examples, see: (a) Möhlmann, L.; Ludwig, S.; Blechert, S. *Beilstein J. Org. Chem.* **2013**, *9*, 602. (b) Toledo, H.; Pisarevsky, E.; Abramovich, A.; Szpilman, A. M. *Chem. Commun.* **2013**, *49*, 4367. (c) Thai, K.; Wang, L.; Dudding, T.; Bilodeau, F.; Gravel, M. *Org. Lett.* **2010**, *12*, 5708. (d) De Sarkar, S.; Studer, A. *Org. Lett.* **2010**, *12*, 1992. (e) Lin, L.; Li, Y.; Du, W.; Deng, W.-P. *Tetrahedron Lett.* **2010**, *51*, 3571. (f) Wong, F. T.; Patra, P. K.; Seayad, J.; Zhang, Y.; Ying, J. Y. *Org. Lett.* **2008**, *10*, 2333. (g) Bode, J. W.; Sohn, S. S. *J. Am. Chem. Soc.* **2007**, *129*, 13798. (h) Vora, H. U.; Rovis, T. *J. Am. Chem. Soc.* **2007**, *129*, 13796. (i) Li, G.-Q.; Li, Y.; Dai, L.-X.; You, S.-L. *Org. Lett.* **2007**, *9*, 3519. (j) Lin, L.; Li, Y.; Du, W.; Deng, W.-P. *Tetrahedron Lett.* **2010**, *51*, 3571.

[38] For examples of NHC-catalyzed thioesterification of aldehydes, see: (a) Zhu, X.; Shi, Y.; Mao, H.; Cheng, Y.; Zhu, C. *Adv. Synth. Catal.* **2013**, *355*, 3558. (b) Ji, M.; Wang, X.; Lim, Y. N.; Kang, Y.-W.; Jang, H.-Y. *Eur. J. Org. Chem.* **2013**, 7881. (c) Uno, T.; Inokuma, T.; Takemoto, Y. *Chem. Commun.* **2012**, *48*, 1901. (d) Singh, S.; Yadav, L. D. S. *Tetrahedron Lett.* **2012**, *53*, 5136. (e) Sohn, S. S.; Bode, J. W. *Angew. Chem. Int. Ed.* **2006**, *45*, 6021. (f) Kageyama, Y.; Murata, S. *J. Org. Chem.* **2005**, *70*, 3140.

[39] (a) Kent, S. B. H. *Angew. Chem. Int. Ed.* **2013**, *52*, 11988. (b) Modha, S. G.; Mehta, V. P.; Van der Eycken, E. V. *Chem. Soc. Rev.* **2013**, *42*, 5042. (c) Wang, P.; Danishefsky, S. J. *J. Am. Chem. Soc.* **2010**, *132*, 17045. (d) Matsuo, K.; Shindo, M. *Org. Lett.* **2010**, *12*, 5346. (e) Crich, D.; Sharma, I. *Angew. Chem. Int. Ed.* **2009**, *48*, 2355. (f) Crich, D.; Sasaki, K. *Org. Lett.* **2009**, *11*, 3514. (g) Li, H.; Yang, H.; Liebeskind, L. S. *Org. Lett.* **2008**, *10*, 4375. (h) Utsumi, N.; Kitagaki, S.; Barbas, C. F. III *Org. Lett.* **2008**, *10*, 3405. (i) Alonso, D. A.; Kitagaki, S.; Utsumi, N.; Barbas, C. F. III *Angew. Chem. Int. Ed.* **2008**, *47*, 4588. (j) Yang, H.; Li, H.; Wittenberg, R.; Egi, M.; Huang, W.; Liebeskind, L. S. *J. Am. Chem. Soc.* **2007**, *129*, 1132. (k) Iimura, S.; Manabe, K.; Kobayashi, S. *Org. Lett.*

2003, *5*, 101. (l) Dawson, P. E.; Kent, S. B. H. *Annu. Rev. Biochem.* **2000**, *69*, 923. (m) Dawson, P. E.; Muir, T. W.; Clark-Lewis, I.; Kent, S. B. H. *Science* **1994**, *266*, 776.
[40] Rastetter, W. H.; Adams, J.; Frost, J.W.; Nummy, L. J.; Frommer, J. E.; Roberts, K. B. *J. Am. Chem. Soc.* **1979**, *101*, 2752.
[41] Hirano, K.; Piel, I.; Glorius, F. *Adv. Synth. Cat.* **2008**, *350*, 984.
[42] Cesati, R. R.; Cheesman, E. H.; Lazewatsky, J.; Radeke, H. S.; Castner, J. F.; Mongeau, E.; Zdankiewicz, D. D.; Siegler, R. W.; Devine, M. Methods and Apparatus for Synthesizing Imaging Agents, and Intermediates Thereof. PCT WO2011097649, Aug 11, 2011.
[43] Screiber, S. L.; Shair, M. D.; Tan, D. S.; Foley, M. A.; Stockwell, B. R. Synthesis of Combinatorial Libraries of Compounds Reminiscent of Natural Products. U.S. Patent 6,448,443, Sep 10, 2002.
[44] Nowrouzi, N.; Mehranpour, A.; Rad, J. *Tetrahedron* **2010**, *66*, 9596.
[45] Kadkin, O.; Osajda, K.; Kaszynski, P.; Barber, T. *J. Poly. Sci. A: Poly. Chem.* **2003**, *141*, 1114.
[46] Bose, A.; Manhas, M.S.; Chib, J.S.; Chawla, H.P.S.; Dayal, B. *J. Org. Chem.* **1974**, *39*, 2877.
[47] Chia, C.S.; Taylor, M.; Dua, S.; Blanksby, S.; Bowie, J. *J. Chem. Soc., Perkin Trans. 2* **1998**, 1435.
[48] Chau, W.; Turner, R.; Braslau, R. *React. Funct. Poly.* **2008**, *68*, 396.
[49] Shono, T.; Ishige, O.; Uyama, H.; Kashimura, S. *J. Org. Chem.* **1986**, *51*, 546.
[50] Lin, L.; Li, Y.; Du, W.; Deng, W. *Tetrahedron. Lett.* **2010**, *51*, 3571.
[51] Garcia, L.; Arias, E.; Moggio, I.; Romero, J.; Ledezmna, A.; Ponce, A.; Perez, O. *Polymer* **2011**, *52*, 5326.
[52] Ochiai, M.; Yoshimura, A.; Hoque, M.; Okubo, T.; Saito, M.; Miyamoto, K. *Org. Lett.* **2011**, *13*, 5568.
[53] Guin, J.; De Sarkar, S.; Grimme, S.; Studer, A. *Angew. Chem., Int. Ed.* **2008**, *47*, 1.
[54] Imashiro, R.; Seki, M. *J. Org. Chem.* **2004**, *69*, 4216.
[55] Rivero-Cruz, B.; Rivero-Cruz, I.; Rodriguez-Sotres, R.; Mata, R. *Phytochemistry* **2007**, *68*, 1147.
[56] Xie, L.; Wang, Z. *Angew. Chem., Int. Ed.* **2011**, *50*, 4901.
[57] Lam, K.; Marko, I. *Tetrahedron* **2009**, *65*, 10930.
[58] Clennan, E. L.; Speth, D. R.; Bartlett, P. D. *J. Org. Chem.* **1983**, *48*, 1246–1250.
[59] Connelly, N. G.; Geiger, W. E. *Chem. Rev.* **1996**, *96*, 877.
[60] Hasnip, S.; Duckett, S.; Sleigh, C.; Taylor, D.; Barlow, G.; Taylor, M. *Chem. Commun.* **1999**, 1717.
[61] Burk, M.; McGrath, M.; Wheeler, R.; Crabtree, R. *J. Am. Chem. Soc.* **1988**, *110*, 5034.
[62] Rahim, M.; Ahmed, K. *Inorg. Chem.* **1994**, *33*, 3003.
[63] Inoue, T.; Takeda, T.; Kambe, N.; Ogawa, A.; Ryu, I.; Sonoda, N. *J. Org. Chem.* **1994**, *59*, 5824.

[64] Watson, D.; Fan, X.; Buchwald, S. *J. Org. Chem.* **2008,** *73*, 7096.
[65] Takido, T.; Sato, K.; Nakazawa, T.; Seno, M. *Sulfur Letters* **1995**, *19*, 67.
[66] Connelly, N. G.; Geiger, W. E. *Chem. Rev.* **1996**, *96*, 877.

Chapter 2 – Electrochemistry of Azolium/Azolinium Salts[4]

Section 1: Introduction

Figure 2.1: Generalized structures of azolium and azolinium cations used in this study.

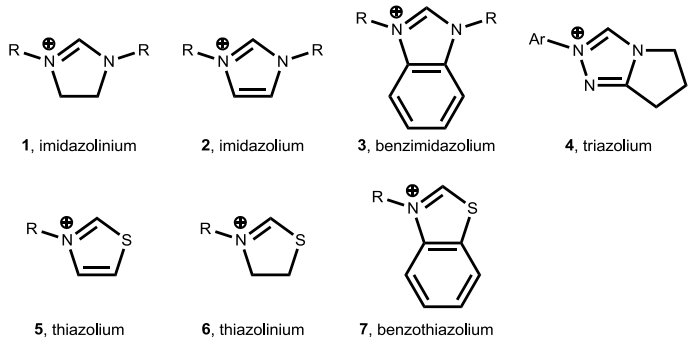

The azolium cation (**Figure 2.1**) is a versatile centerpiece for multiple applications in organic chemistry. Of particular note is their use as synthetic precursors to *N*-heterocyclic carbenes (NHCs),[1,2] ionic liquids for various synthetic reactions[3] and electrochemical procedures,[4] redox reagents or mediators,[5] and building blocks for organic materials.[6] The electrochemical behavior of azolium salts is thus of particular interest since it impacts each of these areas, and continued tabulation of redox properties of new azolium species is necessary to expand beyond this scope. For example, we recently observed undesirable thiolate oxidation by thiazolium-based NHC precursors, which may be avoided in future studies through judicious selection of azolium precatalysts based upon their reduction potentials.[5] Unfortunately, few studies have been reported on the electrochemical behavior of azolium salts, with specific noteworthy

[4] Reproduced with permission from Ogawa, K. A.; Boydston, A. J. "Electrochemical Characterization of Azolium Salts" *Chem. Lett.* **2014**, *43*, 907 – 909. Copyright 2014 The Chemical Society of Japan.

examples by Pichon, Clyburne, Coughlin, and Sun.[7] To our knowledge, C2-unsubstituted thiazolium salts, which are commonly used precursors to thiazolylidene-based NHCs, were not investigated. Moreover, *N*-aryl thiazolinium salts are unreported in the literature, although their *N*-alkyl counterparts have received limited attention.[2f,8] Herein, we describe a systematic comparison of reduction potentials of various classes of azolium cations, including a series of electronically varied thiazolium species, and introduce the first report of *N*-aryl thiazolinium salts.

Section 2: Results and Discussion

To address the paucity of reported thiazolinium compounds, we prepared *N*-aryl thiazolinium iodides **6a** and **6b** as depicted in **Scheme 2.1**. Previously reported *N*-alkyl thiazolinium salts, which were used as chiral ionic liquids and Brønsted acid catalysts, were prepared by alkylation of thiazoline precursors.[2f,8] It was not obvious to us, however, that this approach could be used to access the desired *N*-aryl analogues. Our initial attempts at synthesizing the *N*-aryl thiazolinium moieties via cyclization of 2-aminoethane thiols (**8**) with $(EtO)_3CH$ and Brønsted acids were unsuccessful,[9] as were double alkylation approaches via **9**, which are similar to those reported by Grubbs for the synthesis of imidazolinium salts.[10] A successful route was finally realized via iodine-catalyzed cyclization of **8** with $(EtO)_3CH$. This reaction is envisioned to be facilitated by stabilization of iodonium species via complexation with the orthoester, as described by Shono and coworkers.[11] This approach provided the desired thiazolinium iodides (**6**) in

moderate to good yields after purification by recrystallization, although attempts to improve the yield by increasing the amount of I_2 were not fruitful.

Scheme 2.1: Synthesis of thiazolinium iodides.

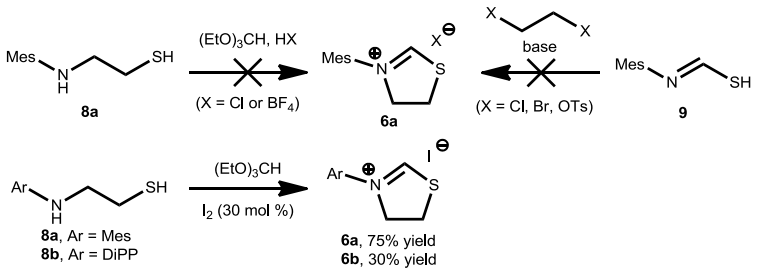

Mes = 2,4,6-trimethylphenyl, DiPP = 2,6-diisopropylphenyl.

Each of the thiazolinium iodides were characterized by single crystal X-ray diffraction analysis (**Figure 2.2**). The N-C-S bond angle in each thiazolinium ring was found to be ca. 122°, which is about 10° greater than that reported for thiazolium rings.[12] The C-S-C bond angles were found to be ca. 90°, which is consistent with reported thiazolium systems. Additionally, the bond lengths within the thiazolinium moieties were consistently longer than those reported in thiazolium analogues, as expected.

Figure 2.2: Molecular structures obtained via single crystal X-ray analysis of (left) 6a, and (right) 6b. Ellipsoids drawn at the 50% probability level, CH_2Cl_2 solvent molecules and iodide counter ions have been removed for clarity.

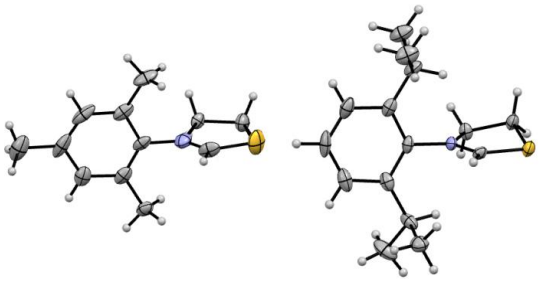

We evaluated the redox properties of each azolium salt in the series using cyclic voltammetry. Our setup involved an undivided cell, glassy carbon working electrode (3 mm diameter), platinum basket counter electrode, and $Ag/AgNO_3$ reference electrode. Each cyclic voltammogram (CV) was taken with a sweep rate of 100 mV/s. Measurements were carried out in CH_3CN (0.005 M in azolium salt) using Bu_4NBF_4 (0.10 M) as supporting electrolyte under N_2 atmosphere. Ferrocene (0.010 M) was added as an internal standard after CVs were collected. Irreversible reduction peaks were observed in the CVs of each azolium species, and representative examples are shown in **Figure 2.3**. The irreversibility is likely ascribed to one-electron reduction of the azolium species followed by rapid loss of hydrogen to give the corresponding NHC.

Figure 2.3: CVs of representative azolium salts, corrected to Fc/Fc+ redox couple (ferrocene added as an internal standard). Colors correspond to structures shown in figure 2.4.

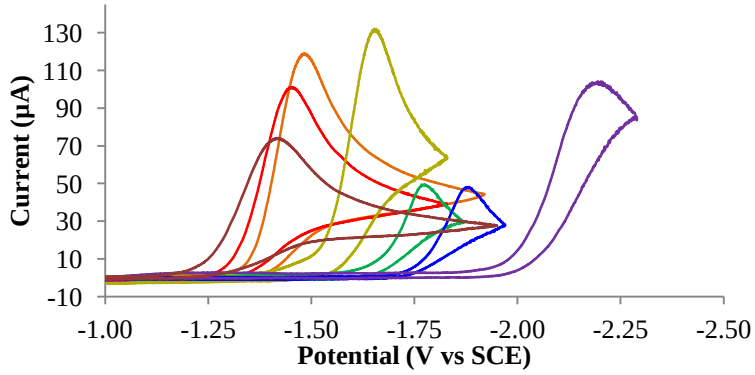

Interesting comparisons can be made from the series of azolium salts; a summary of the half-wave reduction potentials ($E_{1/2}$) are presented in **Figure 2.4** and tabulated in **Table 2.1**. We note that the relative order and values of $E_{1/2}$ were consistent with those observed by Pichon for the five classes of azolium species studied in common. For

example, benzannulation increases $E_{1/2}$ by ca. 200 mV when comparing imidazolium (**2**) to benzimidazolium (**3**), and thiazolium (**5a**) to benzothiazolium (**7a**) cations. In general, small (ca. 50 – 100 mV) shifts in $E_{1/2}$ were observed upon changing from *N*-alkyl to *N*-aryl groups within the same class of azolium species (cf. **5e** and **5h**), consistent with previous studies.[7c]

Interestingly, we discovered that the thiazoliniums **6a** and **6b** were easier to reduce than their unsaturated thiazolium counterparts with the same *N*-aryl groups (**5c** and **5d**). Specifically, the *N*-aryl thiazolinium salts displayed $E_{1/2}$ values of -1.42 and -1.45 V, whereas the *N*-aryl thiazolium cations showed $E_{1/2}$ values between -1.50 and -1.60 V. This was surprising to us considering the relative difficulty in reducing the corresponding saturated imidazolinium species **1**, which could not be reduced within the solvent window in our studies and those previously reported by Pichon. We speculate that this may indicate different secondary reaction rates following one-electron reduction of the varying classes of azolium cations.

Within the series of *N*-aryl thiazolium salts (**5a** – **j)**, a noticeable electronic influence was observed upon variation of the *N*-aryl ring. The *N*-phenyl thiazolium (**5h**) exhibits an $E_{1/2}$ of -1.50 V, and incorporation of inductively electron donating groups such as 2,6-diethylphenyl (DEP, **5b**), 2,4,6-trimethylphenyl (Mes, **5c**), and 2,6-diisopropylphenyl (DiPP, **5d**) shifts the $E_{1/2}$ ca. 100 mV more negative. In contrast, electron deficient 4-(trifluoromethyl)phenyl (**5i**) and 2,4,6-trichlorophenyl (**5j**) groups shifted the $E_{1/2}$ ca. 100 mV more positive. The > 200 mV range of $E_{1/2}$ values for this set is nearly as broad as

that observed across the span of benzothiazolium, thiazolinium, and thiazolium salts combined.

Figure 2.4: Half-wave reduction potentials of azolium salts (counterions omitted for clarity). Values in parentheses are $E_{1/2}$ values (V vs SCE) for the corresponding cation. Mes = 2,4,6-trimethylphenyl, DiPP = 2,6-diisopropylphenyl, PMP = *p*-methoxyphenyl, DEP = 2,6-diethylphenyl. Colors correspond to CVs in figure 2.3.

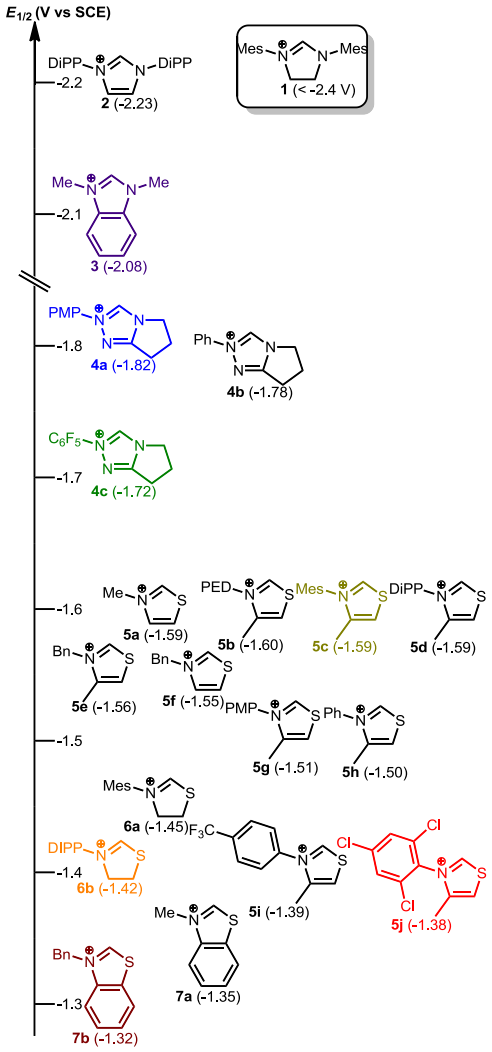

Somewhat surprisingly, incorporation of a *p*-methoxyphenyl (PMP) group at nitrogen (**5g**) resulted in little change in $E_{1/2}$ in comparison with the *N*-phenyl analogue (**5h**). This

result may be due to the inability of the **5g** system to adopt coplanarity of the *N*-aryl and thiazolium rings, due in part to the backbone methyl group of the latter. In contrast, PMP substitution on the triazolium (**4a**) did result in a more negative $E_{1/2}$ (-1.82 V) in comparison with phenyltriazolium analogue **4b** ($E_{1/2}$ = -1.78 V), which in turn was harder to reduce than pentafluorophenyl variant **4c** ($E_{1/2}$ = -1.72 V).

Table 2.1: Half-wave reduction potentials of azolium/azolinium salts.

azolium/azolinium class	compound	$E_{1/2}$ (V vs SCE)
imidazolinium	**1**	n.d.
imidazolium	**2**	-2.23
benzimidazolium	**3**	-2.08
triazolium	**4a**	-1.82
	4b	-1.78
	4c	-1.72
thiazolium	**5a**	-1.59
	5b	-1.60
	5c	-1.59
	5d	-1.59
	5e	-1.56
	5f	-1.55
	5g	-1.51
	5h	-1.50
	5i	-1.39
	5j	-1.38
thiazolinium	**6a**	-1.45
	6b	-1.42
benzothiazolium	**7a**	-1.35
	7b	-1.32

Section 3: Conclusions

In summary, the redox properties of a broad series of azolium salts were systematically investigated via cyclic voltammetry. The series includes several commonly used classes of azolium species for direct comparison, and an expanded set of thiazolium salts that demonstrate the extent to which electronic modification of the *N*-aryl moiety can be used to tune the reduction potential of the thiazolium ring. A new class of *N*-aryl thiazolinium salts were prepared and characterized by cyclic voltammetry and single crystal X-ray analysis. Saturation of the azolium backbone was found to have a significantly different effect on the thiazolium versus imidazolium moiety. Our electrochemical studies may aid in the development of azolium-based materials, NHC precatalysts, electrosynthesis of NHCs, and correlation of electrochemical properties and other fundamental reactivities.

Section 4: Experimental

General Considerations Acetonitrile (CH_3CN) was dried over calcium hydride and distilled prior to use. Electrochemical experiments were performed on a CH Instruments 1100B potentiostat using a 25 mL 3-neck round bottom flask as an undivided cell equipped with a glassy carbon working electrode (3 mm diameter), Pt counter electrode (Premier Lab Supply), and Ag/0.01 M $AgNO_3$ (0.1 M tetrabutylammonium tetrafluoroborate in CH_3CN) reference electrode. The 4-methyl-3-(2,4,6-trimethylphenyl)thiazolium, 3-(2,6-diisopropylphenyl)-4-methylthiazolium, 2-phenyl-

6,7-dihydro-5*H*-pyrrolo[2,1-*c*][1,2,4]triazol-2-ium, and 2-(4-methoxyphenyl)-6,7-dihydro-5*H*-pyrrolo[2,1-*c*][1,2,4]triazol-2-ium salts were prepared according to literature procedures.[13,14] All other reagents and solvents were obtained from commercial sources and stored in a drybox.

General procedures for the synthesis of thiazolium tetrafluoroborates. Procedures for the synthesis of *N*-aryl thiazolium perchlorate salts as reported by Glorius were used with some modifications.[1]

The corresponding aniline (94 mmol) and 20 M aqueous NaOH (96 mmol) were dissolved in 60 mL of dimethylsulfoxide (DMSO). The solution was cooled in an ice bath and carbon disulfide (94 mmol) was added dropwise. After addition of carbon disulfide, the ice bath was removed and the solution was stirred for 1 h. The solution was then cooled in an ice bath and chloroacetone (94 mmol) was added dropwise. After addition of chloroacetone, the ice bath was removed and stirred for 12 h. The solution was then cooled in an ice bath and 60 mL of water was added. The solids that precipitated upon addition of water were collected via filtration and dissolved in 90 mL of ethanol and 6 mL of hydrochloric acid. The resulting solution was heated at reflux for 1 hour and then placed in an ice bath. The solids that precipitated upon cooling were collected via filtration and suspended in 100 mL of glacial acetic acid. Hydrogen peroxide (300 mmol) was added dropwise and the solution was stirred at room temperature for 30 min. The solution was concentrated under reduced pressure and the resulting residue was dissolved in 50 mL of methanol. To this solution, sodium

tetrafluoroborate (395 mmol) in 150 mL of methanol/water (1:2 v/v) was added. The solution was then cooled in an ice bath and the solids that precipitated were collected via filtration. The solids were then dissolved in chloroform and any remaining solids were removed by filtration through a sintered glass funnel. The filtrate was concentrated under reduced pressure and dried on high vacuum to give the corresponding thiazolium tetrafluoroborate.

4-methyl-3-(2,4,6-trichlorophenyl) thiazolium tetrafluoroborate

Obtained in 39% yield. ^{1}H NMR (500 MHz, DMSO-d_6) δ = 10.63 (s, 1 H) 8.40 (s, 1 H) 8.22 (s, 2 H) 2.30 (s, 3 H). ^{13}C NMR (125 MHz, DMSO-d_6) δ = 163.7, 145.8, 137.9, 132.7, 130.5, 129.7, 123.9, 12.15.

4-methyl-3-(4-trifluoromethylphenyl) thiazolium tetrafluoroborate

Obtained in 21% yield. ^{1}H NMR (500 MHz, DMSO-d_6) δ = 10.43 (s, 1 H) 8.22 (s, 1 H) 8.13 (d, J = 10.0 Hz, 2 H) 8.02 (d, J = 5.0 Hz, 2 H) 2.34 (s, 3 H). ^{13}C NMR (125 MHz, DMSO-d_6) δ = 161.4, 146.1, 139.7, 131.6, 131.3, 127.8, 127.2, 122.0, 13.5.

4-methyl-3-(4-methoxyphenyl) thiazolium tetrafluoroborate

Obtained in 16% yield. ^{1}H NMR (500 MHz, DMSO-d_6) δ = 10.32 (s, 1 H) 8.17 (s, 1 H) 7.67 (d, J = 5.0 Hz, 2 H) 7.22 (d, J = 5.0 Hz, 2 H) 3.87 (s, 3 H) 2.32 (s, 3 H). ^{13}C NMR (125 MHz, DMSO-d_6) δ = 161.0, 160.7, 146.4, 129.2, 127.6, 121.4, 114.9, 55.8, 13.6.

4-methyl-3-(2,6-diethylphenyl) thiazolium tetrafluoroborate

Obtained in 56% yield. ^{1}H NMR (500 MHz, $CDCl_3$) δ = 9.82 (s, 1 H) 8.24 (s, 1 H) 7.56 (t, J = 10.0, 5.0 Hz, 1 H) 7.35 (d, J = 5.0 Hz, 2 H) 2.23 (s, 3 H) 2.20 (m, 2 H) 2.13 (m, 2

H) 1.13 (t, J = 10.0, 5.0 Hz, 6 H). ^{13}C NMR (125 MHz, $CDCl_3$) δ = 159.9, 146.7, 139.8, 133.5, 132.4, 127.9, 123.2, 23.8, 14.2, 13.5.

General procedures for the synthesis of 2-amino alcohols and their corresponding 2-aminoethyl iodides. Procedures for the synthesis of 2-aminoethanols and 2-aminoethyl iodides as reported by Gilberston were used.[15]

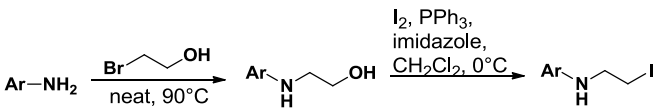

The corresponding aniline (120 mmol) and 2-bromoethanol (90 mmol) were heated to 90 °C for 12 h in a screw cap vial sealed with a Teflon-lined screw cap. The resulting solid was treated with saturated sodium bicarbonate ($NaHCO_3$) and extracted with ethyl acetate (2 × 50 mL). The organic layers were washed with water (3 x 100 mL) and dried over Na_2SO_4. The solvent was removed under reduced pressure and the resulting residue was purified by flash column chromatography (20:80 ethyl acetate:hexanes then 60:40 ethyl acetate:hexanes) to give the amino alcohol.

Triphenylphosphine (67 mmol), imidazole (67 mmol), and iodine (67 mmol) were dissolved in 100 mL of dry dichloromethane (CH_2Cl_2) under N_2 atmosphere and cooled in an ice bath. After this solution was stirred for 10 min, a solution of the amino ethanol (61 mmol) dissolved in 40 mL of dry CH_2Cl_2 was added. The resulting mixture was stirred for 45 min in an ice bath and then a saturated aqueous solution of $Na_2S_2O_3$ was added. The top layer was extracted with ether, washed with water, and dried over Na_2SO_4. The solvent was removed under reduced pressure and the resulting solid was

dissolved in a minimal amount of diethyl ether (Et_2O) and filtered through a plug of silica gel to give the 2-aminoethyl iodides. A small amount of triphenylphosphine oxide remained, and the mixture was used directly in the next step without further purification. Yields of thioacetates reported below are based upon the corresponding intermediate aminoethanols (reported over two steps).

General procedures for the synthesis of 2-aminoethyl thioacetates and their corresponding 2-amino ethane thiols.[16,17]

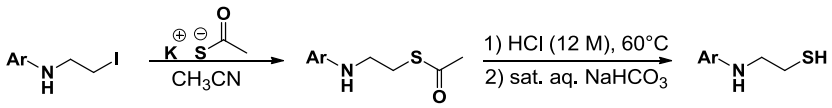

The corresponding 2-aminoethyl iodide (48 mmol) was dissolved in 150 mL of CH_3CN and then potassium thioacetate (56 mmol) was added. The resulting mixture was stirred for 1 h at room temperature and then diluted with water (100 mL). The organic layer was separated, washed with water (2 × 100 mL), and dried over Na_2SO_4 giving the pure 2-aminoethyl thioacetate.

The corresponding 2-aminoethyl thioacetate (47 mmol) was dissolved in 96 mL aq. HCl (12 M). The resulting mixture was heated at 60 °C under N_2 atmosphere for 12 h. The mixture was then removed from heat, neutralized with saturated aqueous $NaHCO_3$, and extracted with Et_2O. The organic layers were combined, washed with water (2 × 50 mL), and dried over Na_2SO_4. The Na_2SO_4 was filtered off from the organic layers. Then the solvent was removed under reduced pressure giving the pure 2-aminoethane thiols.

2-(2,4,6-trimethylphenylamino)ethyl thioacetate

Obtained in 72% yield. ^{1}H NMR (300 MHz, $CDCl_3$) δ = 6.83 (s, 2 H) 3.15 (m, 2 H) 3.06 (m, 2 H) 2.38 (s, 3 H) 2.27 (s, 6 H) 2.24 (s, 3 H). ^{13}C NMR (125 MHz, $CDCl_3$) δ = 142.3, 131.6, 129.8, 129.5, 47.7, 30.7, 30.0, 20.5, 18.4.

2-(2,4,6-trimethylphenylamino)ethyl thiol

Obtained in 90% yield. ^{1}H NMR (300 MHz, $CDCl_3$) δ = 6.76 (s, 2 H) 3.04 (t, *J* = 6.0, 6.0 Hz, 2 H) 2.64 (m, 2 H) 2.22 (s, 6 H) 2.17 (s, 3 H). ^{13}C NMR (125 MHz, $CDCl_3$) δ = 142.4, 131.3, 129.7, 129.3, 50.9, 25.6, 20.4, 18.3.

2-(2,6-diisopropylphenylamino)ethane thioacetate

Obtained in 84% yield. ^{1}H NMR (300 MHz, $CDCl_3$) δ = 7.09 (m, 3 H) 3.27 (m, 2 H) 3.12 (m, 4 H) 2.39 (s, 3 H) 1.24 (d, *J* = 6.0 Hz, 12 H). ^{13}C NMR (125 MHz, $CDCl_3$) δ = 142.7, 142.2, 124.1, 123.6, 50.7, 30.7, 30.0, 27.7, 24.2.

2-(2,6-diisopropylphenylamino)ethane thiol

Obtained in 90% yield. ^{1}H NMR (300 MHz, $CDCl_3$) δ = 7.15 (m, 3 H) 3.36 (m, 2 H) 3.10 (t, *J* = 6.0, 6.0 Hz, 2 H) 2.84 (t, *J* = 6.0, 6.0 Hz, 2 H) 1.30 (d, *J* = 6.0 Hz, 12 H). ^{13}C NMR (125 MHz, $CDCl_3$) δ = 142.7, 142.3, 124.1, 123.6, 53.9, 27.6, 25.7, 24.2.

General procedures for the synthesis of *N*-aryl thiazolinium iodides. Procedures similar to the procedures reported by Zhang for the cyclization of 1,2-phenylenediamines were used with some modification for the cyclization of 2-aminoethane thiols.[18]

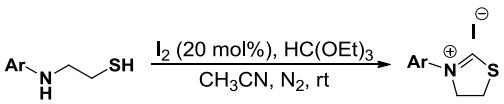

The corresponding 2-aminoethane thiol (24 mmol) was dissolved in 47 mL dry CH_3CN under inert atmosphere. Triethylorthoformate (47 mmol) and iodine (5 mmol) were added to the solution. The resulting mixture was stirred in the dark at room temperature for 2 h. The solvent was removed under reduced pressure and the residue was triturated in Et_2O. The solids were collected by filtration giving pure *N*-aryl thiazolinium iodide.

N-(2,4,6-trimethylphenyl)thiazolinium iodide

Obtained in 75% yield. ^{1}H NMR (300 MHz, $CDCl_3$) δ = 10.30 (s, 1 H) 6.97 (s, 2 H) 4.83 (t, *J* = 6.0, 3.0 Hz, 2 H) 4.44 (t, *J* = 3.0, 6.0 Hz, 2 H) 2.36 (s, 6 H) 2.31 (s, 3 H). ^{13}C NMR (125 MHz, $CDCl_3$) δ = 184.7, 141.5, 133.3, 133.2, 130.2, 61.2, 33.9, 21.0, 18.4.

N-(2,6-diisopropylphenyl)thiazolinium iodide

Obtained in 30% yield. ^{1}H NMR (300 MHz, $CDCl_3$) δ = 10.37 (s, 1 H) 7.49 (t, *J* = 6.0, 3.0 Hz, 1 H) 7.29 (d, *J* = 6.0 Hz, 2 H) 4.81 (t, *J* = 6.0, 6.0 Hz, 2 H) 4.54 (t, *J* = 6.0, 6.0 Hz, 2 H) 2.90 (m, 2 H) 1.32 (dd, *J* = 6.0, 3.0, 6.0, 9.0 Hz). ^{13}C NMR (125 MHz, $CDCl_3$) δ = 185.2, 144.4, 132.7, 132.0, 125.4, 63.2, 34.5, 29.1, 25.2, 24.2.

X-ray crystallography report for *N*-(2,4,6-trimethylphenyl) thiazolinium iodide. A colorless needle, measuring 0.60 x 0.06 x 0.04 mm^3 was mounted on a loop with oil. Data was collected at -173^{o}C on a Bruker APEX II single crystal X-ray diffractometer, Mo-radiation.

Crystal-to-detector distance was 40 mm and exposure time was 30 seconds per frame for all sets. The scan width was 0.5^o. Data collection was 98.2% complete to 25^o

in 9. A total of 62202 reflections were collected covering the indices, h = -32 to 32, k = -25 to 25, l = -18 to 18. 7769 reflections were symmetry independent and the R_{int} = 0.0772 indicated that the data was of average quality (0.07). Indexing and unit cell refinement indicated a C-centered monoclinic lattice. The space group was found to be C 2/c (No.15).

The data was integrated and scaled using SAINT, SADABS within the APEX2 software package by Bruker.[19]

Solution by direct methods (SHELXS, SIR97[20]) produced a complete heavy atom phasing model consistent with the proposed structure. The structure was completed by difference Fourier synthesis with SHELXL97.[21,22] Scattering factors are from Waasmair and Kirfel.[23] Hydrogen atoms were placed in geometrically idealised positions and constrained to ride on their parent atoms with C---H distances in the range 0.95-1.00 Angstrom. Isotropic thermal parameters U_{eq} were fixed such that they were $1.2U_{eq}$ of their parent atom Ueq for CH's and $1.5U_{eq}$ of their parent atom U_{eq} in case of methyl groups. All non-hydrogen atoms were refined anisotropically by full-matrix least-squares.

Sulfur – Carbon disorder at about 3:1 and similar of Iodine plus a few percent of additional disorder visible mainly in Iodine was refined to remove almost all rest-electron density. One of the two dichloromethane solvent molecules in the asymmetric cell occupies infinite channels in the structure and appears heavily disordered.

The structure is of high quality and ready for publication. **Figure 2.5** shows an ORTEP of the asymmetric unit.[24]

Figure 2.5: ORTEP of the structure with thermal ellipsoids at the 50% probability level. Disorder omitted for clarity.

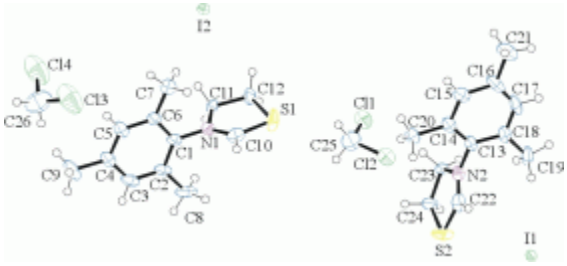

X-ray crystallography report for *N*-(2,6-diisopropylphenyl) thiazolinium iodide. A colorless prism, measuring 0.50 x 0.30 x 0.20 mm^3 was mounted on a loop with oil. Data was collected at -173^{o}C on a Bruker APEX II single crystal X-ray diffractometer, Mo-radiation.

Crystal-to-detector distance was 40 mm and exposure time was 10 seconds per frame for all sets. The scan width was 0.5^o. Data collection was 99.7% complete to 25^o in ϑ. A total of 102387 reflections were collected covering the indices, h = -12 to 12, k = -20 to 20, l = -22 to 22. 10499 reflections were symmetry independent and the R_{int} = 0.0435 indicated that the data was of much better than average quality (0.07). Indexing and unit cell refinement indicated a triclinic lattice. The space group was found to be $P\bar{1}$ (No.2).

The data was integrated and scaled using SAINT, SADABS within the APEX2 software package by Bruker.[19]

Solution by direct methods (SHELXS, SIR97[20]) produced a complete heavy atom phasing model consistent with the proposed structure. The structure was completed by

difference Fourier synthesis with SHELXL97.[21,22] Scattering factors are from Waasmair and Kirfel.[23] Hydrogen atoms were placed in geometrically idealised positions and constrained to ride on their parent atoms with C---H distances in the range 0.95-1.00 Angstrom. Isotropic thermal parameters U_{eq} were fixed such that they were $1.2U_{eq}$ of their parent atom Ueq for CH's and $1.5U_{eq}$ of their parent atom U_{eq} in case of methyl groups. All non-hydrogen atoms were refined anisotropically by full-matrix least-squares.

Some minor disorder in terminal moieties and DCM solvent was addressed which required introducing restraints.

The structure is of high quality and ready for publication. **Figure 2.6** shows an ORTEP of the asymmetric unit.

Figure 2.6: ORTEP of the structure with thermal ellipsoids at the 50% probability level. Disorder omitted for clarity

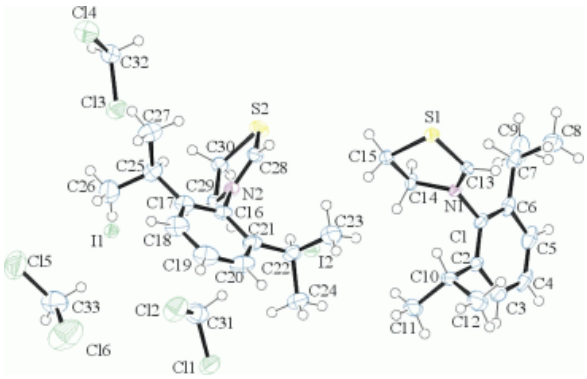

General procedures for cyclic voltammetry. Representative cyclic voltammograms are depicted in **Figure 2.7**. The general procedure was as follows: In a drybox, a 3-neck round bottom flask was charged with a magnetic stir bar, anhydrous CH_3CN (15 mL), and tetrabutylammonium tetrafluoroborate (1.50 mmol). The indicated azolium (0.075 mmol) was then added to the mixture. The flask was equipped with a glassy carbon anode (3 mm diameter), Pt basket cathode, and $Ag/AgNO_3$ reference electrode (0.01 M $AgNO_3$/0.1 M tetrabutylammonium tetrafluoroborate in CH_3CN) and then the apparatus was sealed using rubber septa. The electrochemical cell was then removed from the drybox and the solution was placed under a positive pressure of N_2 and stirred at room temperature. Stirring was stopped prior to connecting to the potentiostat. The cyclic voltammograms for the azolium salts were typically taken from -1.0 V to -2.5 V vs. $Ag/AgNO_3$ with a sweep rate of 0.10 V/s. Ferrocene (0.15 mmol) was added as an internal standard after each voltammogram.[25] All potentials are reported in V vs. SCE. Not all of the azolium salts were fully soluble in CH_3CN. 4-methyl-3-phenylthiazolium tetrafluoroborate and 1,3-bis(2,6-diisopropylphenyl)imidazolium chloride showed poorer solubility in CH_3CN than did the other azolium salts. This resulted in lower observed currents during cyclic voltammetry.

Figure 2.7: Cyclic voltammograms of azolium salts.

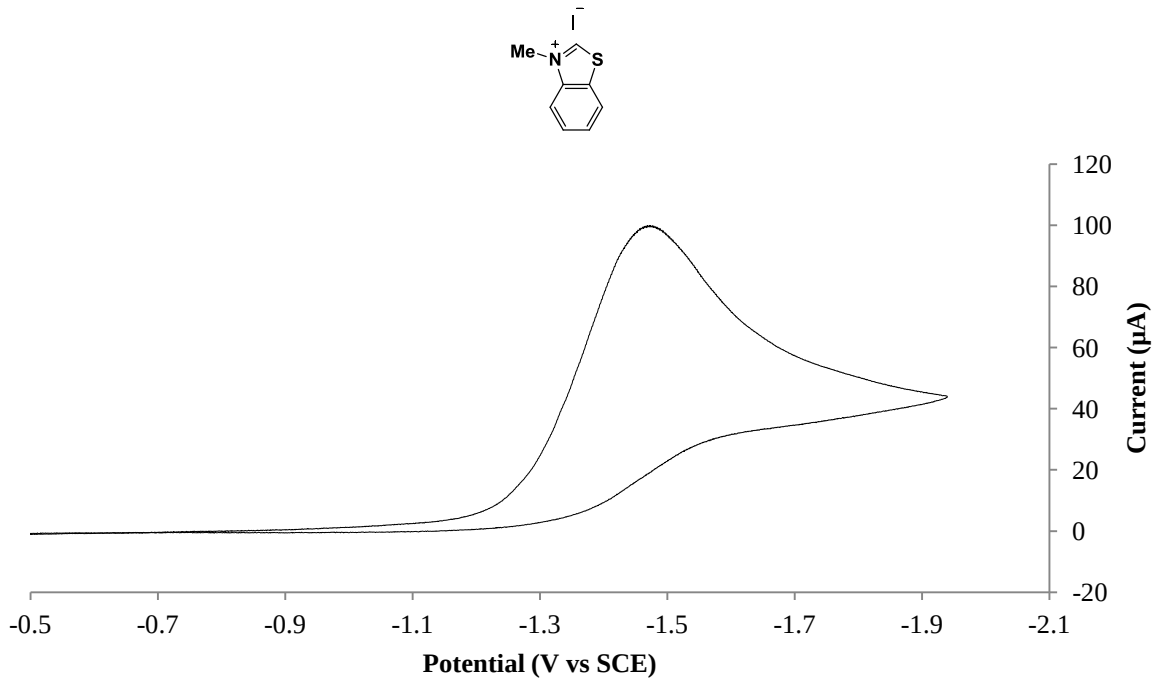

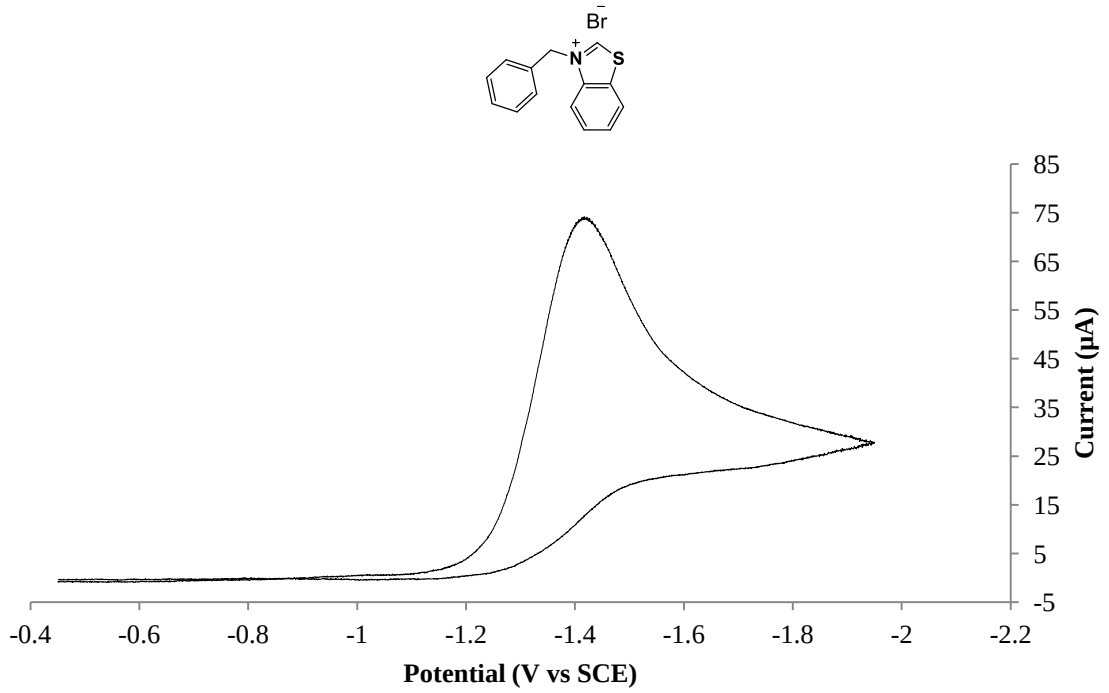

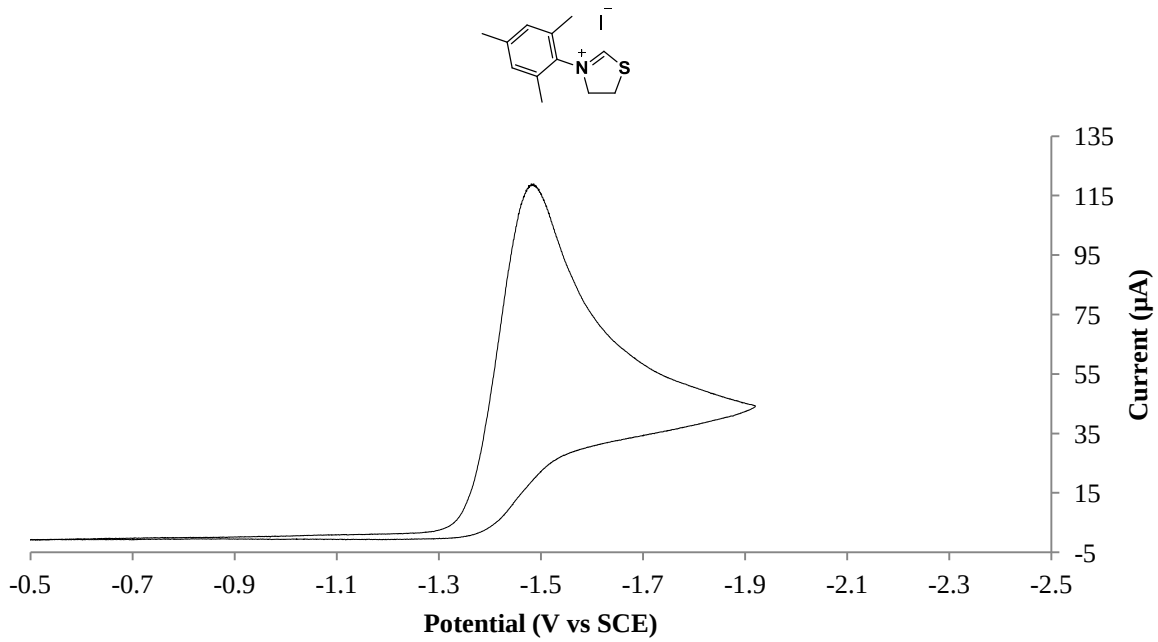
135
115
95
75
55
35
15
-5
Current (µA)
-0.5
-0.7
-0.9
-1.1
-1.3
-1.5
-1.7
-1.9
-2.1
-2.3
-2.5
Potential (V vs SCE)

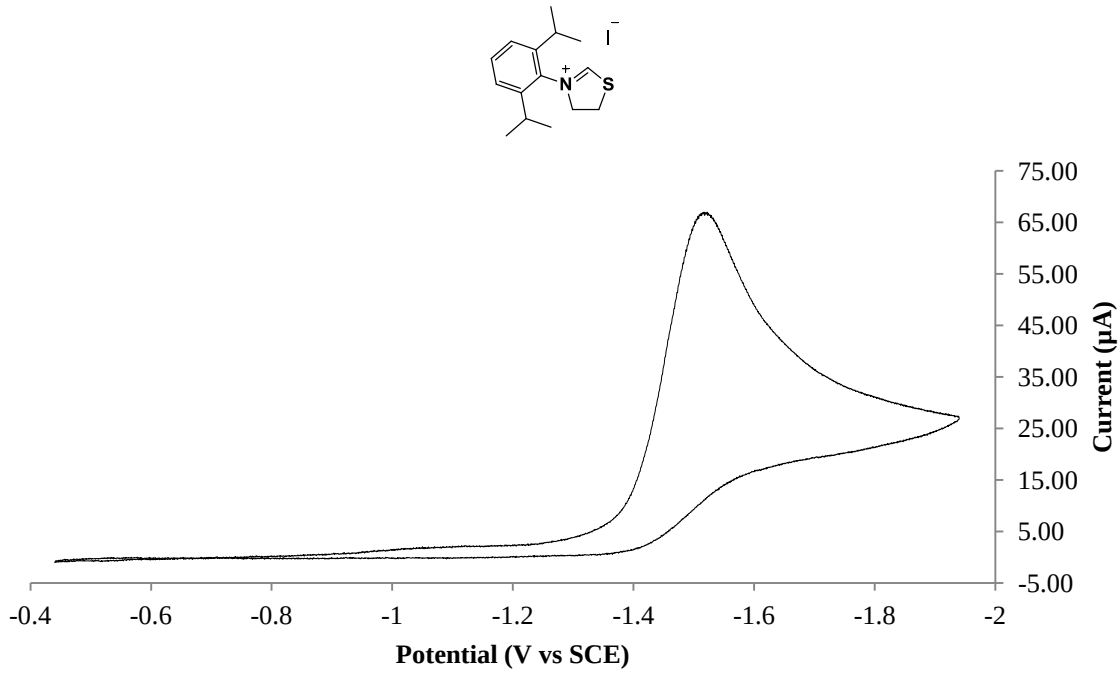
75.00
65.00
55.00
45.00
35.00
25.00
15.00
5.00
-5.00
Current (µA)
-0.4
-0.6
-0.8
-1
-1.2
-1.4
-1.6
-1.8
-2
Potential (V vs SCE)

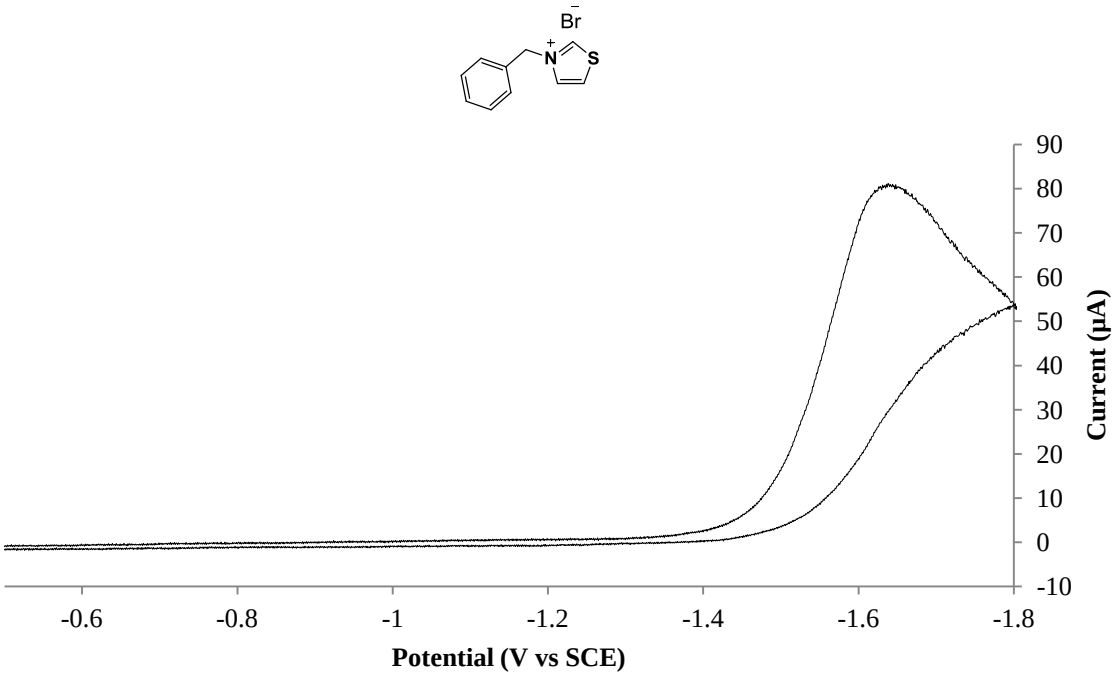
Br
N
S
90
80
70
60
50
40
30
20
10
0
-10
Current (µA)
-0.6
-0.8
-1
-1.2
-1.4
-1.6
-1.8
Potential (V vs SCE)

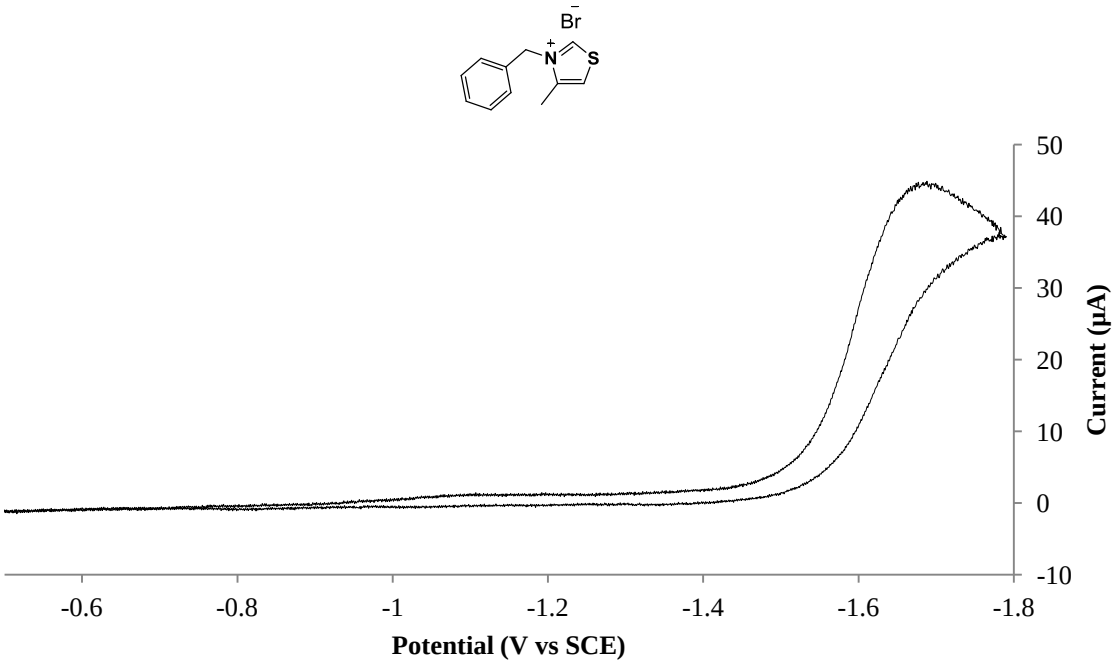
Br
N
S
50
40
30
20
10
0
-10
Current (µA)
-0.6
-0.8
-1
-1.2
-1.4
-1.6
-1.8
Potential (V vs SCE)

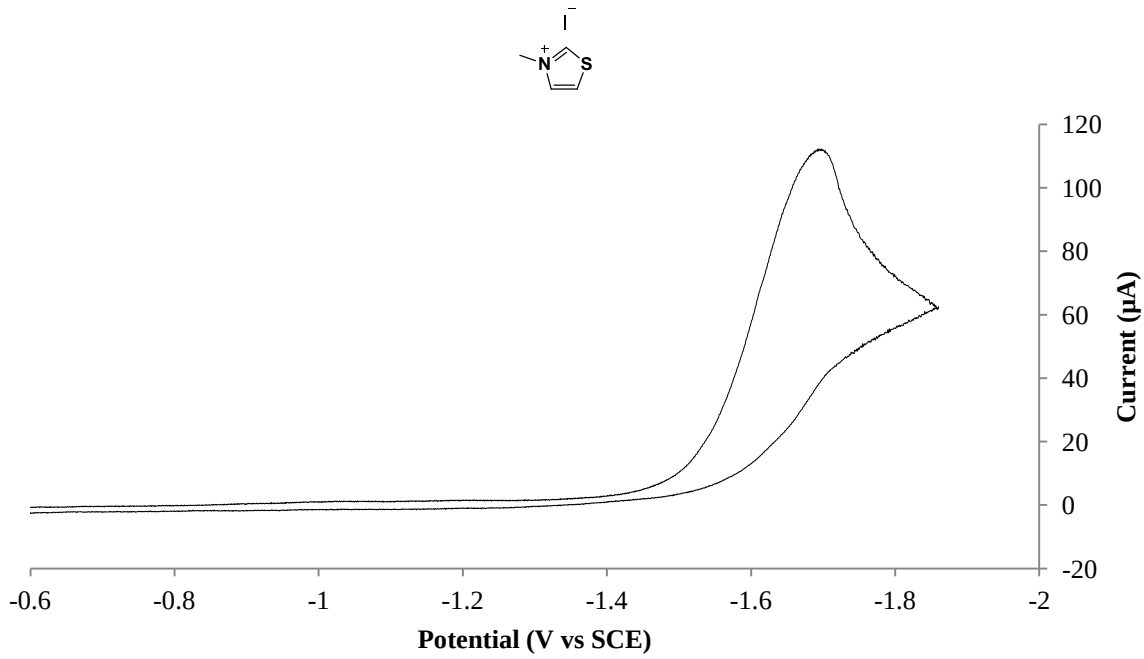
I⁻
N⁺
S
120
100
80
60
40
20
0
-20
Current (µA)
-0.6
-0.8
-1
-1.2
-1.4
-1.6
-1.8
-2
Potential (V vs SCE)

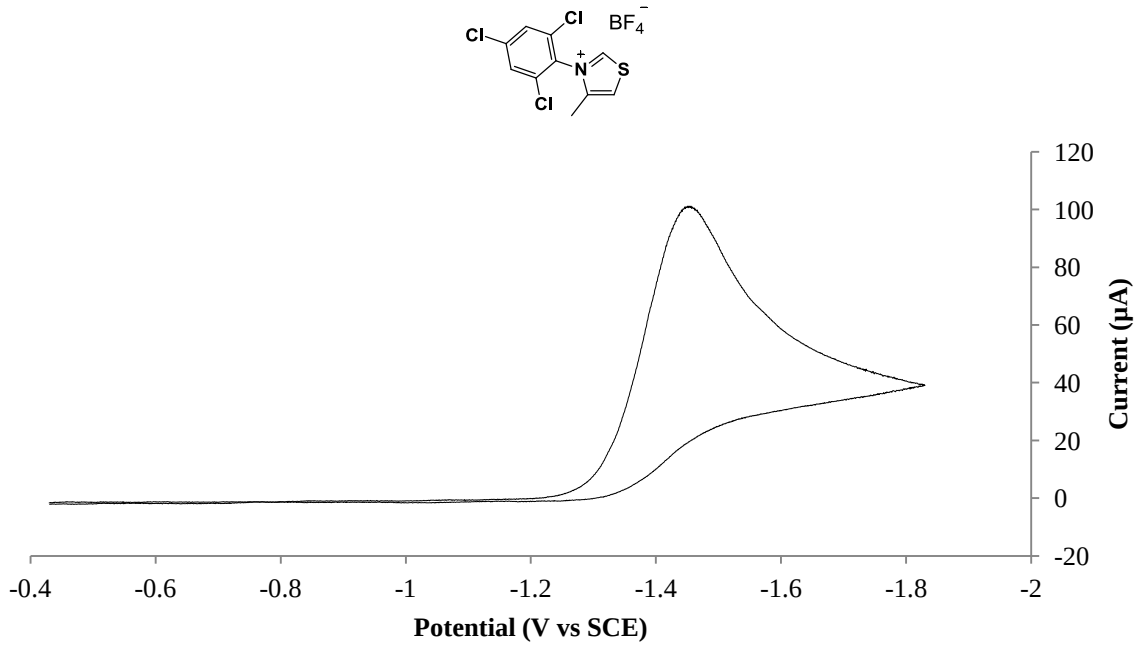
Cl
Cl
Cl
BF4⁻
N⁺
S
120
100
80
60
40
20
0
-20
Current (µA)
-0.4
-0.6
-0.8
-1
-1.2
-1.4
-1.6
-1.8
-2
Potential (V vs SCE)

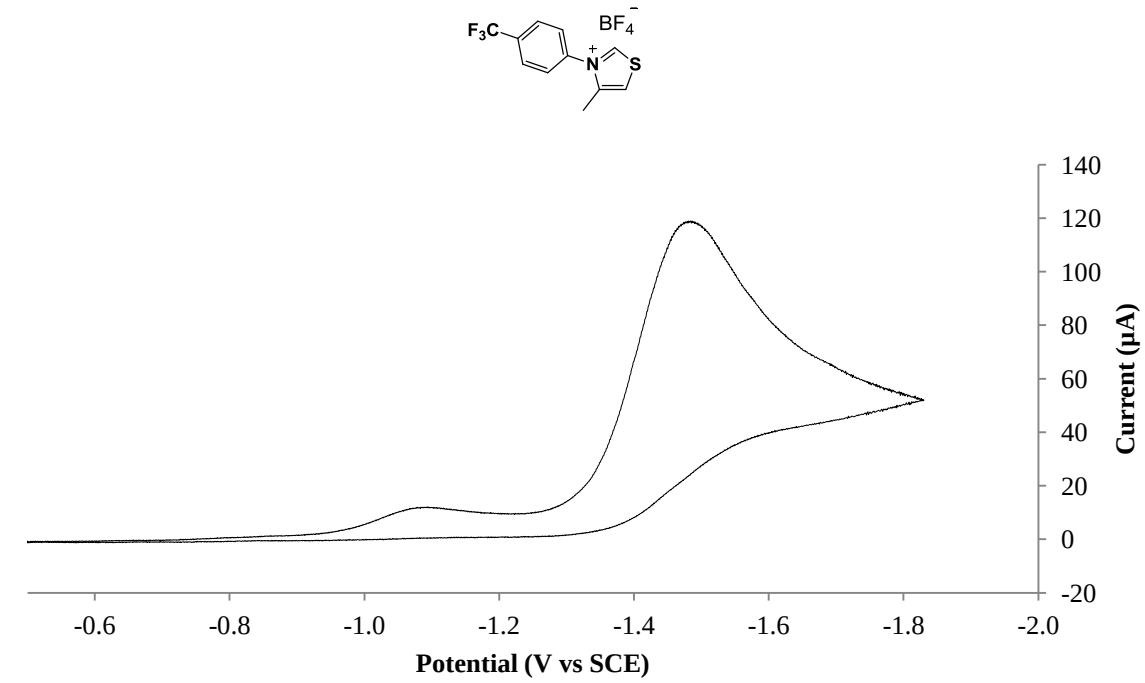
F3C
BF4−
N+
S
140
120
100
80
60
40
20
0
-20
Current (µA)
-0.6
-0.8
-1.0
-1.2
-1.4
-1.6
-1.8
-2.0
Potential (V vs SCE)

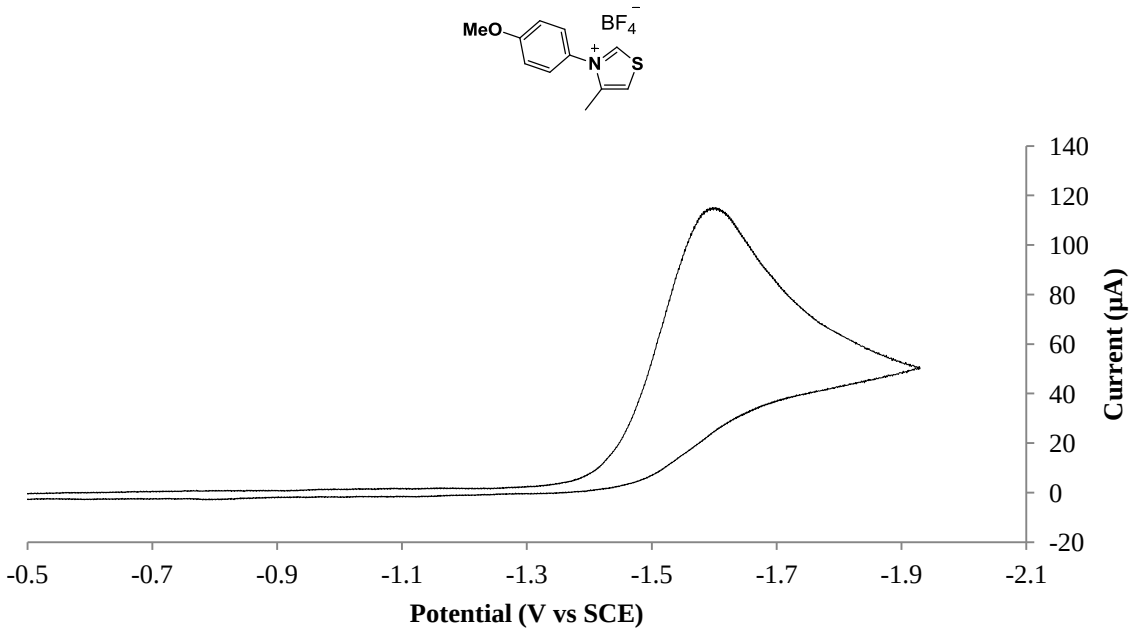
MeO
BF4−
N+
S
140
120
100
80
60
40
20
0
-20
Current (µA)
-0.5
-0.7
-0.9
-1.1
-1.3
-1.5
-1.7
-1.9
-2.1
Potential (V vs SCE)

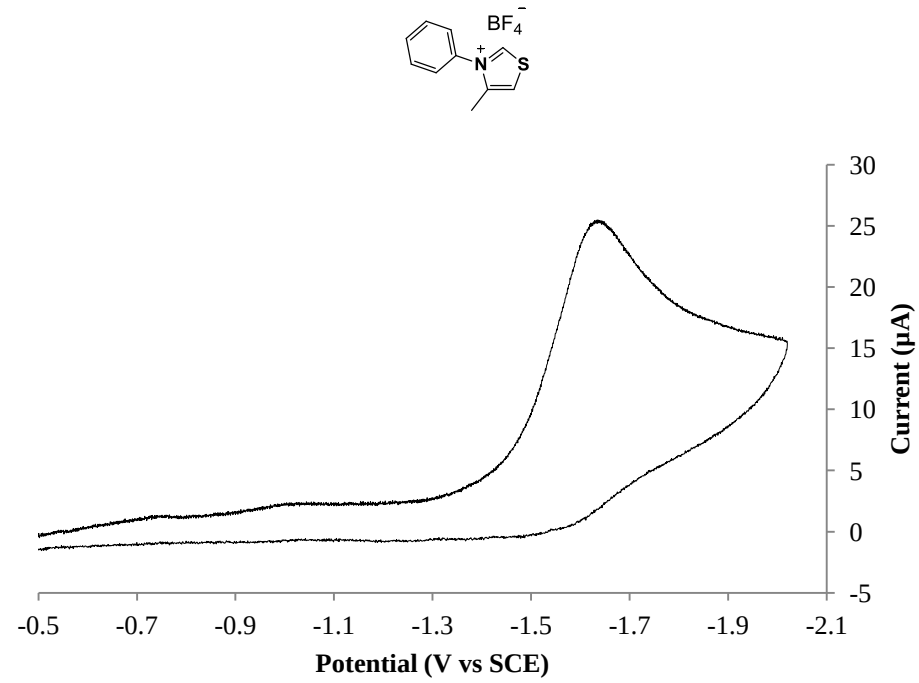
BF4−
N+
S
30
25
20
15
10
5
0
-5
Current (µA)
-0.5
-0.7
-0.9
-1.1
-1.3
-1.5
-1.7
-1.9
-2.1
Potential (V vs SCE)

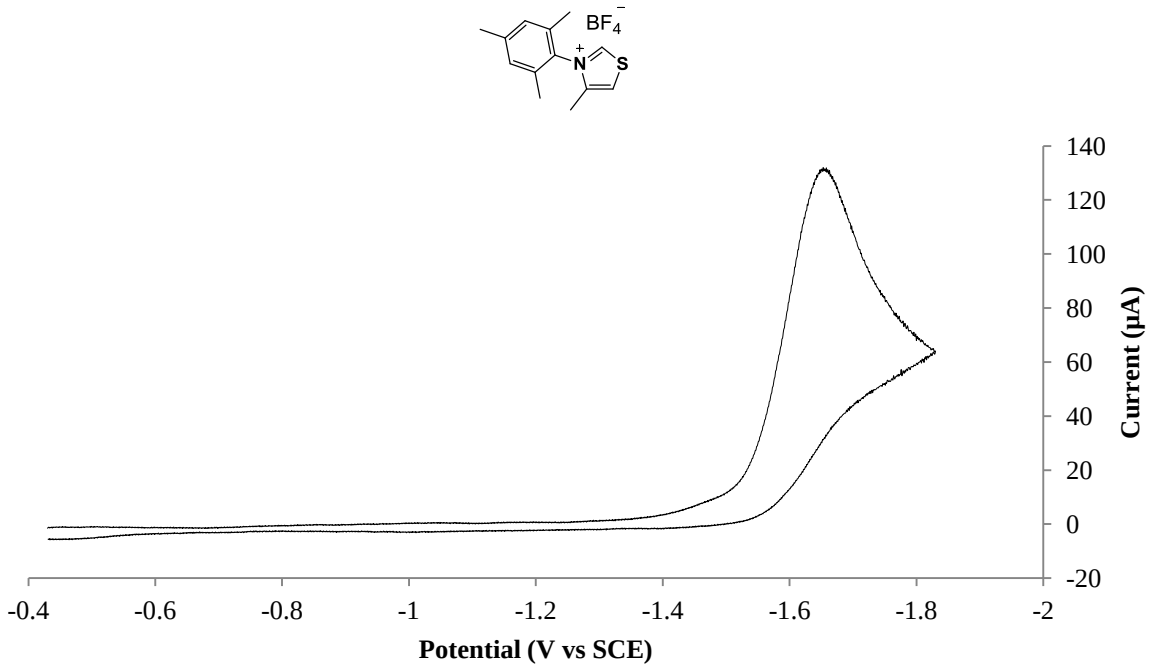
BF4−
N+
S
140
120
100
80
60
40
20
0
-20
Current (µA)
-0.4
-0.6
-0.8
-1
-1.2
-1.4
-1.6
-1.8
-2
Potential (V vs SCE)

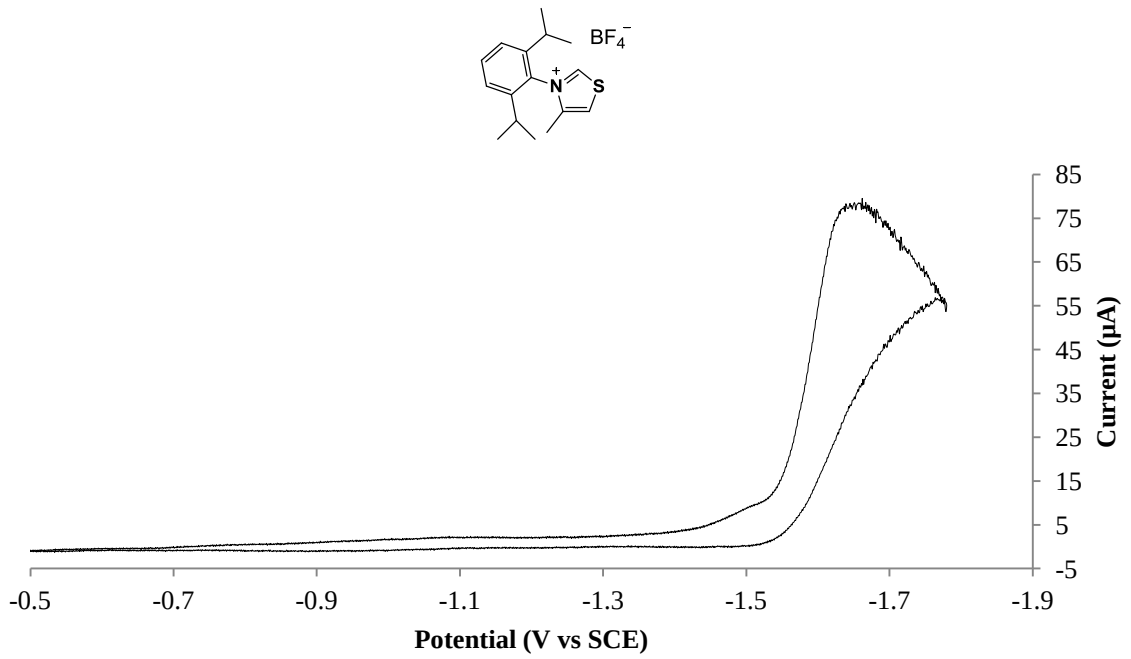
BF4−
N+
S
85
75
65
55
45
35
25
15
5
-5
Current (µA)
-0.5
-0.7
-0.9
-1.1
-1.3
-1.5
-1.7
-1.9
Potential (V vs SCE)

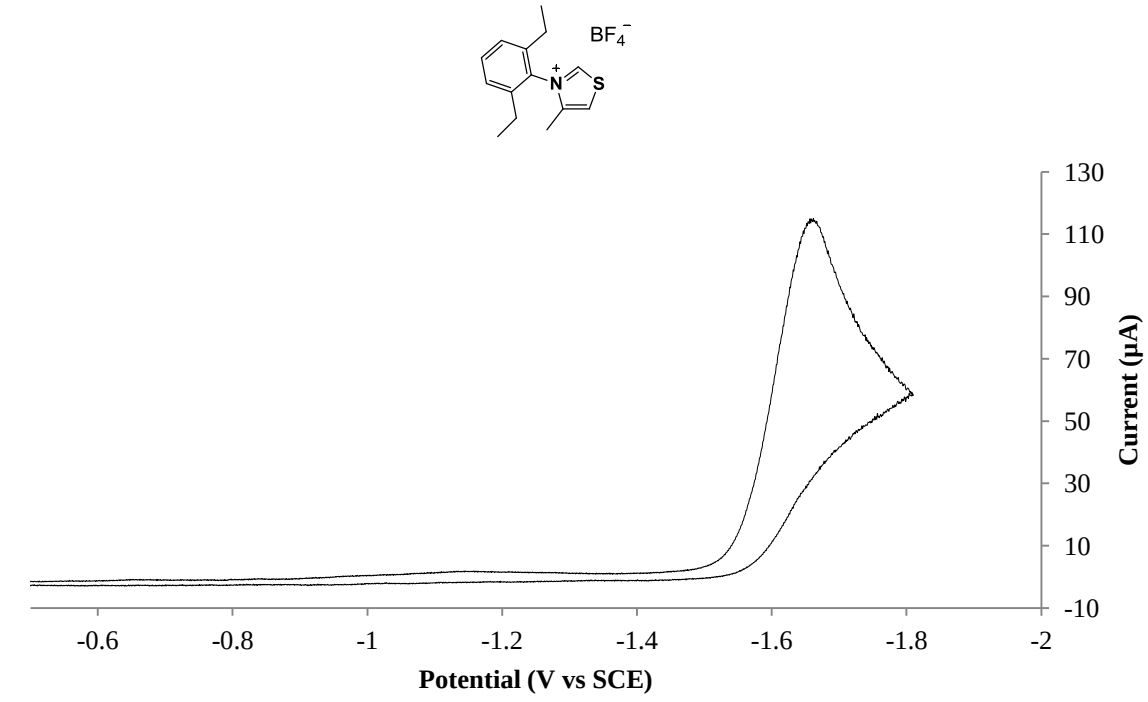
BF4−
N+
S
130
110
90
70
50
30
10
-10
Current (µA)
-0.6
-0.8
-1
-1.2
-1.4
-1.6
-1.8
-2
Potential (V vs SCE)

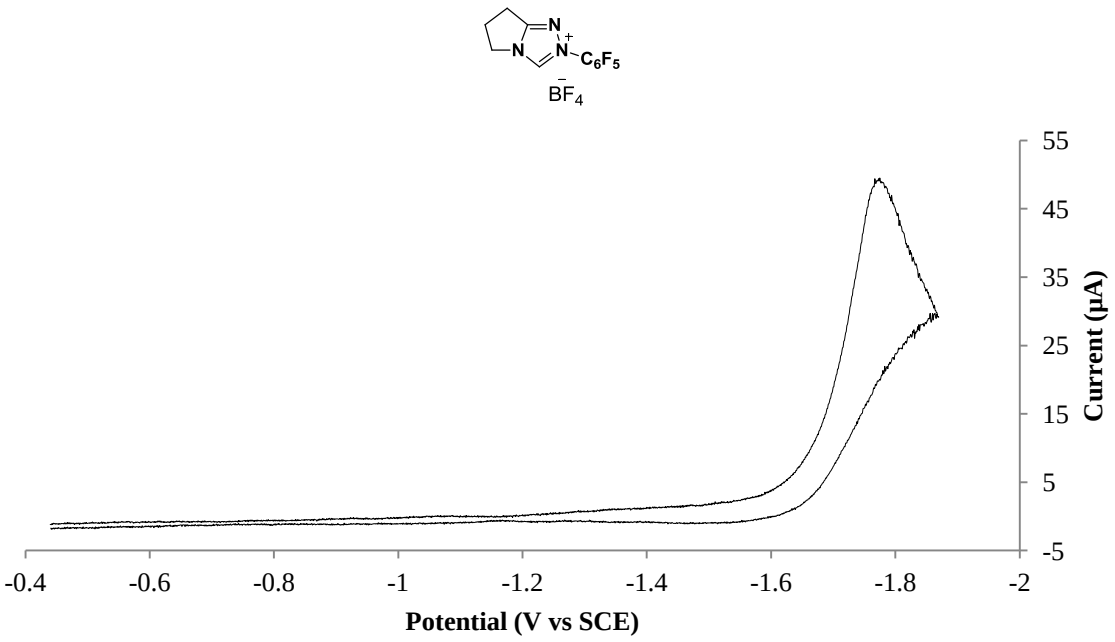
55
45
35
25
15
5
-5
Current (µA)
-0.4
-0.6
-0.8
-1
-1.2
-1.4
-1.6
-1.8
-2
Potential (V vs SCE)

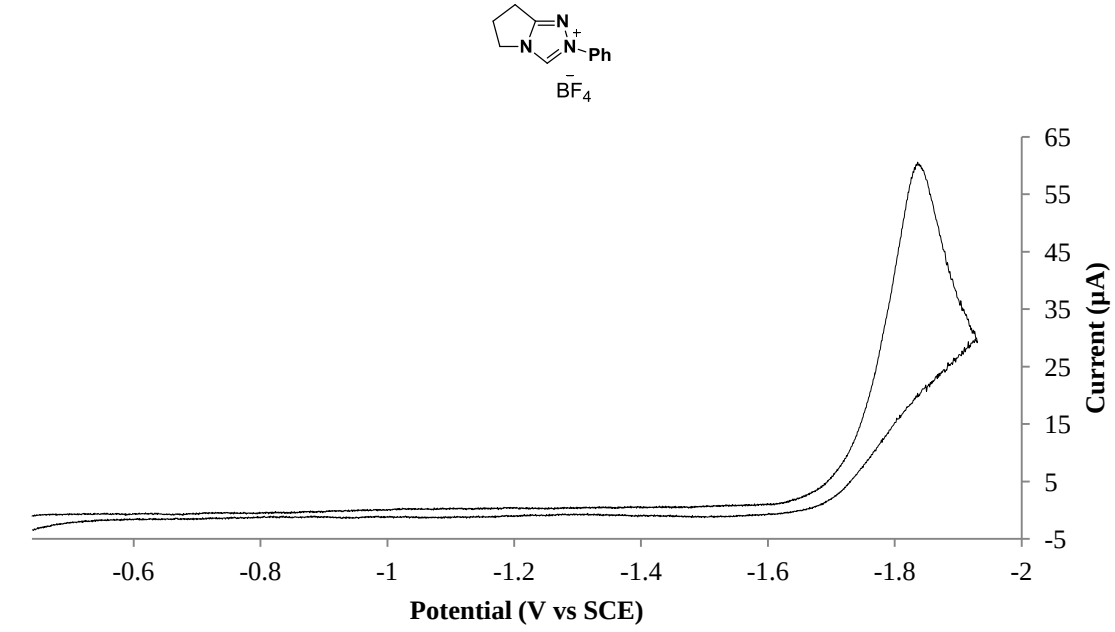
65
55
45
35
25
15
5
-5
Current (µA)
-0.6
-0.8
-1
-1.2
-1.4
-1.6
-1.8
-2
Potential (V vs SCE)

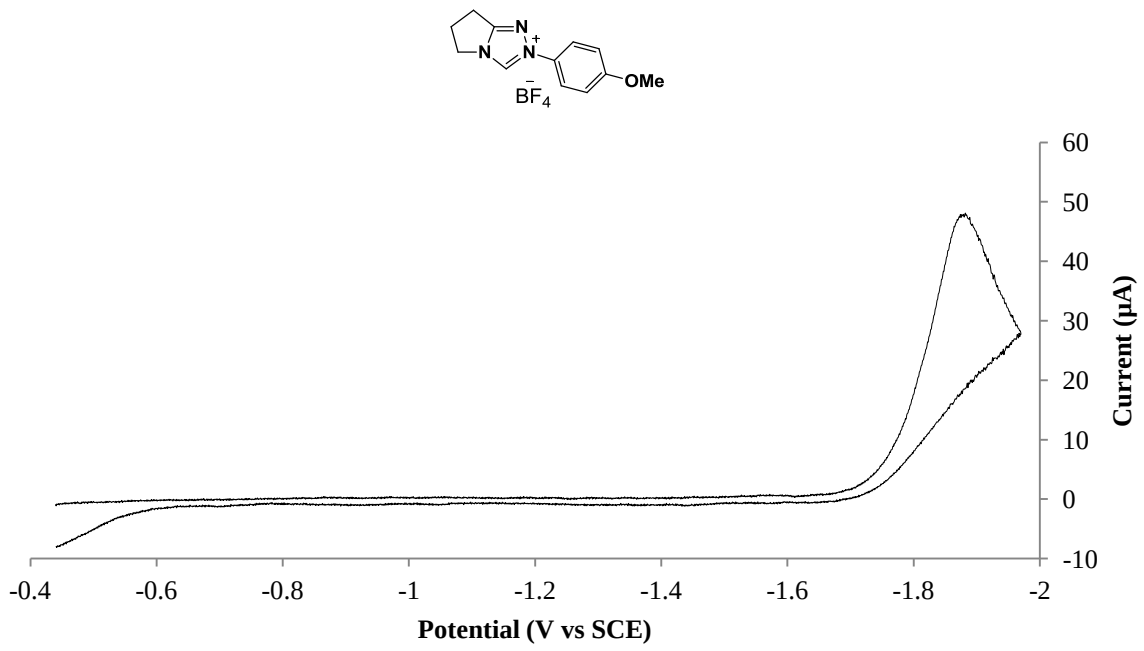
OMe
BF4
60
50
40
30
20
10
0
-10
Current (µA)
-0.4
-0.6
-0.8
-1
-1.2
-1.4
-1.6
-1.8
-2
Potential (V vs SCE)

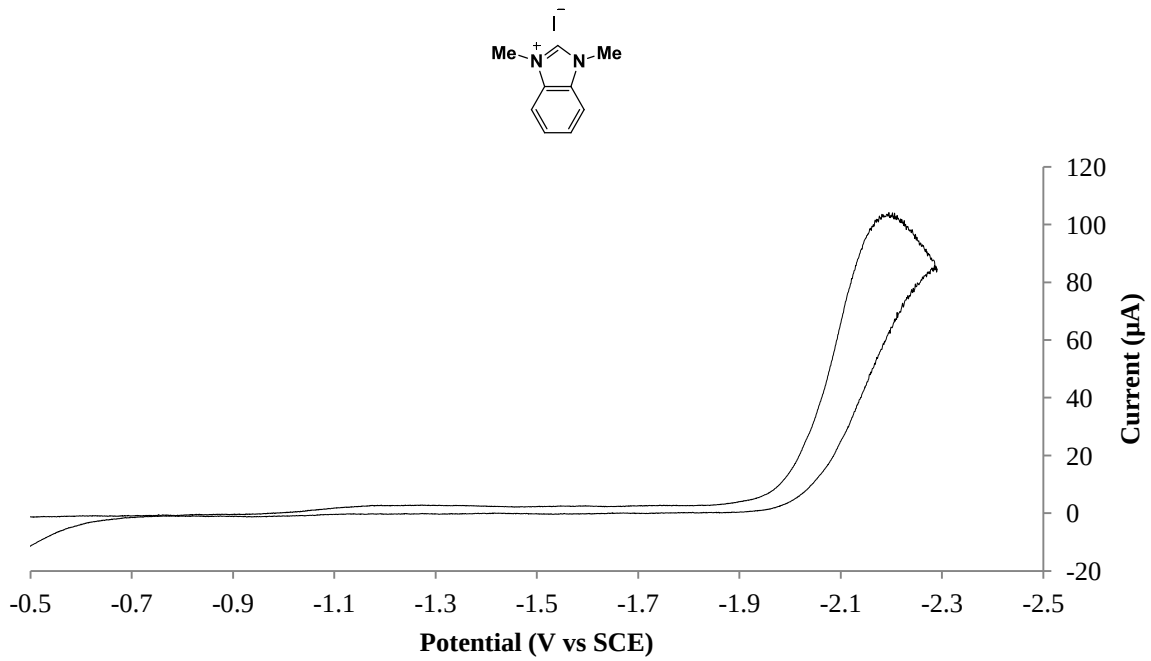
Me
Me
120
100
80
60
40
20
0
-20
Current (µA)
-0.5
-0.7
-0.9
-1.1
-1.3
-1.5
-1.7
-1.9
-2.1
-2.3
-2.5
Potential (V vs SCE)

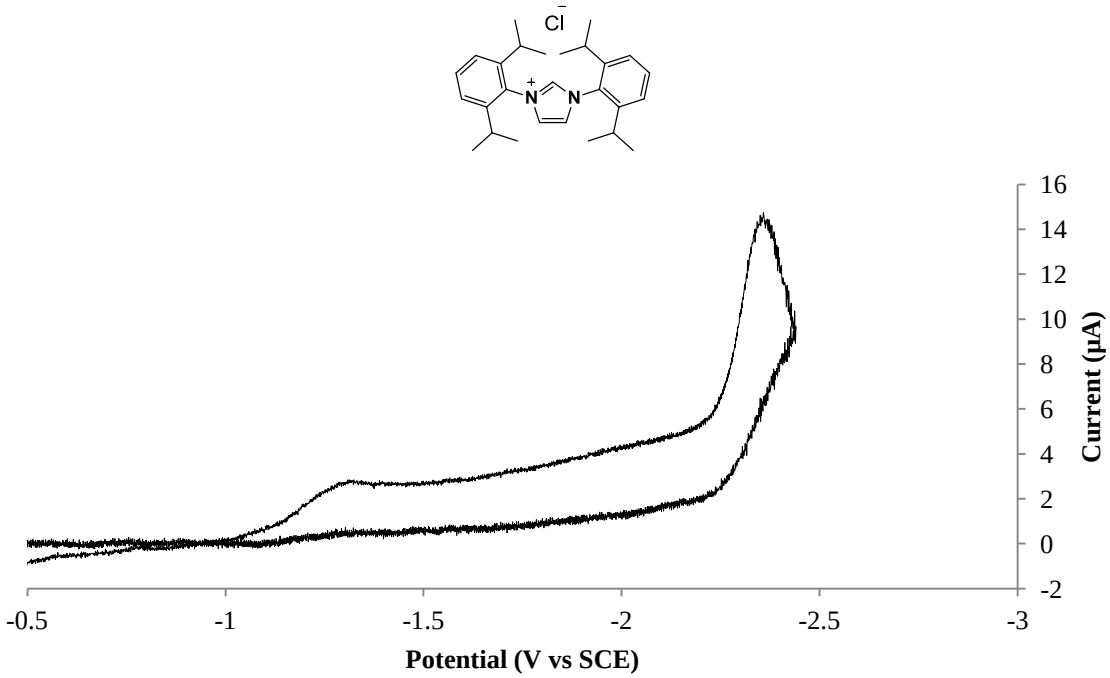
Cl
N
N
16
14
12
10
8
6
4
2
0
-2
-0.5
-1
-1.5
-2
-2.5
-3
Current (µA)
Potential (V vs SCE)

Notes and References to Chapter 2

[1] For recent reviews, see: (a) Chiang, P.-C.; Bode, J. W. in *N-Heterocyclic Carbenes: From Laboratory Curiosities to Efficient Synthetic Tools*; Díez-Gonsálzes, S., Ed.; RSC Catalysis Series, No. 6; Royal Society of Chemistry: Cambridge, U.K., 2010; pp. 399 – 435. (b) Moore, J. L.; Rovis, T. *Top. Curr. Chem.* **2009**, *291*, 77. (c) Enders, D.; Niemeier, O.; Henseler, A. *Chem. Rev.* **2007**, *107*, 5606.

[2] For examples of electrosynthesis of NHCs via cathodic reduction of azolium salts, see: (a) de Robillard, G.; Devillers, C.; Kunz, D.; Cattey, H.; Digard, E.; Andrieu, J. *Org. Lett.* **2013**, *15*, 4410. (b) Feroci, M.; Chiarotto, I.; Inesi, A. *Electrochim. Acta* **2013**, *89*, 692. (c) Chiarotto, I.; Feroci, M.; Sotgiu, G.; Inesi, A. *Eur. J. Org. Chem.* **2013**, 326. (d) Gierz, V.; Melomedov, J.; Förster, C.; Deiβler, C.; Rominger, F.; Kunz, D.; Heinze, K. *Chem. Eur. J.* **2012**, *18*, 10677. (e) Liu, B.; Zhang, Y.; Xu, D.; Chen, W. *Chem. Commun.* **2011**, *47*, 2883. (f) Orsini, M.; Chiarotto, I.; Feeney, M. M. M.; Feroci, M.; Sotgiu, G.; Inesi, A. *Electrochem. Commun.* **2011**, *13*, 738. (g) Feroci, M.; Chiarotto, I.; Orsini, M.; Inesi, A. *Chem. Commun.* **2010**, *46*, 4121. (h) Feroci, M.; Chiarotto, I.; Orsini, M.; Sotgiu, G.; Inesi, A. *ECS Transactions* **2010**, *25*, 1. (i) Orsini, M.; Chiarotto, I.; Sotgiu, G.; Inesi, A. *Electrochim. Acta* **2010**, *55*, 3511. (j) Orsini, M.; Chiarotto, I.; Elinson, M. N.; Sotgiu, G.; Inesi, A. *Electrochem. Commun.* **2009**, *11*, 1013.

[3] For recent reviews, see: (a) Hallett, J.; Welton, T. *Chem. Rev.* **2011**, *111*, 3508. (b) van Rantwijk, F.; Sheldon, R. *Chem. Rev.* **2007**, *107*, 2757. (c) Dupont, J.; de Souze, R.; Suarez, P. *Chem. Rev.* **2002**, *102*, 3667.

[4] (a) Endres, F.; Höfft, O.; Borisenko, N.; Gasparotto, L. H.; Prowald, A.; Al-Salman, R.; Carstens, T.; Atkin, R.; Bund, A.; Abedin, S. Z. E. *Phys. Chem. Chem. Phys.* **2010**, *12*, 1724. (b) Hapiot, P.; Lagrost, C. *Chem. Rev.* **2008**, *108*, 2238. (c) Buzzeo, M. C.; Evans, R. G.; Compton, R. G. *Chem. Phys. Chem.* **2004**, *5*, 1106. (d) Wilkes, J. S.; Levisky, J. A.; Wilson, R. A.; Hussey, C. L. *Inorg. Chem.* **1982**, *21*, 1263.

[5] Ogawa, K. A.; Boydston, A. J. *Org. Lett.*, **2014**, *16*, 1928.

[6] (a) Yan, X.; Gu, S.; He, G.; Wu, X.; Benziger, J. *J. Power Sources* **2014**, *250*, 90. (b) Naka, K.; Shinke, R.; Yamada, M.; Belkada, F. M.; Aijo, Y.; Irie, Y.; Shankar, S. R.; Smaran, K. S.; Matsumi, N.; Tomita, S.; Sakurai, S. *Polym. J. (Tokyo)* **2014**, *46*, 42. (c) Robertson, L. A.; Schenkel, M. R.; Wiesenauer, B. R.; Gin, D. L. *Chem. Commun*. **2013**, *49*, 9407. (d) Rao, A. H. N.; Kim, H.-J.; Nam, S.; Kim, T.-H. *Polymer* **2013**, *54*, 6918. (e) Lu, W.; Shao, Z.-G.; Zhang, G.; Zhao, Y;. Li, J.; Yi, B. *Int. J. Hydrogen Energy* **2013**, *38*, 9285. (f) Lin, B.; Dong, H.; Li, Y.; Si, Z.; Gu, F.; Yan, F.; *Chem. Mater.* **2013**, *25*, 1858. (g) Green, O.; Grubjesic, S.; Lee, S.; Fireston, M. A *J. Macromol. Sci. Polym. Rev.* **2009**, *49*, 339. (h) Boydston, A. J.; Vu, P. D.; Dykhno, O. L.; Chang, V.; Wyatt, II, A. R.; Stockett, A. S.; Ritschdorff, E. T.; Shear, J. B.; Bielawski, C. W. *J. Am. Chem. Soc.* **2008**, *130*, 3143. (i) Suisse, J.-M.; Douce, L.; Bellemin-Laponnaz, S.; Maisse-François, A.;

Welter, R.; Miyake, Y.; Shimizu, Y. *Eur. J. Inorg. Chem.* **2007**, 3899. (j) Boydston, A. J.; Bielawski, C. W. *Dalton Trans.* **2006**, 4073.
[7] (a) Sanghi, S.; Willett, E.; Versek, C.; Tuominen, M.; Coughlin, E. B. *RCS Adv.* **2012**, *2*, 848. (b) Liao, C.; Shao, N.; Han, K. S.; Sun, X.-G.; Jiang, D.-E.; Hagaman, E.; Dai, S. *Phys. Chem. Chem. Phys.* **2011**, *13*, 21503. (c) Abdellah, I.; Cassirame, B.; Condon, S.; Nédélec, J.-Y.; Pichon, C. *Curr. Top. Electrochem.* **2011**, *16*, 81. (d) Gorodetsky, B.; Ramnial, T.; Branda, N. R.; Clyburne, J. *Chem. Commun.* **2004**, 1972.
[8] (a) Mercey, G.; Lohier, J.-F.; Gaumont, A.-C.; Levillain, J.; Gulea, M. *Eur. J. Org. Chem.* **2009**, 4357. (b) Mercey, G.; Brégeon, D.; Baudequin, C.; Guillen, F.; Levillain, J.; Gulea, M.; Plaquevent, J.-C.; Gaumont, A.-C. *Tetrahedron Lett.* **2009**, *50*, 7239.
[9] (a) Bhanu Prasad, B. A.; Gilbertson, S. R. *Org. Lett.* **2009**, *11*, 3710. (b) Zhang, Z.-H.; Li, J.-J.; Gao, Y.-Z.; Liu, Y.-H. *J. Heterocyclic Chem.* **2007**, *44*, 1509. (c) Avenoza, A.; Busto, J.-H.; Jiménez-Osés, G.; Peregrina, J. M. *J. Org. Chem.* **2006**, *71*, 1692. (d) Zheng, T.-C.; Burkart, M.; Richardson, D. E. *Tetrahedron Lett.* **1999**, *40*, 603.
[10] (a) Benhamou, L.; Chardon, E.; Lavigne, G.; Bellemin-Laponnaz, S.; César, V. *Chem. Rev.* **2011**, *111*, 2705. (b) Kuhn, K. M.; Grubbs, R. H. *Org. Lett.* **2008**, *10*, 2075. (c) Saba, S.; Brescia, A.; Kaloustian, M. K. *Tetrahedron Lett.* **1991**, *32*, 5031.
[11] (a) Shono, T.; Matsumura, Y.; Katoh, S.; Fujita, T.; Kamada, T. *Tetrahedron Lett.* **1989**, *30*, 371. (b) Shono, T.; Matsumura, Y.; Katoh, S.; Ikeda, K.; Kamada, T. *Tetrahedron Lett.* **1989**, *30*, 1649.
[12] (a) Piel, I.; Pawelczyk, M. D.; Hirano, K.; Fröhlich, R.; Glorius, F. *Eur. J. Org. Chem.* **2011**, 5475. (b) Pesch, J.; Harms, K.; Bach, T. *Eur. J. Org. Chem.* **2004**, 2025. (c) Shin, W.; Pletcher, J.; Blank, G.; Sax, M. *J. Am. Chem. Soc.* **1977**, *99*, 3491.
[13] Hirano, K.; Piel, I.; Glorius, F. *Adv. Synth. Cat.* **2008**, *350*, 984.
[14] Kerr, M. S.; Read de Alaniz, J.; Rovis, T. *J. Org. Chem.* **2005**, *70*, 5725.
[15] Prasad, B. A. B.; Gilbertson, S. R. *Org. Lett.* **2009**, *11*, 3710.
[16] Zheng, T.-C.; Burkart, M.; Richardson, D. E. *Tetrahedron Lett.* **1999**, *40*, 603.
[17] Avenoza, A.; Busto, J. H.; Jiménez-Osés, G.; Peregrina, J. M. *J. Org. Chem.* **2006**, *71*, 1692.
[18] Zhang, Z.-H.; Li, J.-J.; Gao, Y.-Z.; Liu, Y.-H. *J. Heterocyclic Chem.* **2007**, *44*, 1509.
[19] Bruker (**2007**) APEX2 (Version 2.1-4), SAINT (version 7.34A), SADABS (version 2007/4), BrukerAXS Inc, Madison, Wisconsin, USA.
[20] (a) Altomare A, Burla C, Camalli M, Cascarano G L, Giacovazzo C, Guagliardi A, Moliterni AGG, Polidori G, Spagna R. **(1999)** SIR97: a new tool for crystal structure determination and refinement *Journal of Applied Cryst*allography, ***32,*** 115-119. (b) Altomare A, Cascarano G L, Giacovazzo C, Guagliardi A. **(1993)** Completion and refinement of crystal structures with SIR 92. *Journal of Applied Cryst*allography, ***26,*** 343-350.
[21] Sheldrick GM. **(1997)** SHELXL-97, Program for the Refinement of Crystal Structures. University of Göttingen, Germany.

[22] Mackay, S.; Edwards, C.; Henderson, A.; Gilmore, C.; Stewart, N.; Shankland, K.; Donald, A. **(1997)** *MaXus: a computer program for the solution and refinement of crystal structures from diffraction data*. University of Glasgow, Scotland.
[23] Waasmaier, D.; Kirfel, A. **(1995)** New Analytical Scattering Factor Functions for Free Atoms and Ions. *Acta Crystallographica* A., ***51***, 416-430.
[24] Farrugia LJ. **(1997)** Ortep-3 for Windows. *Journal of Applied Cryst*allography, ***30,*** 565.
[25] Connelly, N. G.; Geiger, W. E. *Chem. Rev.* **1996**, *96*, 877.

Chapter 3 -Metal-free Ring-opening Metathesis Polymerization[5]

Section 1: Introduction

3.1.a Metal-free Olefin Metathesis

The anodic oxidation of enol ethers to form radical cations has been extensively studied.[1] These reactive intermediates are known to participate in intramolecular cyclizations. Moeller and coworkers have studied the intramolecular reactivity of radical cations generated from enol ether substrates. In 2001, enol ether radical cation intermediates were intramolecularly trapped by an alcohol moiety to form tetrahydrofuran type products (**Scheme 3.1**).[1l] This electrochemical approach was used to synthesize linalool oxide in high yield. Moeller's group was also able to successfully form acetals via oxidative cyclization of enol ether radical cations with intramolecular trapping groups, such as alcohols and enol ethers (**Scheme 3.2**).[1a]

Scheme 3.1: Representative oxidative cyclization of enol ether to form tetrahydrofurans.

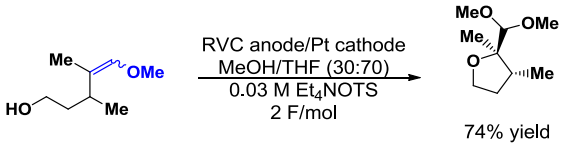

[5] Reproduced with permission from Ogawa, K. A.; Goetz, A. E.; Boydston, A. J. "Metal-free Ring-opening Metathesis Polymerization" *J. Am. Chem. Soc.*, **2015**, *137*, 1400 – 1403. Copyright 2015 American Chemical Society.

Scheme 3.2: Representative oxidative cyclization of enol ether to form acetals.

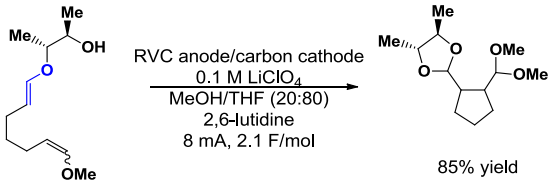

The intermolecular reactivity of enol ether radical cations has also been studied previously. In 2001, Chiba and coworkers reported the intermolecular [2 + 2] cycloaddition of enol ethers following anodic oxidation (**Scheme 3.3**, top).[1k] Interestingly, 1 M $LiClO_4$ in CH_3NO_2 was the only electrolyte solution to provide any measurable amount of the desired product. They proposed that the addition of the radical cation to another olefin resulted in the formation of a cyclobutane radical cation and that the fate of this intermediate depended upon the electronic nature of the starting enol ether. Enol ethers containing neutral aryl rings or aliphatic groups gave no cyclized product. However, substrates containing electron-rich aromatic systems gave cyclobutane products in good yields due to the increased ability for intramolecular electron transfer from the aromatic system to the cyclobutane radical cation. During the development of this method, they noted that intermolecular cross coupling rather than cyclobutane formation could be occurring when electron neutral aromatic and aliphatic systems were employed.

Scheme 3.3: (top) Formal [2 + 2] cycloaddition as reported by Chiba and coworkers (bottom) and stoichiometric electrochemical olefin cross-metathesis as reported by Chiba and coworkers.

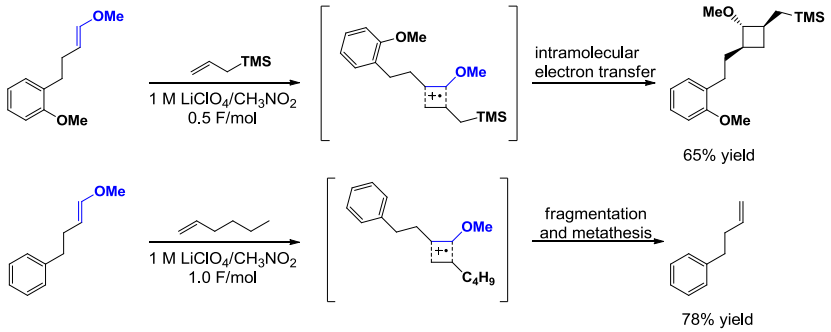

Scheme 3.4: (top) Fate of the cyclobutane radical cation in electrochemical [2 + 2] cycloaddition (bottom) and cross-metathesis.

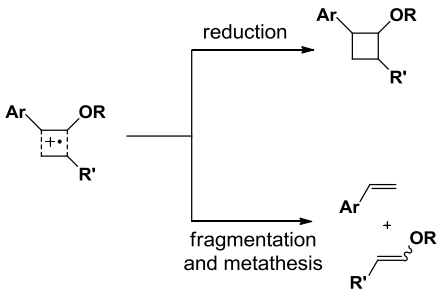

In 2006, Chiba reported the first example of metal-free electrochemical olefin metathesis (**Scheme 3.3**, bottom).[1i] They proposed that this reaction goes through a similar cyclobutane radical cation intermediate as the cycloaddition reported previously. The main difference being that cyclobutane intermediates formed from enol ethers with electron neutral aromatic or aliphatic systems favored fragmentation over reduction with fragmentation ultimately leading to metathesis (**Scheme 3.4**). This electrochemical approach to cross-metathesis was successfully demonstrated with a limited set of olefins. Notably, $LiClO_4$ and CH_3NO_2 once again emerged as the only electrolyte solution to

provide measurable amounts of product. Although the ability to achieve cross-metathesis under metal-free conditions was impressive, the substrate scope remained limited and no further development of this method has been reported. Specifically, to the best of our knowledge, enol ethers have not been employed in a catalytic fashion. We envisioned expanding the scope of this method by developing a catalytic variant that would allow us to achieve metal-free ring-opening metathesis polymerization (ROMP).

3.1.b Metal-mediated ROMP

Figure 3.1: Examples of transition metal-based alkylidene initiators.

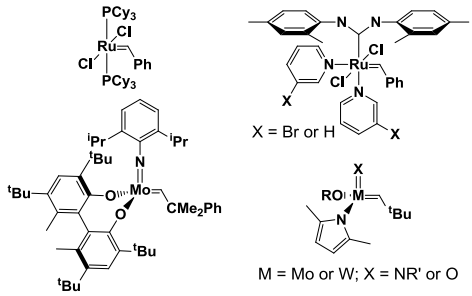

Metal-mediated ROMP is a commonly used polymerization technique in academic as well as industrial settings and has led to breakthroughs in numerous areas such as biomedical devices, drug delivery, photovoltaics, and the production of materials.[2–4] In general, ROMP can be used to achieve living polymerizations that produce polymers of narrow dispersity. The versatility of this technology stems from the development of well-defined transition metal initiators, specifically Ru- and Mo-based alkylidene initiators (**Figure 3.1**). These initiators allow the incorporation of a broad range of functional groups into polymer scaffolds. It is important to note that initiators

with redox active ligands have also been developed.[5] These redox active ligands can be electrochemically activated or inactivated; however, the mechanism of the polymerization remains the same after initiator activation.

Although metal-mediated ROMP is one of the most widely used polymerization techniques, the final polymer may contain residual metal and metallic byproducts which can be problematic.[6,7] Specifically, residual metal may lead to complications in biological and optical applications. Additionally, the presence of metallic byproducts is known to lower the oxidative stability of the final material. Numerous protocols have been developed to combat these problems; however, these processes often require additional processing steps or derivatization of the initiator as well as quantification by advanced analytical techniques.[8] A metal-free approach to ROMP could provide a complimentary method that would avoid the issues regarding residual metal. In this account, we will discuss the development of the first metal-free ROMP method that can be achieved electrochemically as well as photochemically.

Section 2: Results and Discussion

3.2.a Electro-organic ROMP

In Chiba's work, the key to achieving metathesis over cyclobutane formation was to favor fragmentation over reduction of the cyclobutane radical cation intermediate.[1i,k] The ability to use the relief of ring strain to outcompete reduction would allow us to

expand the scope of this electrochemical approach and access a new mechanism for ROMP.

We envisioned initiating ROMP via one-electron oxidation of electron-rich vinyl ethers (**Scheme 3.5**).[9] Oxidation of a vinyl ether would form radical cation intermediate **B** that would go on to form a [2 + 2] complex with a strained cycloalkene giving cyclobutane radical cation **C**. Fragmentation and opening of this complex would relieve ring strain and form radical cation **D**. Further reaction with additional cycloalkene monomers would result in the formation of polymeric species **E** with reactive radical cation chain ends. Competitive reversible reductions of radical cations **D** and **E** are likely to occur. These reversible reductions would lead to reiterative termination-initiation cycles that would eventually lead to final polymer **F**. Inspired by the propensity for ring strain to drive metal-mediated ROMP, we looked towards developing an electro-organic approach to ROMP using vinyl ether initiators and strained cycloalkene monomers.

Scheme 3.5: Envisioned mechanism for metal-free ROMP.

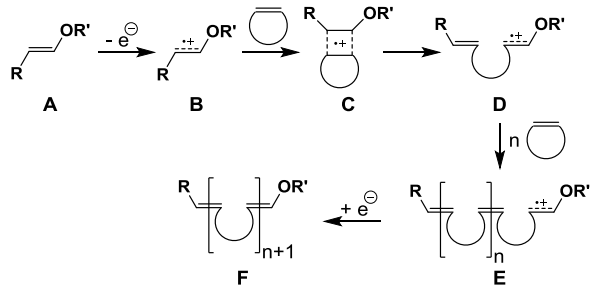

To begin our investigations, we chose readily available vinyl ethers (**1a – c**) and norbornene (**NB**) as our model strained monomer due to its relatively high ring strain and

frequent use in metal-mediated ROMP (**Figure 3.2**). Cyclic voltammograms of the initiators exhibited irreversible oxidation peaks with oxidation potentials (E_{ox}) ranging from 1.43 – 1.30 V vs SCE, consistent with literature data (see experimental). We began our electrochemical investigations using an undivided cell consisting of a 3-neck round bottom flask, carbon fiber electrodes, and a nonaqueous $Ag/AgNO_3$ reference electrode (**Figure 3.3**). As mentioned previously, Chiba's group observed that 1 M $LiClO_4/CH_3NO_2$ was necessary for the success of their electrochemical [2 + 2] cycloadditions and olefin metatheses. Building off of this observation, we used 1 M $LiClO_4/CH_3NO_2$ for the bulk electrolyses of vinyl ether initiator **1a** in the presence of **NB**. Notably, **NB** has limited solubility in $LiClO_4/CH_3NO_2$ with a saturated concentration of 0.5 M as determined by ^{1}H NMR spectroscopy with an internal standard.

Figure 3.2: Monomer and initiators used in metal-free ROMP.

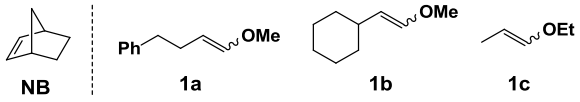

Figure 3.3: Electrochemical cell set up for electro-organic ROMP.

Our initial conditions were modeled after Chiba's olefin metathesis and consisted of a monomer concentration of 0.5 M and initiator concentration of 0.015 M. Unfortunately, no polymer formation was observed in the bulk solution; however, during the cleaning of the carbon fiber anode, we noticed that the surface of the anode was coated with a white residue that was insoluble in acetone and methanol. This observation led us to attempt characterization of the residue. Characterization of this residue using ^{1}H-NMR spectroscopy was consistent with polynorbornene (**PNB**) synthesized using metal initiators and gel-permeation chromatography (GPC) analysis revealed a number-average molecular weight (M_n) of 11.8 kDa (Đ = 2.2), confirming that the polymerization had indeed taken place.

Although this initial result was exciting, the isolated yield of polymer was only 3%. This low yield was most likely due to the limited solubility of **NB** and insolubility of the polymer in the $LiClO_4/CH_3NO_2$. During electrolysis, the insolubility of **PNB** resulted in the coating of the anode surface with growing polymer. The surface adhesion of the polymer prevented further electrolysis of the initiator and resulted in the rapid decrease in current to background levels prior to reaching 1 F/mol. We envisioned that moving to a better solvent or finding conditions that would prevent the blockage of the anode would be key to overcoming these challenges and improving the yield.

Solubility tests revealed that **NB** has increased solubility in CH_3CN and is fully soluble in CH_2Cl_2, THF, and toluene while **PNB** is not soluble in CH_3NO_2 and CH_3CN but is soluble in THF and CH_2Cl_2. Looking towards solving the solubility issue, we

investigated a variety of solvents containing 1 M $LiClO_4$ as electrolyte (**Table 3.1**). Lower concentrations of $LiClO_4$ (0.1 M) in CH_3CN gave similar yields to CH_3NO_2 (entries 2 – 3, **Table 3.1**). The use of THF as solvent and cosolvent (entries 4 – 5, **Table 3.1**) resulted in only trace amounts of polymer despite increased solubility of monomer and polymer. Unfortunately, $LiClO_4$ is not fully soluble in CH_2Cl_2 and toluene precluding their use as solvents for the bulk electrolysis. Although the use of toluene as a cosolvent was unsuccessful (entry 5, **Table 3.1**), CH_2Cl_2 as cosolvent yielded similar results to pure CH_3NO_2.

Table 3.1: Solvent screen for bulk electrolysis.[a]

entry	**solvent**	**yield (%)**
1	CH_3NO_2	3
2	CH_3CN	1
3	CH_3CN	4
4	THF	trace
5	THF/CH_3NO_2 (1:2)	<1
6	toluene/CH_3NO_2 (1:2.5)	0
7	CH_2Cl_2/CH_3NO_2 (1:2)	4

[a]Polymerizations conducted with $LiClO_4$ (1.0 M) as supporting electrolyte, **NB** as the monomer (saturated concentration of 0.5 M), initiator **1c**, and a constant voltage of 1.00 V (vs $Ag/AgNO_3$).

We also examined the influence of other electrolytes on the success of the polymerization. Unfortunately attempts to use tetrabutylammonium salts (NBu_4X, X =

ClO_4, PF_6, or BF_4) as the electrolyte led to no polymer formation, whereas the use of $LiBF_4$, LiCl, and $NaClO_4$ were unsuccessful due to the insolubility of these salts in CH_3NO_2. Ultimately, $LiClO_4$ emerged as the only successful electrolyte.

We next looked into the effect of the electrode material (**Table 3.2**). All other carbon electrodes (entries 3 – 6, **Table 3.2**) were unsuccessful. Anodes made from silver and copper (entries 8 – 9, **Table 3.2**) were incompatible with the oxidation potentials used for the bulk electrolysis and platinum electrodes (entry 2 and 7, **Table 3.2**) were found to be unsuccessful. In the end, we found that carbon fiber was the only electrode material that resulted in polymer formation.

Table 3.2: Electrode screen for bulk electrolysis.[a]

entry	anode	cathode	yield (%)
1	carbon fiber	carbon fiber	3
2	carbon fiber	platinum basket	0
3	RVC	RVC	0
4	glassy carbon	carbon fiber	0
5	carbon fiber	glassy carbon	0
6	graphite	graphite	0
7	platinum basket	platinum basket	0
8	silver coil	platinum basket	0
9	copper wire	platinum basket	0

[a]Polymerizations conducted in CH_3NO_2 with $LiClO_4$ (1.0 M) as supporting electrolyte, **NB** as the monomer (saturated concentration of 0.5 M), initiator **1c**, and a constant voltage of 1.00 V (vs $Ag/AgNO_3$).

Following all of these reaction screens, it became apparent that carbon fiber electrodes, $LiClO_4$, and CH_3NO_2 were crucial for the success of the electro-organic ROMP. Attempts to increase the solubility of the polymer through the use of cosolvents did not increase the yields significantly. The inability to increase solubility while maintaining the desired reactivity led us to consider other strategies to prevent the coating of the anode during electrolysis. Decreasing the $[M]_0/[I]_0$ ratio to 28/1 (limit of the solubility of **NB**) and replacing the anode with a fresh electrode after the current reached low levels improved the yield to 13%. Although this resulted in significantly higher yields, the need to replace the anode 6 – 8 times throughout the electrolysis was not ideal. We were able to achieve similar yields with only one anode replacement by sonicating the cell in an ultrasonic bath throughout the electrolysis. With these optimized conditions in hand, the electro-organic ROMP of **NB** and **1a** gave 6.7 kDa **PNB** in 13% yield with a cis/trans ratio of 1:2 (entry 1, **Table 3.3**). Similar yields were obtained using initiators **1b** and **1c** (14% and 12% yields, respectively).

Table 3.3: Summary of results from the electro-organic ROMP of **1** and initiators **1a – c**.[a]

entry	initiator	$[M]_0/[I]_0$	M_n (kDa)	Đ	yield (%)
1	**1a**	28/1	6.7	1.5	13
2	**1b**	28/1	4.8	1.5	14
3	**1c**	28/1	6.2	1.4	12

[a]Polymerizations conducted in CH_3NO_2 with $LiClO_4$ (1.0 M) as supporting electrolyte, carbon fiber anode and cathode, and constant voltage of 1.13, 1.09, or 1.00 V (vs $Ag/AgNO_3$). M_n determined by GPC analysis using multi-angle laser light scattering (MALS).

We were able to demonstrate the first example of electro-organic ROMP for the polymerization of norbornene with various enol ether initiators. Although this proof of concept was exciting, the yields remained low due to challenges associated with limited solubility of the monomer, insolubility of the polymer, and inefficient heterogeneous oxidation of the initiator at the surface of the anode. Attempts to overcome these challenges resulted in mild success; however, the need to replace the electrodes and sonicate the solution during electrolysis limited the practicality of this method.

3.2.b Photoredox-mediated ROMP

Although electro-organic ROMP was an exciting breakthrough, the need for an incompatible electrolyte solution remained essential and ultimately limited the practicality of this method. We began to explore other avenues that would fulfill two main goals, homogeneous oxidations and compatibility with a wider range of solvents. Inspired by recent reports utilizing photoredox mediators to achieve metal-free polymerizations with spatiotemporal control, we investigated the viability of organic

photoredox mediators in metal-free ROMP.[10] Notably, photoredox polymerization strategies have focused almost exclusively on controlled radical addition polymerizations in which a redox process is inherent in the activation/deactivation of the polymer chain end. Traditional metal-mediated ROMP (**Scheme 3.6**), on the other hand, is redox-neutral at all stages, and the metal complex is covalently attached to each chain end until chemically cleaved at the end of the polymerization.[2]

Scheme 3.6: Generalized depiction of ROMP using transition metal alkylidene initiators.

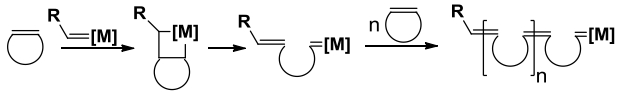

Photoredox mediators are also capable of achieving one-electron oxidations of enol ethers and the reactivity of the resulting radical cations is consistent with previously reported electrochemical approaches.[11] In 2013, Nicewicz and coworkers reported the oxidative [2 + 2] cycloaddition of styrenes using an organic photoredox mediator (**Scheme 3.7**).[11d] They proposed that the excited pyrylium facilitates the one-electron oxidation of the styrene substrate. The resulting radical cation then goes on to form the desired cyclobutane product in good yields. Although the method of oxidation is different, the reactivity of the radical cation intermediates is consistent with Chiba's work. Notably, oxidative [2 + 2] cycloadditions have also been accomplished using metal-based photoredox mediators. Recently, Yoon's group has reported the oxidative [2 + 2] cycloadditions of styrenes, dienes, and enones using Ru and Ir-based photoredox

mediators.[11] These examples suggest that photoredox chemistry might be amenable to metal-free ROMP.

Scheme 3.7: Representative example of organic photoredox-mediated [2 + 2] cycloadditon of styrenes.

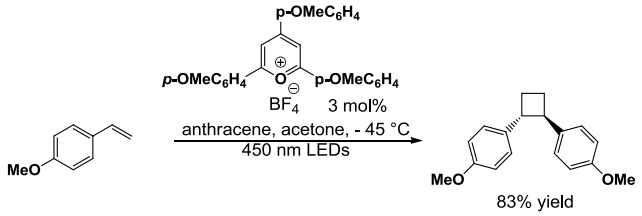

Figure 3.4: Photoredox mediators used in this study.

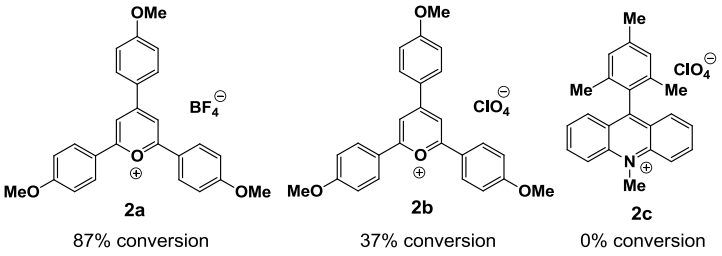

Pyrylium and acridinium salts (**2a** – **c**, **Figure 3.4**) have been identified as good candidates for facilitating photo-oxidation.[11] These mediators are capable of facilitating electron transfer when in the photo-excited state, and were expected to be good oxidizers for the vinyl ether initiators (**1**). Whereas the initiators **1a** – **c** display oxidation potentials in the range of 1.43 to 1.30 V vs SCE, the oxidizing power of excited state pyrylium and acridinium cations have been calculated to be 1.74 and 2.06 V vs SCE, respectively.[12,13] To explore photoredox-mediated ROMP, we used an initial monomer concentration of ca. 1.9 M in CH_2Cl_2, with a monomer to initiator (**NB**:**1a**) molar ratio of ca. 100:1. Using a blue LED light source (λ = 450 – 480 nm) in the presence of **2**, the best yields were

obtained from the pyrylium tetrafluoroborate salt **2a** (**Figure 3.5**). In general, **2b** gave lower yields than **2a**, and **2c** failed to produce any detectable **PNB**.

Figure 3.5: Photoredox-mediated ROMP reaction setup with blue LEDs.

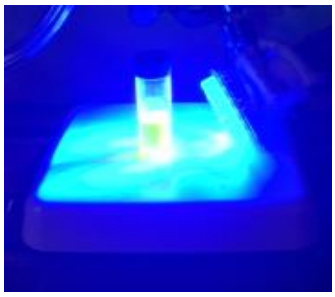

The structure of the **PNB** was confirmed by ^{1}H NMR analysis in comparison with an authentic sample prepared via traditional ROMP using the Grubbs 1st-generation initiator (see experimental). The glass transition temperature (T_g) of samples prepared by either traditional or photoredox-mediated ROMP were also found to be consistent with one another. Specifically, the T_g of PNB prepared by Ru-mediated ROMP (M_n = 49.5 kDa) was found to be 53.3 °C, versus 49.5 °C for a sample prepared by the photoredox-mediated approach (M_n = 43.9 kDa).

Each initiator (**1**) gave **PNB** in good yield via the photoredox method (**Table 3.4**, entries 1-3). Whereas **1a** provides a distinguishable NMR handle (see experimental), the majority of the polymerizations were conducted with **1c** simply due to commercial availability of this initiator. The amount of photoredox mediator **2a** that was required for successful polymerization was found to be quite low. Specifically, we observed

consistent M_n values and % conversions when using mediator to initiator ratios (**2a**:**1**) of 0.03 to 0.25 (entries 3 – 5).

Table 3.4: Polymerization results and GPC data for photoredox-mediated ROMP.

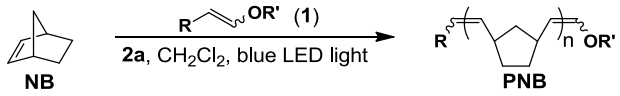

entry	initiator	**NB** : **1** : **2**[a]	$[\mathbf{NB}]_0$ (M)[b]	conversion (%)[c]	time (min)	$M_{n,\ theo}$ [kDa]	$M_{n,\ exp}$ [kDa]	Đ
1	**1a**	97 : 1 : 0.03	1.9	88 (73)	30	8.0	15.1	1.7
2	**1b**	97 : 1 : 0.03	1.9	92 (80)	30	8.4	14.9	1.6
3	**1c**	106 : 1 : 0.03	2.0	87 (67)	30	9.0	15.8	1.6
4	**1c**	104 : 1 : 0.10	1.9	80 (76)	150	7.8	13.5	1.4
5	**1c**	104 : 1 : 0.25	1.9	90 (73)	120	8.9	19.2	1.6
6	**1c**	48 : 1 : 0.03	1.8	95 (78)	60	4.3	8.1	1.4
7	**1c**	57 : 1 : 0.03	1.2	93 (58)	120	5.0	11.5	1.4
8	**1c**	491 : 1 : 0.03	5.3	51 (25)	120	23.6	22.2	1.5
9	**1c**	494 : 1 : 0.03	1.8	72 (50)	60	33.4	43.9	1.5
10	**1c**	1000 : 1 : 0.03	1.9	61 (47)	120	57.4	60.2	1.6
11[d]	**1c**	103 : 1 : 0.03	1.9	53 (29)	2580	5.0	7.2	1.3
12[e]	**1c**	102: 1: 0.03	1.9	88 (53)	90	8.5	15.5	1.4

[a]Initial molar ratio of **NB**, **1**, and **2**. [b]Initial concentration of **NB**. [c]Conversion of **NB**, as determined by ^{1}H NMR analysis; isolated yields after precipitation given in parentheses. [d]Reaction mixture exposed only to ambient light from fume hood. [e]Reaction mixture exposed to blue LED light with half of the bulbs blocked out. $M_{n,\ theo}$ is theoretical number-average molecular weight calculated from initial **NB**:**1** ratio and % conversion of **NB**. $M_{n,\ exp}$ is experimental number-average molecular weight, calculated from a weight-average molecular weight determined by GPC using multi-angle laser light scattering (MALLS). Dispersities (Đ) determined by GPC analysis.

Higher loading of mediator did manifest some bimodality in the GPC traces, with high MW shoulders appearing with increasing amounts of mediator. We speculate that

this may be due to increased concentration of active chain ends and therefore greater extent of chain-chain coupling. Additionally, the complexity of reversible chain end deactivation/re-activation is likely influenced by the amount of mediator.

Varying the initial monomer to initiator ratio provided some degree of control over the final M_n (entries 3, 6 – 10). We observed a consistent correlation between the theoretical and experimental M_n values, with experimental values generally being greater than expected for the given monomer to initiator ratios and % conversions. Dispersities were found to vary between 1.3 and 1.7 across different experiments, and remained fairly consistent during the course of each polymerization. We also found that the initial monomer concentration could be varied, with even very high (5.3 M) concentrations giving successful polymerizations (entry 8). This suggests that bulk polymerization using liquid monomers may be possible in the future with this approach.

Importantly, the initiator, mediator, and light source were each found to be required for the polymerization. In absence of blue LED light, but with exposure to ambient lighting from the fume hood, we observed slow conversion to give **PNB** (entry 11). Similarly, using blue LED light with half of the bulbs blocked out also gave **PNB** at an expected longer reaction time (entry 12). It is noteworthy that the reduced light intensity in each case gave lower Đ in comparison with other experiments, although the extent and origin of this trend are not yet clear. In complete absence of light, no **PNB** was observed.

During the course of the polymerization, we observed a gradual increase in M_n with increasing conversion of monomer, consistent with the chain growth nature of ROMP (**Figure 3.6**). Although there was a positive correlation, the linearity was not as precise as traditional "living" ROMP using, for example, Grubbs 3rd-generation initiator.[2c,14] This could be ascribed to the relative rates of initiation and propagation in the photoredox-mediated method, or any number of early termination events.

Figure 3.6: Plot of M_n (circles) and Đ (triangles) vs % conversion of monomer using initial **NB**:**1c** of (top) 100:1 and (bottom) 500:1.

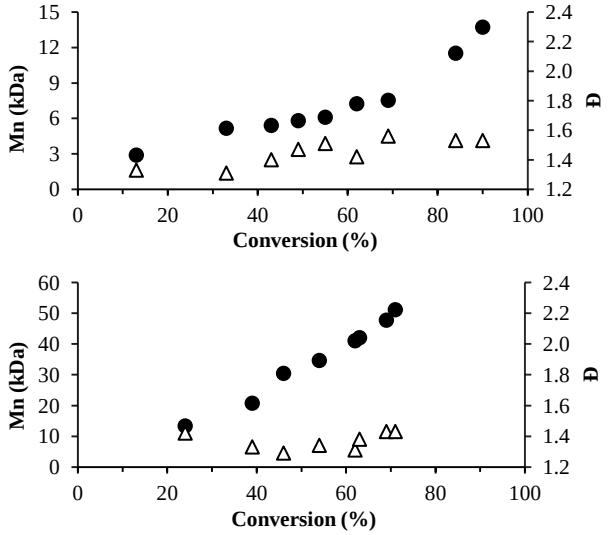

Mechanistically, we envision oxidation of the vinyl ether via electron transfer to the excited pyrylium cation to give the vinyl ether radical cation (e.g., **A → B**, **Scheme 3.5**). Notably, the propagating radical cation chain end likely forms a dynamic redox couple with the reduced pyrylium species. The reversibility would manifest an ability for the radical cation chain end to be reduced to terminate polymerization, and then oxidize and reinitiate upon exposure to light. We investigated this temporal control by monitoring

the polymerization with intermittent exposure to blue LED light. As shown in **Figure 3.7**, polymerization ceased in the dark and was reinitiated upon exposure to blue light. Specifically, we observed little to no further conversion of monomer in the dark as determined by ^{1}H NMR spectroscopy, and no significant changes in M_n as judged by GPC analysis (**Figure 3.8**). This suggested to us that the pyrylium cation and vinyl ether form a dynamic redox couple. Furthermore, the correlation between % conversion and increasing M_n during the alternating light/dark cycles is consistent with chain end activation/deactivation cycles, as opposed to photo-mediated initiation of new polymer chains upon re-exposure to light.

Figure 3.7: Plot of % conversion of monomer vs time, solid lines indicate periods of exposure to blue LED light. Dotted lines indicate periods in the dark, data point labels indicate M_n values (kDa). Initial conditions: **NB**:**1a** = 100:1, $[\mathbf{NB}]_0$ = 1.9 M.

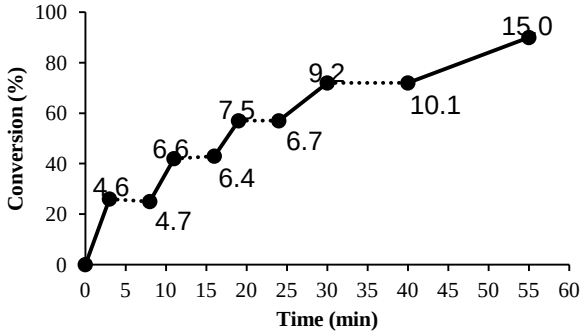

Figure 3.8: GPC traces for light/dark cycles during photoredox-mediated ROMP. From right to left (decreasing retention time) the sequence of GPC traces corresponds to increasing % conversion of monomer. The solid lines represent GPC traces following exposure to blue LED light and the dotted lines refer to GPC traces of periods in the dark immediately following a period of light (colors are coordinated).

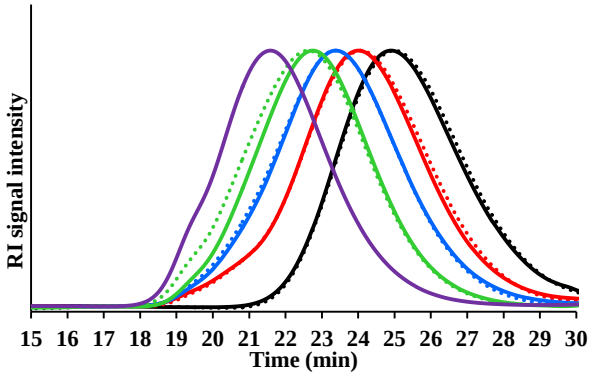

Section 3: Conclusions

In summary, we have developed the first protocol for achieving metal-free ROMP. The approach utilizes one-electron oxidation of electron-rich vinyl ethers to initiate the process, which can be achieved either electrochemically or via photoredox-mediated processes. A photoredox approach enabled high yields of polymerization in short reaction times under mild conditions. This demonstration may lead to a complementary approach to synthesizing ROMP polymers via a metal-free protocol, with the potential to offer unique synthetic control over end group functionality. The success of the photoredox mediation may also provide new opportunities for spatiotemporal control over production of ROMP-based polymers and materials.

Overall, our projects focused on developing greener alternatives to traditional methods in synthetic organic chemistry by discovering new reactivity and strategies at the interface of organocatalysis and redox chemistry. In doing so, we have introduced a

series of aldehyde oxidations that require neither transition metal reagents nor stoichiometric, sacrificial oxidants. Evolution of this project later arrived at the first demonstrated method for achieving ring-opening metathesis polymerization without using metal-based catalysts or initiators. This new polymerization strategy has opened the door for new capabilities in polymer and materials science. The mechanism, product properties, temporal control, and many other features of metal-free ROMP differ significantly from those arising from traditional methods. We hope that this discovery sparks new expansive and upward growth for creative applications of ROMP and cross metathesis.

Section 4: Experimental

Materials and Methods. Acetonitrile (CH_3CN) and nitromethane (CH_3NO_2) were dried over calcium hydride and distilled prior to use. Dichloromethane (CH_2Cl_2) and tetrahydrofuran (THF) were obtained from a solvent purification system. ^{1}H and ^{13}C NMR spectra were recorded on Bruker AVance 300 MHz or 500 MHz spectrometers. Chemical shifts are reported in delta (δ) units, expressed in parts per million (ppm) downfield from tetramethylsilane using the residual protio-solvent as an internal standard ($CDCl_3$, ^{1}H: 7.27 ppm and ^{13}C: 77.0 ppm). Data are reported as follows: chemical shift, multiplicity (s = singlet, d = doublet, dd= doublet of doublets, br = broad, m = multiplet), coupling constants (Hz) and integration. UV-visible spectroscopy data were collected on an Agilent 8453 UV-vis spectrophotometer. Gel permeation chromatography (GPC) was performed using a GPC setup consisting of: a Shimadzu pump, 3 in-line columns, and

Wyatt light scattering and refractive index detectors with tetrahydrofuran (THF) as the mobile phase. Number-average molecular weights (M_n) and weight-average molecular weights (M_w) were calculated from light scattering. All polymerizations were carried out under an inert atmosphere of nitrogen in standard borosilicate glass vials purchased from Fisher Scientific with magnetic stirring unless otherwise noted. Irradiation of photochemical reactions was done using a 2 W Miracle blue LED indoor gardening bulb purchased from Amazon. Electrochemical experiments were performed on a CH Instruments 1100B potentiostat using a 25 mL 3-neck round bottom flask as an undivided cell. Cyclic voltammetry experiments were done using a glassy carbon working electrode (3 mm diameter), Pt counter electrode (Premier Lab Supply), and Ag/0.01 M $AgNO_3$ (0.1 M tetrabutylammonium tetrafluoroborate in CH_3CN) reference electrode. Electro-organic ROMP experiments were done using a carbon fiber (Zoltek) working electrode, carbon fiber counter electrode, and Ag/0.01 M $AgNO_3$ (0.1 M tetrabutylammonium tetrafluoroborate in CH_3CN) reference electrode. T_g values were determined using a Perkin-Elmer DMA 8000. Analysis was performed on powdered samples held within material pockets supplied by Perkin-Elmer. Samples were analyzed using the Single-Cantilever Geometry Fixture with the following settings: heating rate = 3.0 ^oC/min, frequency = 1 Hz, static force = 1.0 N. Reported T_g values refer to the temperature corresponding to the peak of the tan delta curve. Initiators **1a** and **1b** were prepared according to literature procedures.[15] The pyrylium tetrafluoroborate (**2a**) and perchlorate (**2b**) salts were prepared according to literature procedures.[12] All other

reagents and solvents were obtained from commercial sources and used as received unless otherwise noted.

General procedure for the preparation of initiators 1a and 1b. Procedures for the synthesis of enol ether initiators as reported by Stambuli were used.[15]

Scheme 3.8: Preparation of initiators **1a** and **1b**.

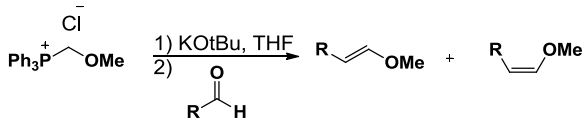

A solution of potassium *tert*-butoxide (5.1 g, 45.0 mmol, 1.5 equiv.) in 10 mL of dry THF was slowly added to a solution of (methoxymethyl)triphenylphosphonium chloride (15.4 g, 45.0 mmol, 1.5 equiv.) in 40 mL of dry THF. After stirring the red solution at 23°C for 45 min, a solution of the corresponding aldehyde (30.0 mmol, 1.0 equiv.) in 10 mL of dry THF was slowly added and allowed to stir at 23°C for an additional 2 h. The solvent was removed under vacuum and the residue was diluted with hexanes. The organic layer was washed with water (3 x 100 mL) and dried over Na_2SO_4. The solvent was removed under reduced pressure and the resulting residue was purified by filtering through a plug of silica with diethyl ether as the eluent. In some cases, residual triphenylphosphine was removed by stirring overnight with 10 equiv of iodomethane and filtration through a plug of silica with diethyl ether as the eluent.

1-methoxy-4-phenyl butene (1a).

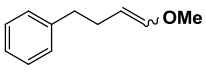

Prepared according to the above procedure in 92% yield (1:2 *cis* to *trans* ratio); spectral data were consistent with literature values.[1i]

2-cyclohexyl-1-methoxyethylene (1b).

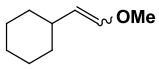

Prepared according to literature procedures in 82% yield (1:2 *cis* to *trans* ratio).[15] ^{1}H NMR (300 MHz, $CDCl_3$) δ = 6.29 (d, *J* = 12 Hz, 1 H, *trans*) 5.79 (d, *J* = 6.0 Hz, 0.5 H, *cis*) 4.70 (dd, *J* = 6.0 Hz, 9 Hz, 1 H, *trans*) 4.24 (dd, *J* = 3 Hz, 6 Hz, 0.5 H, *cis*) 3.58 (s, 1.5 H, *cis*) 3.50 (s, 3 H, *trans*) 2.42 (m, 0.5 H, *cis*) 1.88 (m, 1 H, *trans*) 1.68 (m, 4 H, *cis/trans*) 1.16 (m, 9 H, *cis/trans*). ^{13}C NMR (125 MHz, $CDCl_3$) δ = 145.7, 144.5, 113.4, 109.7, 59.5, 55.8, 36.9, 34.4, 35.4, 33.4, 26.2, 26.1, 26.0

Scheme 3.9: Preparation of 2,4,6-tri-(*p*-methoxyphenyl) pyrylium tetrafluoroborate (**2a**).

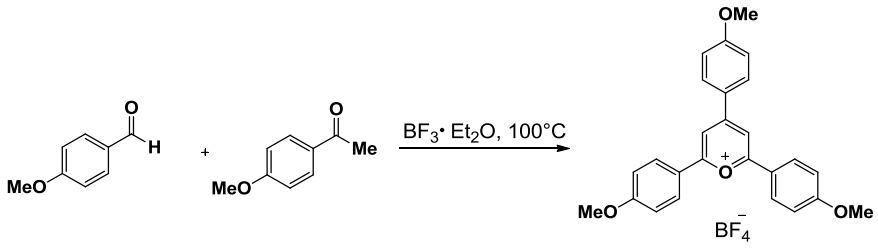

To a flask containing *p*-anisaldehyde (6.1mL, 50.3 mmol, 1 equiv) and *p*-acetylanisole (15.07g, 100.4 mmol, 2 equiv) was added BF_3•Et_2O (15.0mL, 121.5 mmol, 2.4 equiv) dropwise over 5 min. The solution was heated in an oil bath set to 100 ºC. After 2 h, the reaction was removed from heat. Once at room temperature, the crude material was diluted with acetone (200 mL) and Et_2O (250 mL) and filtered to give a rust-colored

solid. The solids were washed with warm acetone (175 mL) and dried under vacuum to give the pyrylium tetrafluoroborate as an orange solid (5.01 g, 20%). Spectral data matched those previously reported.

Preparation of 2,4,6-tri-(*p*-methoxyphenyl) pyrylium perchlorate (2b).

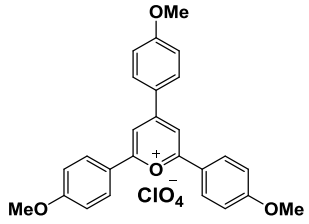

Prepared according to literature procedures in 10% yield, spectral data were consistent with literature values.[17]

General procedure for cyclic voltammetry of initiators 1a – 1c. Representative cyclic voltammograms are depicted in **Figure 3.9 – 3.11**. The general procedure was as follows: In a drybox, a 3-neck round bottom flask was charged with a magnetic stir bar, anhydrous CH_3NO_2 (15 mL), and lithium perchlorate (15.0 mmol). The indicated initiator (0.075 mmol) was then added to the mixture. The flask was equipped with a glassy carbon anode (3 mm diameter), Pt basket cathode, and $Ag/AgNO_3$ reference electrode (0.01 M $AgNO_3$/0.1 M tetrabutylammonium tetrafluoroborate in CH_3CN) and then the apparatus was sealed using rubber septa. The electrochemical cell was then removed from the drybox and the solution was placed under a positive pressure of N_2 and stirred at room temperature. Stirring was stopped prior to connecting to the potentiostat. The cyclic voltammograms for the initiators were typically taken from 0.5 V to 2.5 V vs. $Ag/AgNO_3$

with a sweep rate of 0.10 V/s. Ferrocene (0.15 mmol) was added as an internal standard after each voltammogram.[18] All potentials are reported in V vs. SCE.

Figure 3.9: Cyclic voltammogram of initiator **1a.**

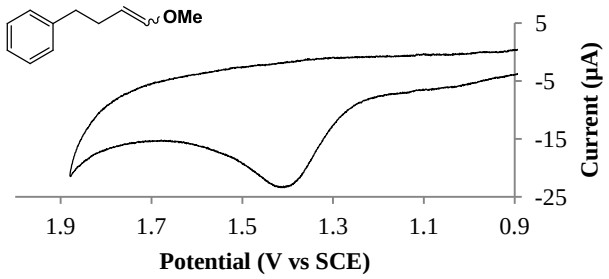

Figure 3.10: Cyclic voltammogram of initiator **1b.**

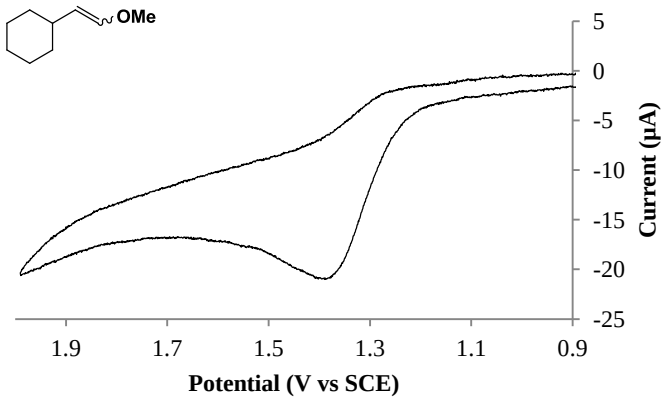

Figure 3.11: Cyclic voltammogram of initiator **1c.**

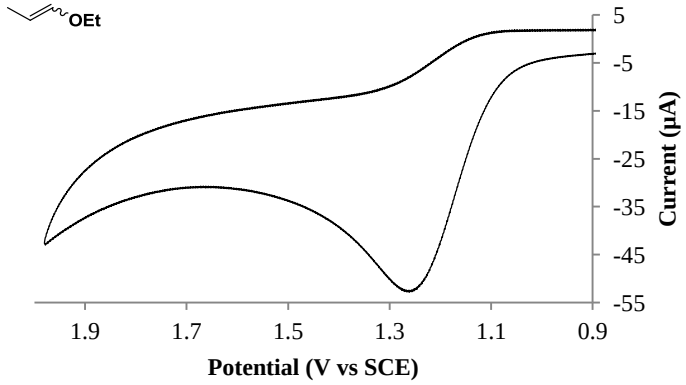

General procedure for electro-organic ROMP. Electro-organic ROMP experiments were done using a carbon fiber (Zoltek) working electrode, carbon fiber counter electrode, and Ag/0.01 M $AgNO_3$ (0.1 M tetrabutylammonium tetrafluoroborate in CH_3CN) reference electrode in a double junction chamber (**Figure 3.12**). The carbon fiber electrodes were 40 mm in length (excluding the copper lead) and 15 mm of the carbon fiber was submerged in the electrolyte solution during electrolysis. In the drybox, a 3-neck round bottom flask was charged with a magnetic stir bar, lithium perchlorate (15.0 mmol) and CH_3NO_2 (15 mL). To the solution was added norbornene (23.2 mmol, 100 equiv.) and initiator (0.23 mmol, 1 equiv.). The electrodes were attached onto the cell and the apparatus was sealed using rubber septa. The electrochemical cell was then removed from the dry box and placed under a positive pressure of N_2. The electrodes were connected to the potentiostat and bulk electrolysis with a constant potential of 1.43 V vs SCE was started with constant stirring. After the current reached background levels,

the electrolysis was stopped and hydroquinone (2.3 mmol, 10 equiv) was then added to the solution. The carbon fiber electrodes were removed and soaked in THF. The quenched solution and electrode soaks were added to rapidly stirring methanol to precipitate the polymer. The resulting solids were redissolved in THF, passed through a syringe filter (2 μm) to remove any carbon fiber particulates, and reprecipitated into methanol. The resulting solids were dried under vacuum and analyzed by ^{1}H NMR spectroscopy and GPC.

Figure 3.12: a) Undivided electrochemical cell with carbon fiber working and counter electrodes, double junction chamber (for the reference electrode), and $Ag/AgNO_3$ reference electrode. b) Carbon fiber electrode with copper lead bound with Teflon tape.

a)  b) 

General procedure for photoredox mediated ROMP. All polymerizations were set up in a drybox under an inert atmosphere of nitrogen. Irradiation of the sealed vials with blue LEDs was done outside of the drybox. A 2-dram vial was equipped with a magnetic stir-bar, 2,4,6-tri-(*p*-methoxyphenyl) pyrylium tetrafluoroborate (**2a**, 3.0 – 25.0 mol %), and norbornene (48 – 1000 equiv. relative to **1**). The solvent, CH_2Cl_2 (1.8 – 1.9 M), and

initiator **1** (1 equiv.) were added to the vial. The vial was sealed with a Teflon-coated screw cap and brought out of the drybox. The mixture was irradiated for the indicated period of time. The reaction progress and M_n were monitored by ^{1}H NMR spectroscopy and GPC, respectively. Upon completion, hydroquinone (5 equiv.) was added to the reaction mixture, which was then passed through a short plug of alumina. The polymer solution was then added dropwise into an excess of methanol (MeOH) or dry acetonitrile (CH_3CN) to cause precipitation of the polymer. *Note: As a control, the same setup was performed outside the drybox, and then the reaction mixture sparged with N_2 for 15 minutes before irradiation. This led to a significant decrease in polymer formation (only ~ 30 % conversion of monomer as determined by ^{1}H NMR spectroscopy) compared to reactions setup inside the drybox.*

NMR Spectra for Structural Comparisons:

Figure 3.13: ^{1}H NMR spectra of (top) polynorbornene (M_n = 49.3 kDa; Đ = 1.2, *cis*/*trans* = 1:8) synthesized using Grubbs 1st-generation initiator, and (bottom) polynorbornene (M_n = 10.1 kDa; Đ = 1.5 by GPC and M_n = 12.7 kDa by NMR; *cis*/*trans* = 1:2) synthesized via metal-free ROMP using initiator **1a**.

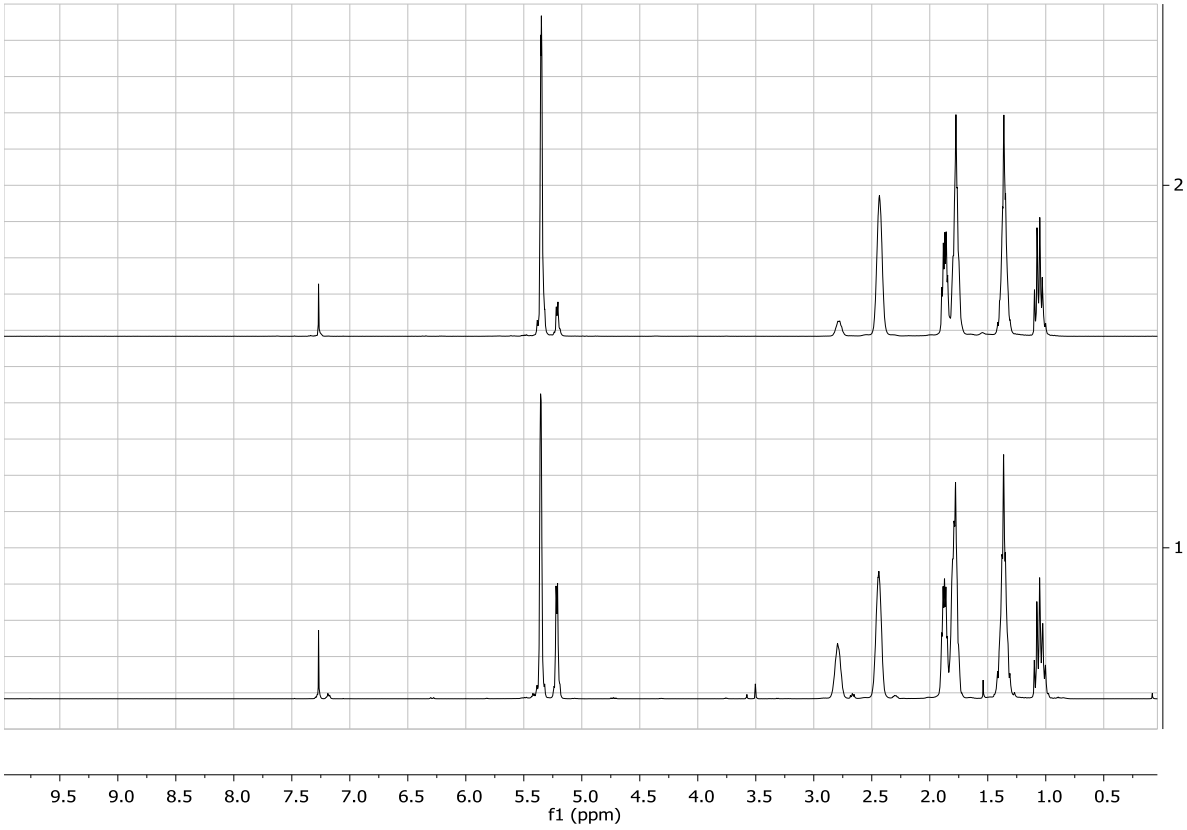

Figure 3.14: Zoomed in **^{1}H NMR** spectra of (top) polynorbornene (M_n = 10.1 kDa; Đ = 1.5) synthesized via metal-free ROMP using initiator **1a**, and (bottom) initiator **1a**.

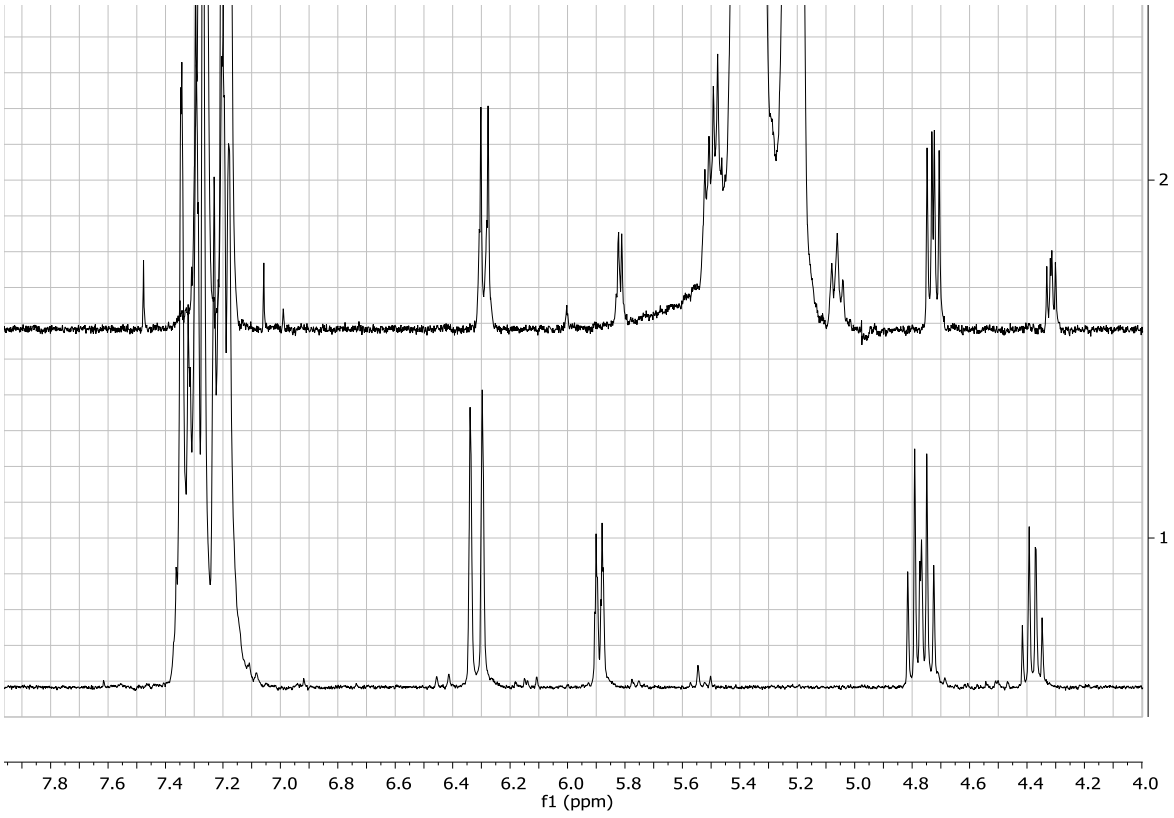

Figure 3.15: ^{1}H NMR spectra of (black) polynorbornene (M_n = 10.1 kDa; Đ = 1.5) synthesized via metal-free ROMP using initiator **1a**, and (red) initiator **1a**.

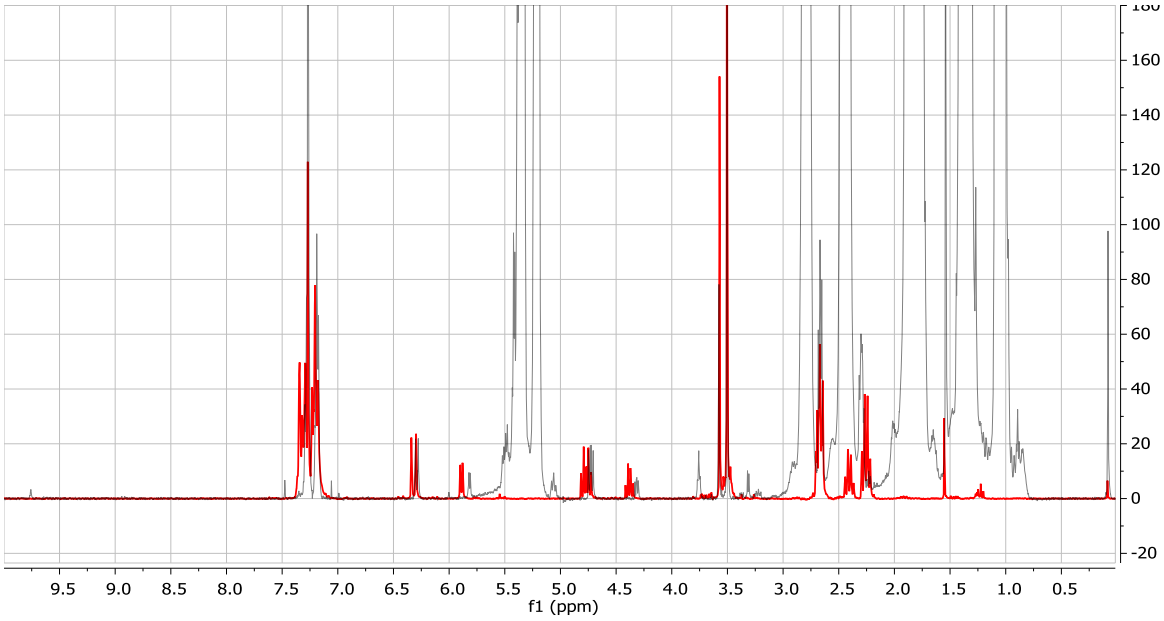

Figure 3.16: Zoomed in **^{1}H NMR** spectra of (black) polynorbornene (M_n = 10.1 kDa; Đ = 1.5) synthesized via metal-free ROMP using initiator **1a**, and (red) initiator **1a**.

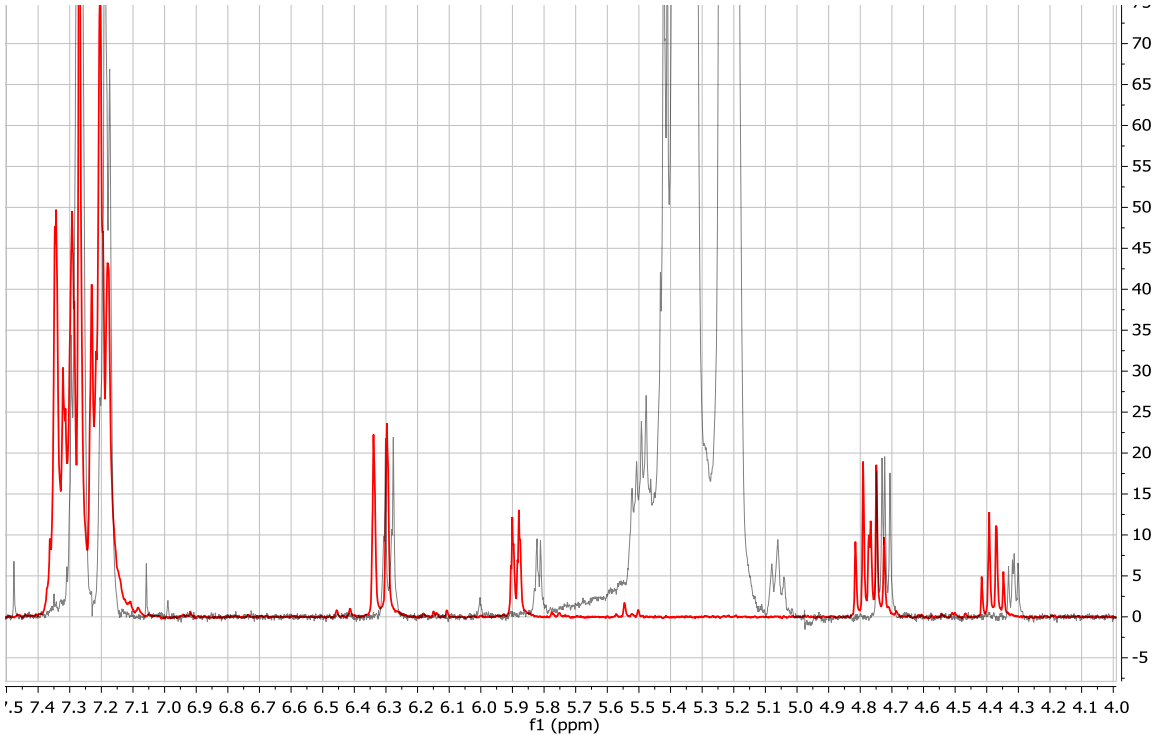

Representative GPC traces:

Figure 3.17: GPC trace of polymer corresponding to Table 3.4, entry 1 of the main text.

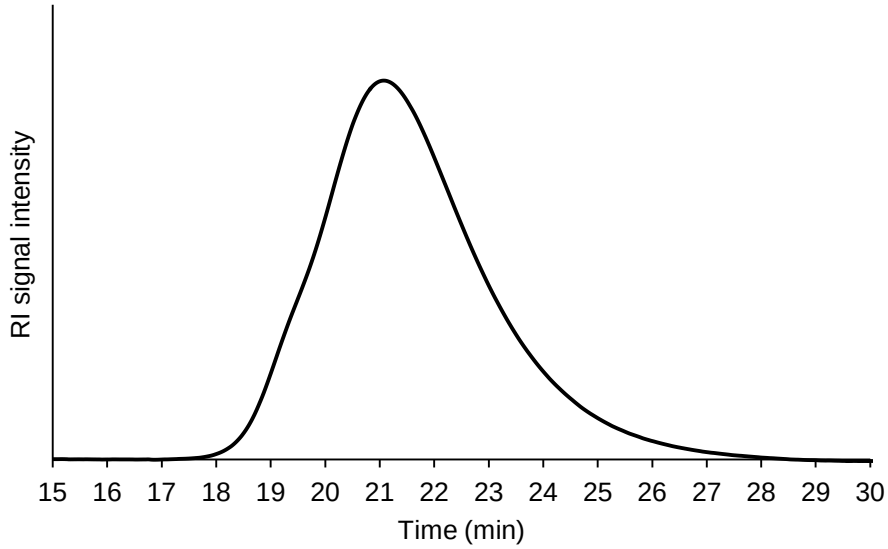

Figure 3.18: GPC trace of polymer corresponding to Table 3.4, entry 2 of the main text.

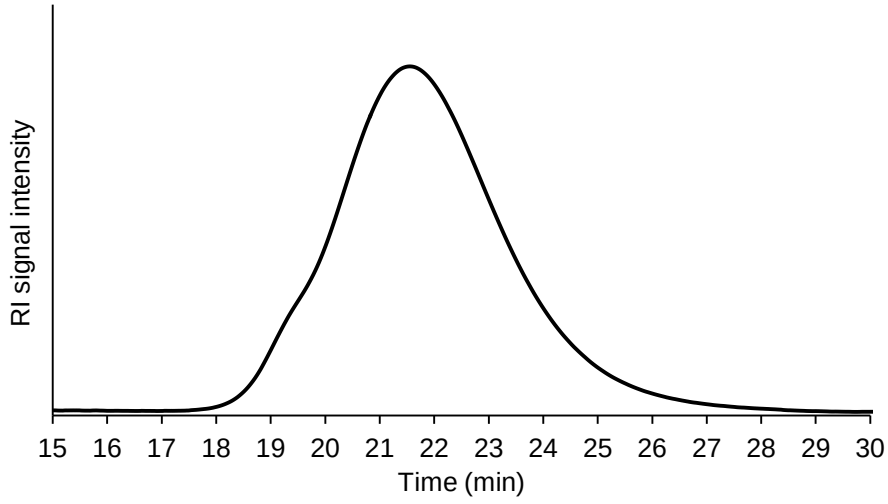

Figure 3.19: GPC trace of polymer corresponding to Table 3.4, entry 3 of the main text.

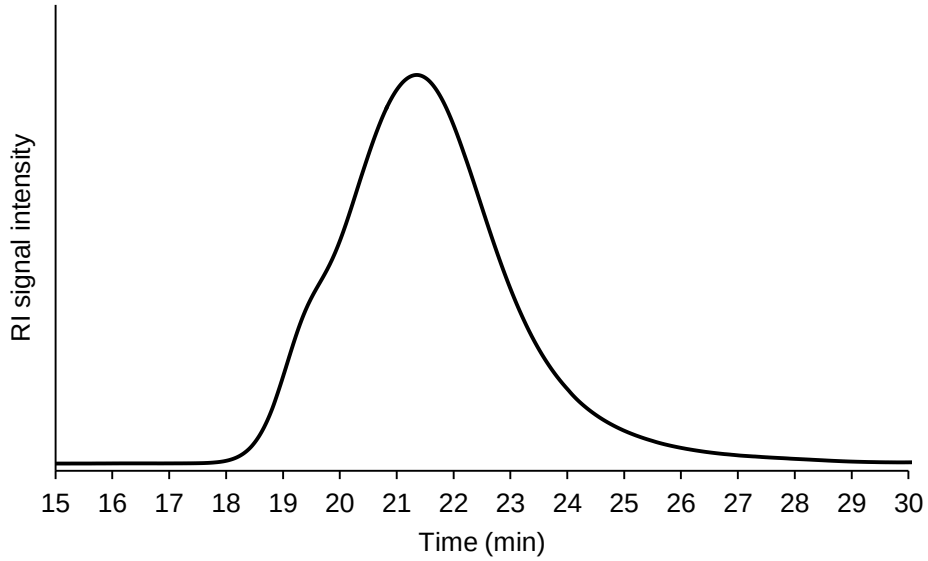

Figure 3.20: GPC trace of polymer corresponding to Table 3.4, entry 4 of the main text.

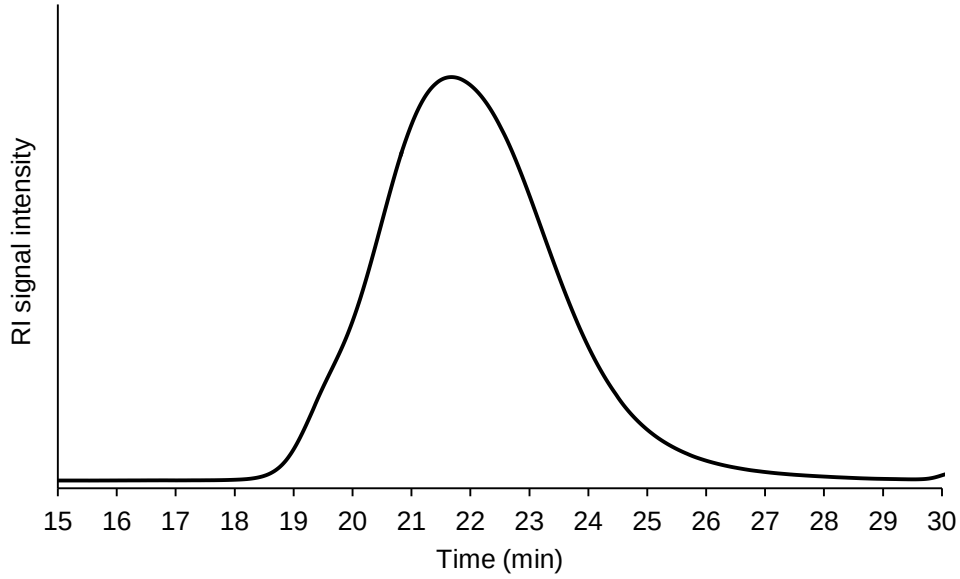

Figure 3.21: GPC trace of polymer corresponding to Table 3.4, entry 5 of the main text.

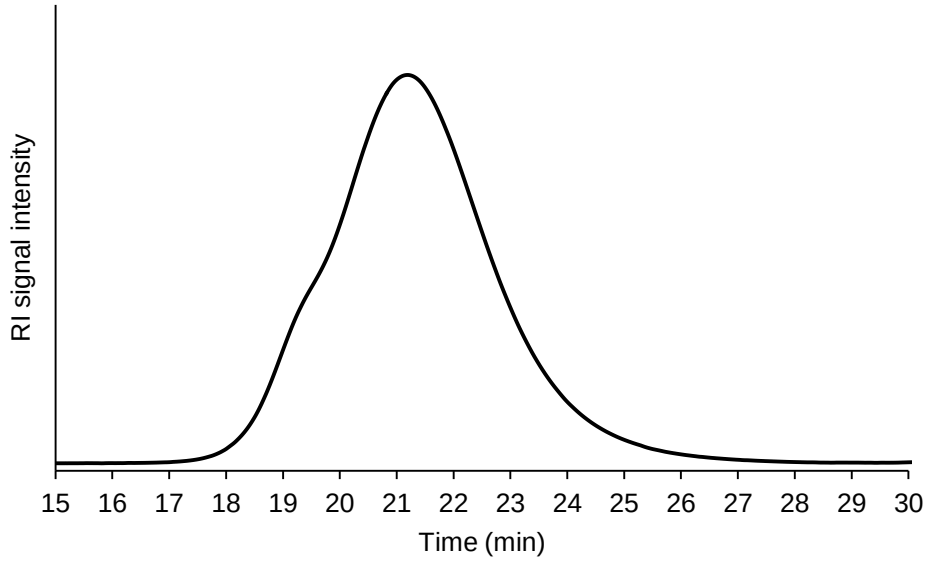

Figure 3.22: GPC trace of polymer corresponding to Table 3.4, entry 6 of the main text.

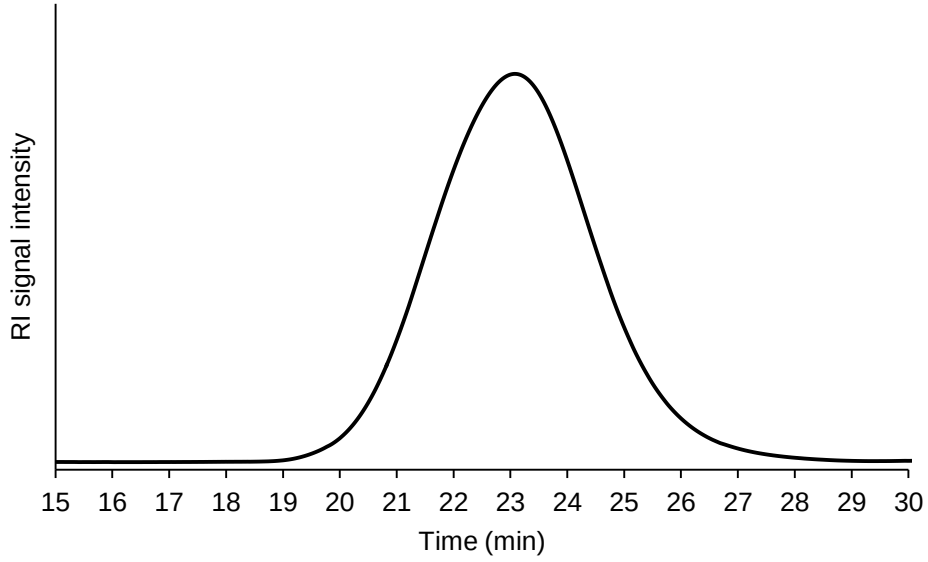

Figure 3.23: GPC trace of polymer corresponding to Table 3.4, entry 7 of the main text.

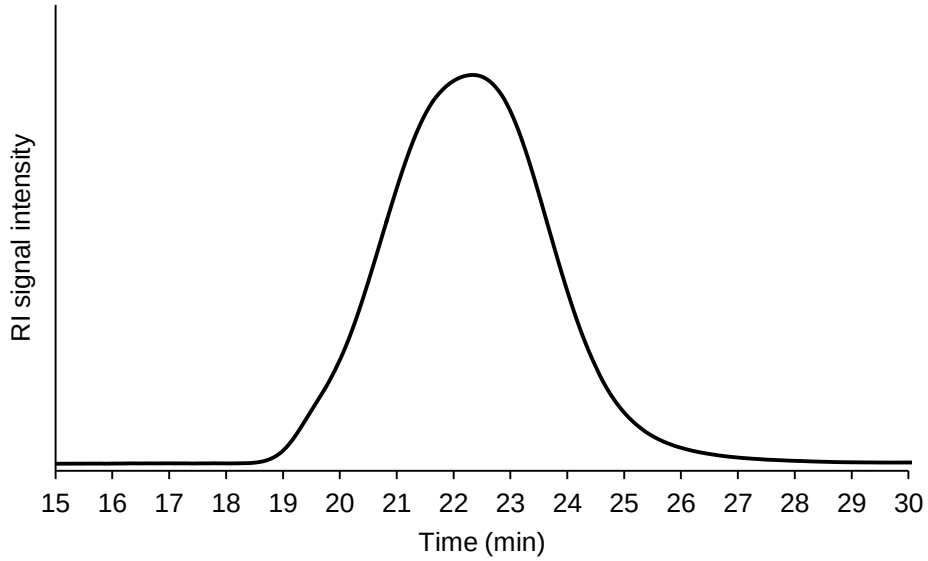

Figure 3.24: GPC trace of polymer corresponding to Table 3.4, entry 8 of the main text.

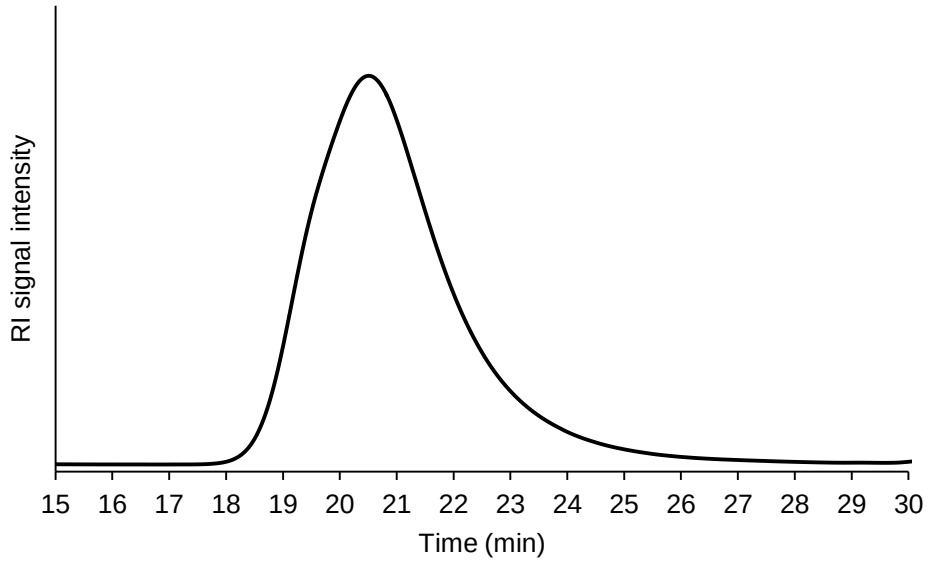

Figure 3.25: GPC trace of polymer corresponding to Table 3.4, entry 9 of the main text.

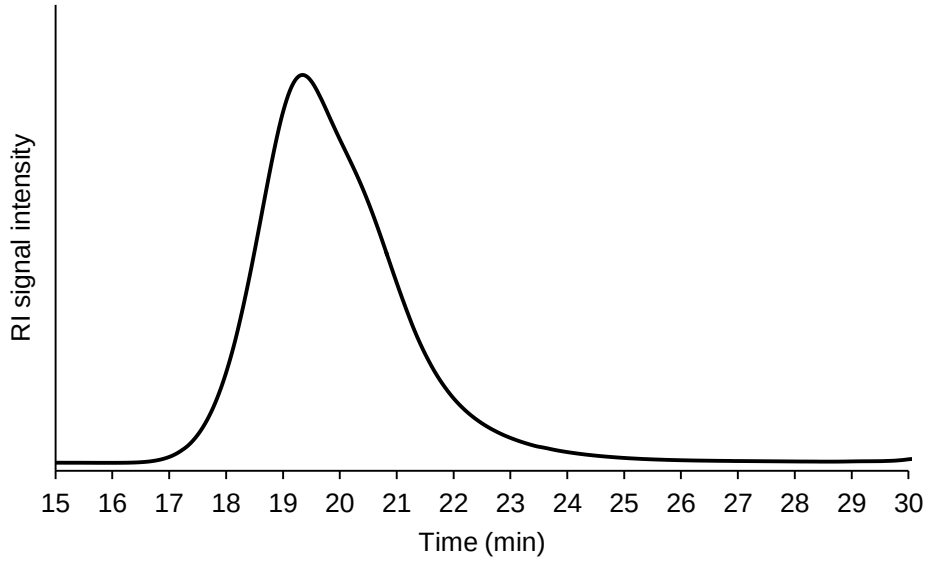

Figure 3.26: GPC trace of polymer corresponding to Table 3.4, entry 10 of the main text.

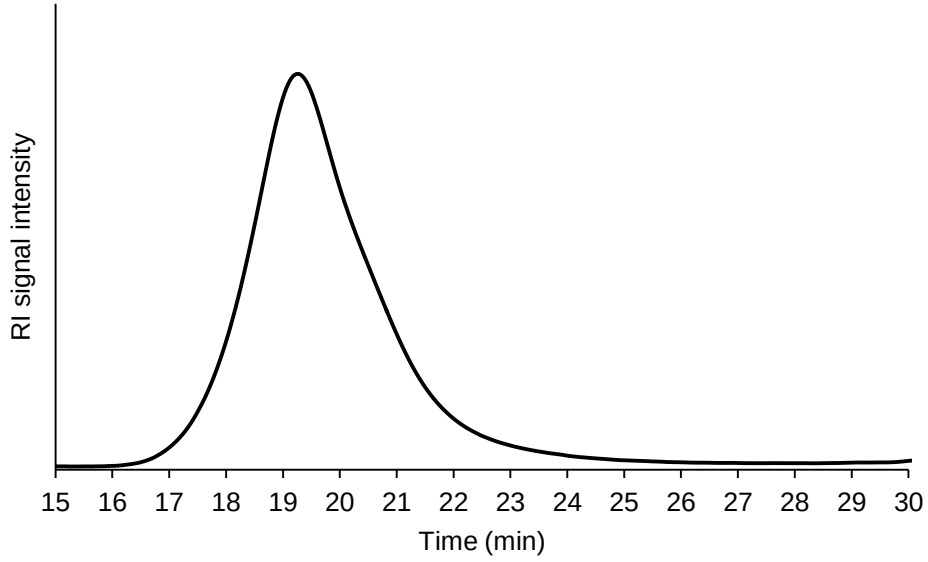

Figure 3.27: GPC trace of polymer corresponding to Table 3.4, entry 11 of the main text.

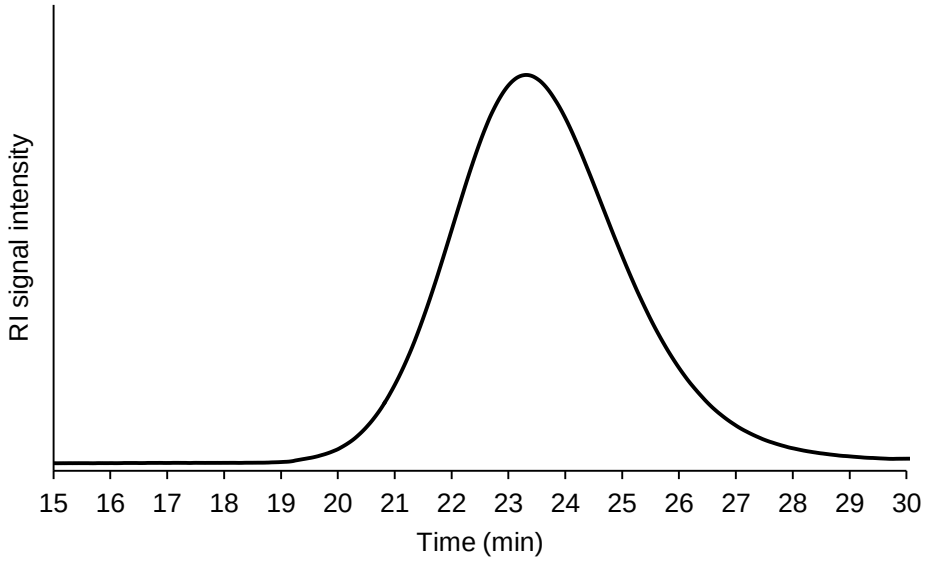

Figure 3.28: Each GPC trace corresponds to a data point in Figure 3.6, top, from the main text. From right (longest retention time) to left (shortest retention time), the sequence of GPC traces corresponds to increased % conversion of monomer as shown in Figure 3.6, top.

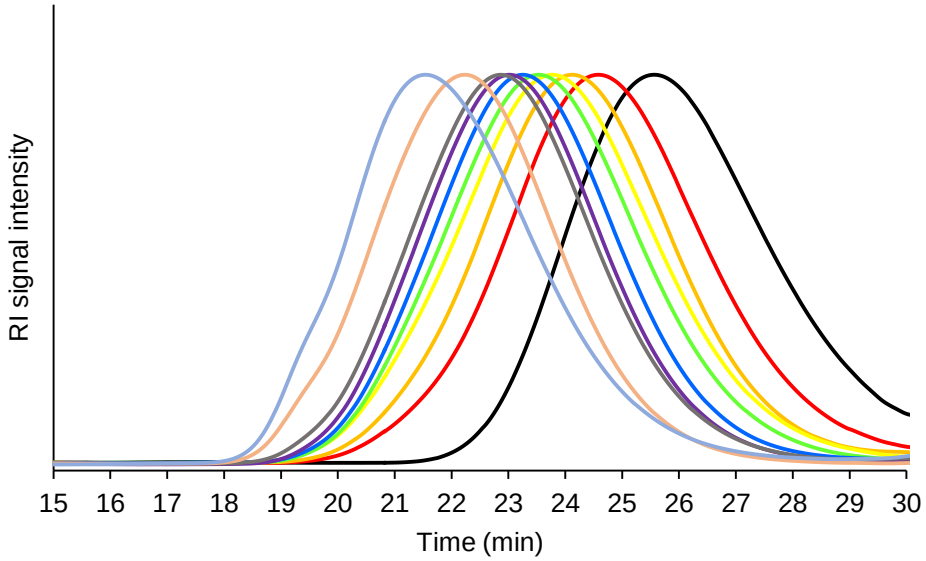

Figure 3.29: Each GPC trace corresponds to a data point in Figure 3.6, bottom, from the main text. From right (longest retention time) to left (shortest retention time), the sequence of GPC traces corresponds to increased % conversion of monomer as shown in Figure 3.6, bottom.

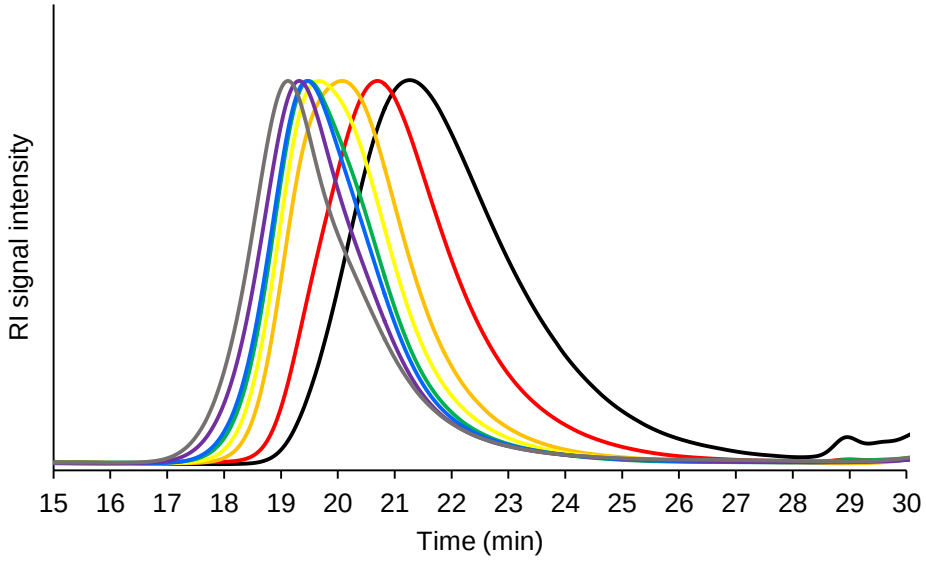

UV-Visible Spectroscopy Data:

Figure 3.30: UV-visible spectrum of a $1.4*10^{-4}$ M solution of pyrylium 2a. Measurements were taken in dichloromethane using a quartz cuvette with a 1 cm pathlength. The measured extinction coefficient of **2a** was 5400 M^{-1} cm^{-1}.

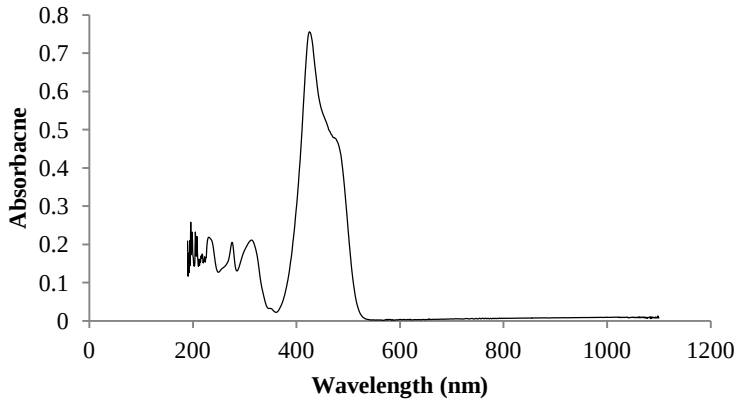

Figure 3.31: UV-visible spectrum of polynorbornene synthesized via metal-free ROMP using initiator **1b**. Measurements were taken in dichloromethane using a quartz cuvette with a 1 cm pathlength.

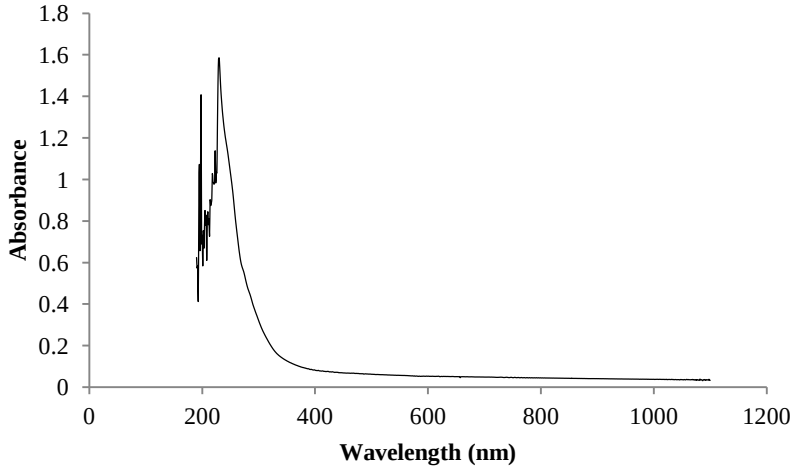

Notes and References to Chapter 3

[1] For electrochemical oxidations: (a) Redden, A.; Perkins, R. J.; Moeller, K. M. *Angew. Chem. Int. Ed.* **2013**, *52*, 12865. (b) Yamaguchi, Y.; Okada, Y.; Chiba, K. *J. Org. Chem.* **2013**, *78*, 2626. (c) Okada, Y.; Akaba, Y.; Chiba, K. *Org. Lett.* **2009**, *11*, 1033. (d) Tang, F.; Moeller, K. M. *Tetrahedron* **2009**, *65*, 10863. (e) Moeller, K. M. *Synlett* **2009**, 1208. (f) Xu, H.-C.; Moeller, K. M. *J. Am. Chem. Soc.* **2008**, *130*, 13542. (g) Tang, F.; Moeller, K. M. *J. Am. Chem. Soc.* **2007**, *129*, 12414. (h) Tang, F.; Chen, C.; Moeller, K. M. *Synthesis* **2007**, 3411. (i) Miura, T.; Kim, S.; Kitano, Y.; Tada, M.; Chiba, K. *Angew. Chem. Int. Ed.* **2006**, *45*, 1461–1463. (j) Liu, B.; Duan, S.; Sutterer, A. C.; Moeller, K. M. *J. Am. Chem. Soc.* **2002**, *124*, 10101. (k) Chiba, K.; Miura, T.; Kim, S.; Kitano, Y.; Tada, M. *J. Am. Chem. Soc.* **2001**, *123*, 11314–11315. (l) Duan, S.; Moeller, K. M. *Org. Lett.* **2001**, *3*, 2685. (m) Moeller, K. M. *Tetrahedron* **2000**, *56*, 9527.

[2] (a) Schrock, R. R. *Acc. Chem. Res.* **2014**, *47*, 2457–2466. (b) Sutthasupa, S.; Shiotsuki, M.; Sanda, F. *Polym. J.* **2010**, *42*, 905–915. (c) Bielawski, C. W.; Grubbs, R. H. *Prog. Polym. Sci.* **2007**, *32*, 1–29. (d) Rosebrugh, L. E.; Marx, V. M.; Keitz, B. K.; Grubbs, R. H. *J. Am. Chem. Soc.* **2013**, *135*, 10032–10035. (e) Jeong, H.; Kozera, D. J.; Schrock, R. R.; Smith, S. J.; Zhang, J.; Ren, N.; Hillmyer, M. A. *Organometallics* **2013**, *32*, 4843–4850. (f) Forrest, W. P.; Axtell, J. C.; Schrock, R. R. *Organometallics* **2014**, *33*, 2313–2325.

[3] (a) Chauvin, Y. *Angew. Chem. Int. Ed.* **2006**, *45*, 3740–3747. (b) Schrock, R. R. *Angew. Chem. Int. Ed.* **2006**, *45*, 3748–3759. (c) Grubbs, R. H. *Angew. Chem. Int. Ed.* **2006**, *45*, 3760–3765.

[4] Mol, J. C. *J. Mol. Catal. A: Chem.* **2004**, *213*, 39–45.

[5] (a) Plamper, F. *Colloid Polym. Sci.* **2014**, *292*, 777. (b) Szczepaniak, G.; Kosiński, K.; Grela, K. *Green Chem.* **2014**, *16*, 4474. (c) Varnado, C. D.; Rosen, E. L.; Collins, M. S.; Lynch, V. M.; Bielawski, C. M. *Dalton Trans.* **2013**, *42*, 13251. (d) Elbert, J.; Mersini, J.; Vilbrandt, N.; Lederle, C.; Kraska, M.; Gallei, M.; Stühn, B.; Plenio, H.; Rehahn, M. *Macromolecules* **2013**, *46*, 4255. (e) Peeck, L. H.; Leuthäusser, S.; Plenio, H. *Organometallics* **2010**, *29*, 4339. (f) Maishal, T. K.; Mondal, B.; Puranik, V. G.; Wadgaonkar, P. P.; Lahiri, G. K.; Sarkar, A. *J. Organomet. Chem.* **2005**, *690*, 1018. (g) Süβner, M.; Plenio, H. *Angew. Chem. Int. Ed.* **2005**, *44*, 6885.

[6] Vougioukalakis, G. C. *Chem. Eur. J.* **2012**, *18*, 8868–8880.

[7] Alcaide, B.; Almendros, P.; Luna, A. *Chem. Rev.* **2009**, *109*, 3817–3858.

[8] It should be noted that low detection limits for most metal byproducts also affords quantitative confirmation of contaminant levels, which can be advantageous.

[9] Ogawa, K. A.; Goetz, A. E.; Boydston, A. J. *J. Am. Chem. Soc.* **2015**, *137*, 1400.

[10] Treat, N. J.; Sprafke, H.; Kramer, J. W.; Clark, P. G.; Barton, B. E.; Read de Alaniz, J.; Fors, B. P.; Hawker, C. J. *J. Am. Chem. Soc.* **2014**, *136*, 16096.

[11] (a) Schultz, D. M.; Yoon, T. P. *Science* **2014**, *343*, 1239716. (b) Nicewicz, D. A.; Nguyen, T. M. *ACS Catalysis* **2014**, *4*, 355–360. (c) Du, J.; Skubi, K. L.; Schultz, D. M.;

Yoon, T. P. *Science* **2014**, *344*, 392–396. (d) Riener, M.; Nicewicz, D. A. *Chem. Sci.* **2013**, *4*, 2625–2629. (e) Lu, Z.; Yoon, T. P. *Angew. Chem. Int. Ed.* **2012**, *51*, 10329–10332.
[12] Martiny, M.; Steckhan, E.; Esch, T. *Chem. Ber.* **1993**, *126*, 1671–1682.
[13] Fukuzumi, S.; Kotani, H.; Ohkubo, K.; Ogo, S.; Tkachenko, N. V.; Lemmetyinen, H. *J. Am. Chem. Soc.* **2004**, *126*, 1600–1601.
[14] Choi, T.-L.; Grubbs, R. H. *Angew. Chem. Int. Ed.* **2003**, *42*, 1743-1746.
[15] Lauer, M. G.; Henderson, W. H.; Awad, A.; Stambuli, J. P. *Org. Lett.* **2012**, *14*, 6000–6003.
[16] VanAllan, J. A.; Reynolds, G. A. *J. Org. Chem.* **1968**, *33*, 1102–1105.
[17] Ye, J.; Zhang, X.; Deng, D.; Ning, G.; Liu, T.; Zhuang, M.; Yang, L.; Gong, W.; Lin, Y. *RSC Adv.* **2013**, *3*, 8232–8235.
[18] Connelly, N. G.; Geiger, W. E. *Chem. Rev.* **1996**, *96*, 877–910.

Vita

Kelli Ogawa is originally from Waipahu, Hawaii and received a B.S. degree in chemistry from the University of Hawaii in 2009. In July, 2010 Kelli joined the Boydston research group at the University of Washington and was awarded the Ringold Fellowship, graduate student merit fellowship, and graduate student travel award from the University of Washington. Her current graduate research focuses on developing new reactions that increase overall efficiency and minimize environmental impact, with recent advancements involving N-heterocyclic carbene catalyzed anodic oxidation of aldehydes and metal-free ROMP.